Spring 1-1-2015

A study on Flash Sintering and Related Phenomena in Titania and its Composites with Alumina

Fnu Shikhar
University of Colorado at Boulder, fnu.shikhar@colorado.edu

A STUDY ON FLASH SINTERING AND RELATED PHENOMENA IN TITANIA AND ITS COMPOSITE WITH ALUMINA.

By,

Shikhar

B.E. Metallurgy and Materials Engineering

Indian Institute of Engineering, Science and technology, Shibpur, 2009

M.E., Materials Engineering,

Indian Institute of Science, Bangalore, 2011

A thesis submitted to the Faculty of the Graduate School of the University of Colorado in partial fulfillment of the requirement for the degree of Doctor of Philosophy

Department of Mechanical Engineering

2015

This thesis entitled:
A study on Flash Sintering and Related Phenomena in
Titania and its Composites with Alumina
Written by Shikhar
has been approved for the Department of Mechanism Engineering

_____

Professor Rishi Raj
Mechanical Engineering, University of Colorado, Boulder

_____

Professor Charles Musgrave
Mechanical Engineering, University of Colorado, Boulder

_____

Professor Se-Hee Lee
Mechanical Engineering, University of Colorado, Boulder

_____

Professor Todd Murray
Mechanical Engineering, University of Colorado, Boulder

_____

Professor Gregory Rieker
Mechanical Engineering, University of Colorado, Boulder

Date _____

The final copy of this thesis has been examined by the signatories, and we find that both the content and the form meet acceptable presentation standards of scholarly work in the above mentioned discipline.

Abstract

A study on Flash Sintering and Related Phenomena in Titania and its Composites with Alumina.

Shikhar (Ph.D., Mechanical Engineering)

Dissertation directed by Professor Rishi Raj

In 2010, Cologna *et. al.* [1] reported that with a help of small electric field 120 Vcm^{-1}, the sintering temperature of 3 mol % yittria stabilized zirconia could be brought down to 850°C from 1450°C. On top of reducing the temperature requirements, the green sample could be sintered from starting density of 50% to near full density in mere 5 seconds, a sintering rate three orders of magnitude higher than conventional methods. This discovery led to the emergence of a new field of enhanced sintering with electric field, named "Flash Sintering".

The objective of this thesis is to understand the phenomenological behavior of flash-sintering and related phenomena on titania and its composites with alumina at elevated temperature. The possible mechanisms to explain flash sintering are discussed: Joule heating and the avalanche of defect generation [2], both induced by the rapid rise in conductivity just before the onset of the flash. Apparently, both mechanisms play a role.

The thesis covers the response of pure titania and composites of titania-alumina under flash and compared with conventional sintering.

We start with the sintering behavior of pure titania and observe lowering of sintering temperature requirements with higher applied electric field. The conductivity of titania during flash

is also measured, and compared with the nominal conductivity of titania at equivalent temperatures. The conductivity during flash is determined to be have a different activation energy.

For the composites of titania-alumina, effect of flash on the constrained sintering was studied. It is a known fact that sintering of one component of composite slows down when the other component of a different densification rate is added to it, called constrained sintering. In our case, large inclusions of alumina particles were added to nano-grained titania green compact that hindered its densification. Flash sintering was found to be overcoming this problem and near full densification was achieved.

In another experiment, effect of high current density and hold time under flash on the chemical reaction (phase transformation) of titania and alumina to form Al_2TiO_5 is studied. It was found that not only flash enhances the kinetics of reaction when compared with conventional heating at equivalent temperatures, but also brought down the phase transformation temperature for this spinel formation, as reported by the phase diagram.

In-situ X-ray diffraction experiments were performed at the synchrotron facility in Argonne National Laboratory. The specimen temperature were measured during the experiment on the basis of peak shift with temperature and were found to be matching with our predicted values by Black-Body-Radiation model. We also observed the instant evolution of texture in grain orientation of pure titania under flash and their disappearance as the fields were switched off. Study on chemical kinetics between titania and alumina were also performed which supported our findings of in-house experiments.

Dedicated to Professor Rishi Raj

Acknowledgement

This research was supported by the Basic Science Division of the Department of Energy under Grant No. DE-FG02-07ER46403.

I thank all the people who inspired me and supported me through my journey of PhD.

Table of Contents

List of Tables

Table of Figures

1. Introduction

Materials have been the backbone behind every technology and every material has its own application depending on its property. On the basis of these unique properties, materials have been divided in four general categories: metals, ceramics, polymers and composites. [3]. Typically Ceramics are the oxides, carbides and nitrides of metals. They are known for their stiffness and hardness but unlike metals they are brittle. Ceramics are also often resistant to chemicals and oxidation. Composites are comprised of two or more of the materials categorized above.

Ceramics [4] have their unique properties that make their applications exclusive sometimes. Electrical properties of ceramics usages varying from an insulator (alumina) to semiconductor (Titania) to superconductors (YBCO). Ceramics are used where stiffness and hardness of the material is critical, such as knives (zirconia and alumina), ball-bearings (silicon nitrides) and tiles among many others. As a heat and environment resistant material, ceramics are used for high temperature applications (furnace components and turbine blades). Ceramics have medical application in form of bio-ceramics, such as hydroxyapatite. Non-stoichiometric ceramics are used as oxygen sensors. Based on the recent discoveries of unique ceramic properties, their applications have touched nearly every field of engineering and science. However, desirable

properties of ceramics can be negated by the difficulty of manufacturing. The high melting point and brittle nature (cannot be formed like metal) render the ceramics difficult to be given a desired shape [5].

Owing to these difficulties, ceramics are fabricated by a process called sintering. Sintering is a thermally activated process in which solid-state mass transport occurs that reduces the particle interface/surface energy to form dense body out of green body [6], [7]. Green body is a compacted powder of ceramics which is pressed into a desired shape with the help of a die.

The process of sintering can also be influenced by pressure, ceramic powder morphology, additives and different heating schedule [8]. This thesis describes the use of electric field along with temperature, as a new method of sintering, called “flash sintering”. Apart from saving a lot of energy in terms of temperature and time requirements by enhancing sintering behavior, this method has also shown some unexpected results such optical-luminescence, controlled grain-growth and synthesizing some composites which was not possible before using conventional methods. Along with discovering new findings such as texture evolution, chemical reactions and constrained sintering, this thesis also tries to explain the theory behind the results on the basis of a mechanism proposed by Raj and coworker [2], [9] , “defect avalanche”.

2. Literature survey

2.1 Sintering

Sintering is a process of forming a solid mass of material, metal/ceramic from compacted powder with the help of thermal energy with or without external pressure. Sintering occurs through neck growth between the particles which is assisted by thermal diffusion. This process can lead to densification where particles eventually come together and pores are eliminated. Elevated temperature is required for the solid-state diffusion in ceramics as atomic bonds are very strong. For example, alumina requires 1400-1500 °C[10] Zirconia 1450 – 1500 °C [1] and Titania 1000 – 1200 °C [11].

An age old example of sintering is Pottery where a clay body is formed into a desired shape and heated in a high temperature kiln, steps shown in Fig 2.1. Firing at high temperature allows the diffusion of matter and reaction that gives strength to clay. On macroscopic level, the shape of

the material remain the same but the size shrinks as a porous body turns into dense solid material as a result of pore removal, schematically shown in Fig 2.2.

Figure 2.1 Clay body being given shape on a wheel and fired at high temperature to give final product, that is, a porcelain bowl. [12] .

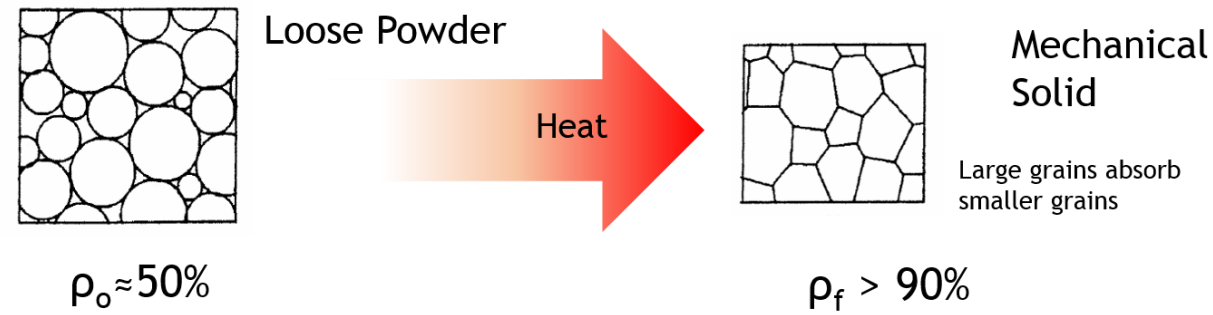

Figure 2.2 Starts with green compact of density 50 % theoretical density and goes to to more than 90% dense material.[6]

On the scale of particles, the driving force for sintering comes from the reduction in total interfacial energy. The total interfacial/surface energy is expressed as γ*A, were γ is surface (interface) energy and A is the total surface area. Differentiation of this total energy gives two components given in Eq. 2.1.[7]

$$\Delta(\gamma A) = \Delta\gamma.A + \gamma.\Delta A \qquad (2.1)$$

First component, $\Delta\gamma.A$, corresponds to reduction in surface energy by replacement of particle-pore (open surface) interface by particle-particle (grain boundaries) interface which leads to densification. The other component, $\gamma.\Delta A$, corresponds to removal of interfacial area by grain coarsening (volume remains the same while pore size grows), schematically shown in Fig 2.3. Sintering is combination of these two processes at different stages.

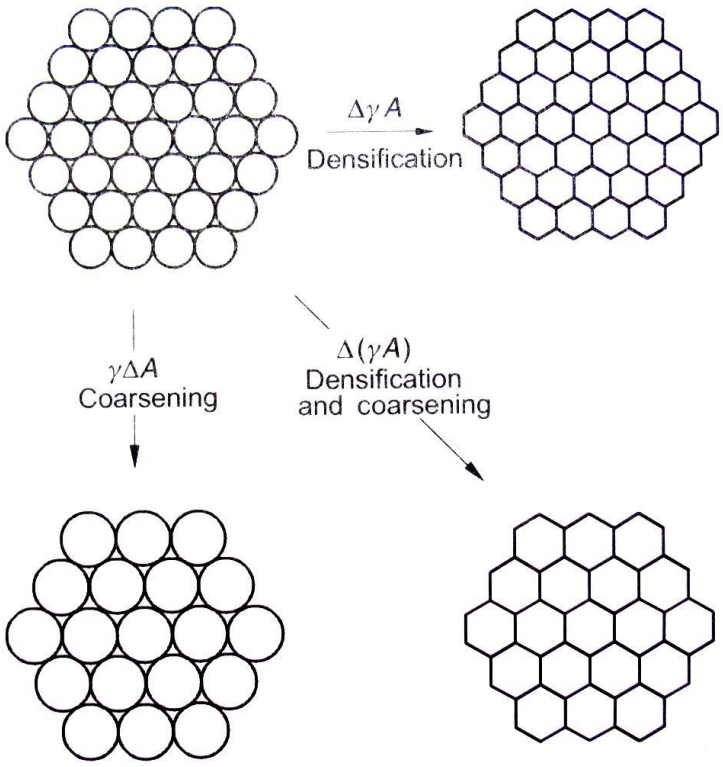

Figure 2.3 Schematic representation of densification and coarsening from green compact.[7]

2.1.1 Mechanism of Sintering

Sintering in polycrystalline material happens by diffusional transport of matter and elimination of pores through solid-state mass diffusion. The diffusion can happen along different paths which determines the mechanism of sintering involved. Matter moves from region of higher chemical potential (the source) towards region of lower chemical potential (the sink). There can be as many as six distinct mechanism that allow the transport of matter [6], [13], schematically shown in Fig. 2.4. All six of them lead to inter-particle neck growth and bonding between the particles which increases the strength but only three of them lead to densification (shrinkage). The first three; surface diffusion, lattice diffusion from surface and vapor transport deposit matter from one surface to neck which leads to neck growth but no pore removal. They also lead to reduction of neck curvature and thus lowers the driving force of sintering. With the last three, the matter is removed from the grain-boundaries and bulk and deposited at the neck, thus bringing the centers of particles together, and densifying along with neck growth.

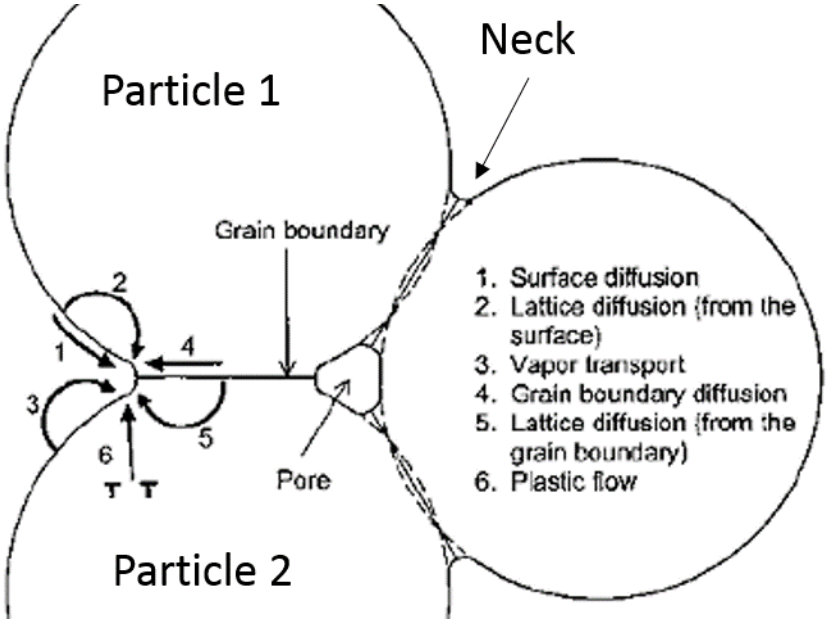

Figure 2.4 Six distinct mechanisms that contributes to the sintering (mass diffusion). [6]

Table 2.1 Mechanisms of Sintering in Polycrystalline materials [6]. Bolded text distinguishes the densifying mechanism from rest of them.

Mechanism	Source	Sink
1. Surface Diffusion	Surface	Neck
2. Lattice Diffusion (From surface)	Surface	Neck
3. Vapor transport	Surface	Neck
4. Grain boundary diffusion	**Grain boundary**	**Neck**
5. Lattice diffusion (from grain boundary)	**Grain Boundary**	**Neck**
6. Plastic flow (through dislocation)	**Bulk**	**Neck**

2.1.2 Sintering Pressure

From mechanical point of view, sintering can also be described in terms of compressive stress that has been experimentally measured with sintering behavior of tape-cast titania, where the time dependent axial strain (parameter of densification) was measured as a function of varying tensile load at a fixed temperature. As the tensile stress (acting against sintering pressure) is increased the densification slows down. The applied stress where the axial strain (due to sintering) becomes zero gives a measurement of sintering pressure. [14]. Values of sintering pressure were in line with earlier findings of sinter-forging experiment on alumina [15]. It was also concluded that sintering pressure decreases with increasing density. A rigorous analysis of sintering pressure was presented by Raj [16] that explained sintering pressure as summation of two terms, one being

surface curvature of pores (*r*) and other is dependent on the grain size (*D*) of particles. The coupled equation being,

$$\sigma_{\sin tering} = \frac{2\gamma_{ss}}{D} + \frac{2\gamma_{sv}}{r} \qquad (2.2)$$

where D is the grain size of particles, γ_{ss} is surface energy at grain boundaries and γ_{sv} is interface energy between surface and vapor (particle - pore). The equation assumes that number density of pores remain the same and the surface of pores have uniform curvature. In Eq. (2.2) '*r*' is the curvature of the pores, which can be either positive or negative depending on whether the curvature is convex with its center points towards middle of pore or vice-versa. The Smaller is the grain size of particle (*D*), the higher is the driving force. The driving force of this process is surface energy reduction. Larger pore size (assuming convex surface) and particle size both implies lower sintering pressure.

2.2 Stages of sintering

The sintering behavior has been broadly categorized in three different stages. A plot of densification with time at a suitable sintering temperature and its corresponding micrograph have been depicted in Fig. 2.5 [17], [18].

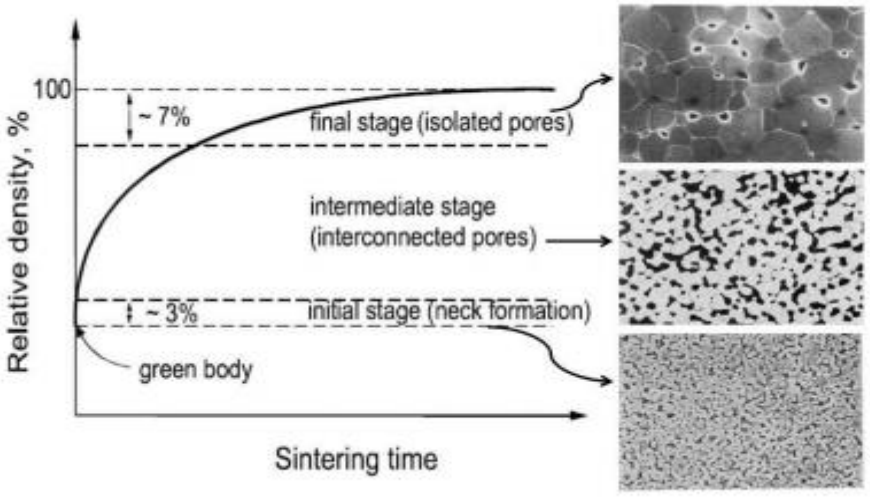

Figure 2.5 Densification rate slows down with higher density and the corresponding microstructures show the grain growth, pore evolution and densification. [17], [18]

1. *Initial stage*:

   Particles come in contact with each other by inter-particle neck growth. Vapor transport is the main contributor for this stage. Large initial differences in surface curvature are removed in this stage and densification accompanies the neck growth. The curvature around the particle-particle –pore region becomes convex that drives densification in next stage. There is very small increment in green density (such as 50 to 55% of T.D., theoretical density).

2. *Intermediate stage*:

   Once the neck formation is over, the pores reach equilibrium shape based on the particle shape-size, packing and surface energy. The pores remain interconnected but shrink in volume. This stage covers densification from 60 % to 85% of theoretical density at which point pores become isolated from their neighbor pores.

3. *Final stage*:

This stage begins when the pores become isolated and cornered on the triple junctions. Depending on the mechanism and temperature, pores may either continue to deplete at a much slower rate than stage II or coalesce to a bigger pore (thus stalling the densification from reaching the theoretical density). Grain growth also takes important role in stage III which reduce the driving force for sintering further.

Interplay between the grain growth and densification during final stage can be understood from the work of Cameron and Raj [19] where the specific surface area and grain size for sintering of alumina have been plotted with respect to relative density in Fig. 2.6. While the specific surface area continues to drop with densification until the pores become isolated and trapped at the triple boundaries when density reaches near 0.95 of its T.D. (theoretical density). It is about the time when the grains starts to grow non-linearly. This can be explained that until pores are isolated, they pin the grain boundaries at the triple junction and therefore preventing grain growth.

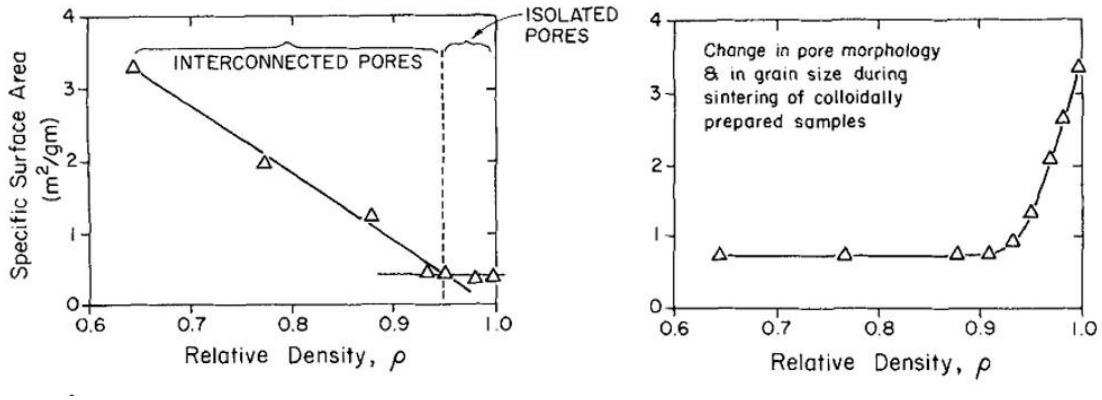

Figure 2.6 (a) shows the depletion of surface area with densification to the point where pores become isolated and trapped at the triple junction. (b) gives an account of how the grain growth becomes effective only after majority of densification is over and no open pores are left. [19]

There can be much more variability in the sintering behavior apart from what has been mentioned above depending on the surface energy, particle size, diffusion coefficient, powder morphology, packing distribution in green compaction and many others.

2.3 Methods of Sintering

For the longest time, temperature and time were the only two parameters of sintering, but with the advancement in understanding of the process, new techniques were developed to save on energy by reducing the temperature requirement of sintering and time of process. To quantify this gain, a map has been developed, Fig. 2.7 which allocates the different methods of sintering on the map of temperature versus time. The example that has been used here is based on sintering of 3 mol % yitrria stabilized zirconia.

2.3.1 Conventional sintering

As mentioned above, conventional sintering requires temperature and time as the only two variables for sintering, however they vary depending on the material, initial grain size, green density and requirements of final product.

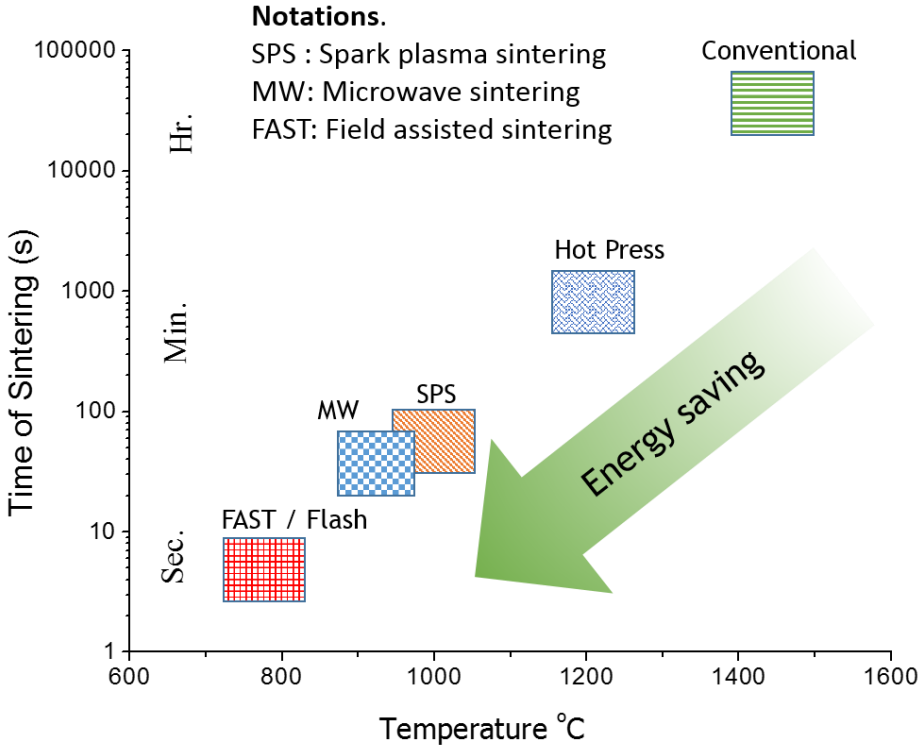

Figure 2.7 Reduction in time and temperature with new techniques of sintering. [20]

2.3.2 Pressure Assisted sintering:

Application of an external pressure results in a direct increase in driving force for densification increases by an additional factor of $\phi.P_a$ where ϕ is stress intensity factor that depends on the density of specimen. At the same time, since grain growth is not related to the

applied external pressure, it enhances the densification without grain growth. There are three ways of applying pressure while sintering, as schematically shown in Fig. 2.8.

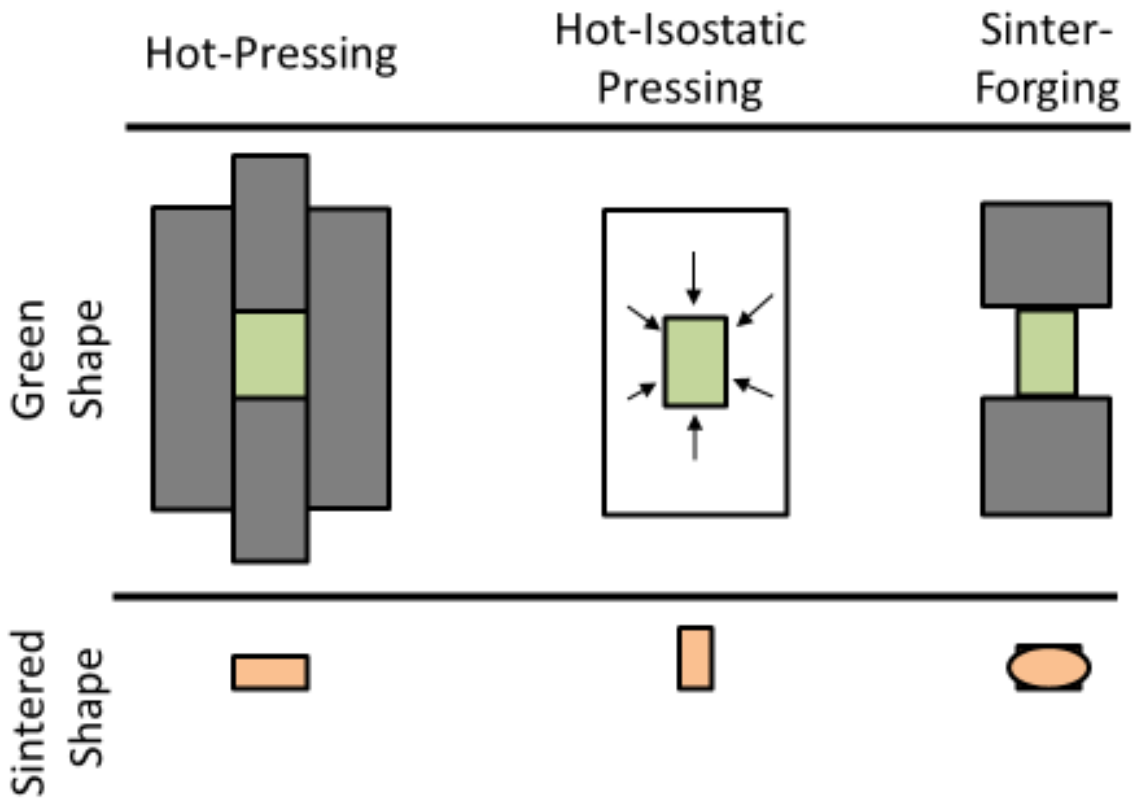

Figure 2.8 Three types of pressure assisted sintering (a) Hot pressing (b) Hot isostatic pressing and (c) Sinter forging.[18]

Hot pressing: Cylindrical graphite dies are used in which the powder are compacted uniaxially compressed while being heated up in the furnace [6]. It is the most commonly used method of pressurized-sintering, however on the other hand, it has its own limitations, for example, it can only produce cylindrical specimens based on die size and die walls (carbon) sometimes reacts chemically with sample. Also, since graphite starts to oxidize at ~ 800 °C so it requires atmosphere controlled (Ar gas) furnace.

Hot Isostatic pressing (HIP): In this technique, near theoretical density can be achieved for any shape of pre-sintered compact, because it eliminates the shear stress under isostatic condition. But this method requires pre-sintered material of density more than 90 %.

Sinter-forging: Sinter forging is similar to hot pressing with an exception that it does not require any die. The specimen is compacted into cylindrical specimen and uniaxially compressed while sintering. It also has shear component that aids in pore mobility and eliminating defects [21].

2.3.3 Microwave Sintering:

Microwave (MW) sintering is a method of heating inside-out as compared to conventional sintering where specimen get heated from outside (surface temperature is higher than core). Heat is generated internally by interaction of microwave radiation (wavelength 1 mm to 1 m) with atomic particles and grain boundaries [22], so a very high heating rate, such as 300 °C/min, can be achieved which leads to very high densification rate as compared to conventional sintering. Since receptibility of ceramics towards microwaves changes with temperature, an additional heater is needed in some cases to make ceramics more receptive. Although microwave sintering is very energy efficient, it has issues of uncontrolled localized heating especially if shape of ceramic body is not simple.

2.3.4 Electric field assisted Sintering:

Electric field has been utilized in two ways to achieve quicker densification. They are (a) Spark plasma sintering, (b) Field assisted sintering (FAST) and (c) Flash sintering.

Spark Plasma Sintering (SPS): Spark plasma sintering set-up is similar to hot pressing with a small difference that graphite die is heated with joule heating, produced by a high current

(hundreds of amperes) passing through the die. For the most part and specially for ceramics, the applied current goes through the graphite-die since it is much more conducting than ceramic powder inside. A schematic of SPS is shown in Fig. 2.9 [23]. Like hot-pressing, significant axial stress, ~ 300 MPa can be applied using the graphite push-rods. This technique too has advantage of very high heating rate (1000 °C/min) and fine grains (almost no grain growth) [24], [25], but as a drawback, it can produce specimens of cylindrical shape only.

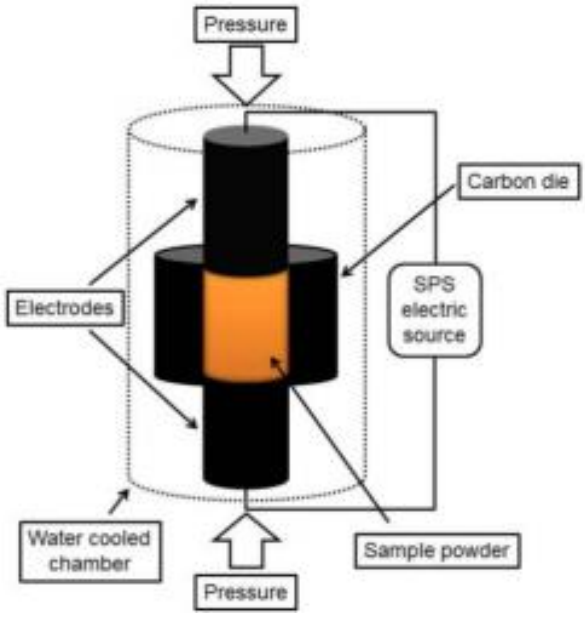

Figure 2.9 Schematic diagram of Spark plasma sintering (SPS) apparatus. [23]

Field assisted sintering was the precursor of Flash sintering, so a detailed description of the development of this method is needed. When a small electric field is applied across the specimen to enhance the sintering rate, it is called field assisted sintering (FAST). Current flowing through the specimen is very little, in this case. When this applied field is amplified high enough, current starts to rise non-linearly until a limit is put on current; this condition has been named Flash sintering.

2.4 FAST Sintering

This section talks about the history behind the development of Flash sintering [26]–[29], the first report of flash sintering by Cologna and Raj [1] and the development thereon. The FAST and flash sintering are fundamentally different from SPS because in the later process most of the electrical energy passes through die resulting in high current and low electric field (1000 A and 27 V/cm [25] but in flash experiments field is applied directly to the specimen and current is made to flow through the sample, so a relatively high electric field ~ 100 V/cm and very low current density ~ (60mAmm^{-2} for 3YSZ) [30] is required. Also, with an exception of Flash sinter forging [31], all the flash sintering experiments are open air and free sintering (with no applied pressure).

2.4.1 Earlier development

In the earliest experiment by Yang and Conrad [27] in 1997 on fully sintered 3 mol % yittria stabilized zirconia (3YSZ), it was showed that an applied electric field of 1kV/cm during the superplastic deformation at 1500 °C can reduce the flow stress and increase the extent of plastic deformation by retarding the grain-growth and cavitation, shown in Fig. 2.10.

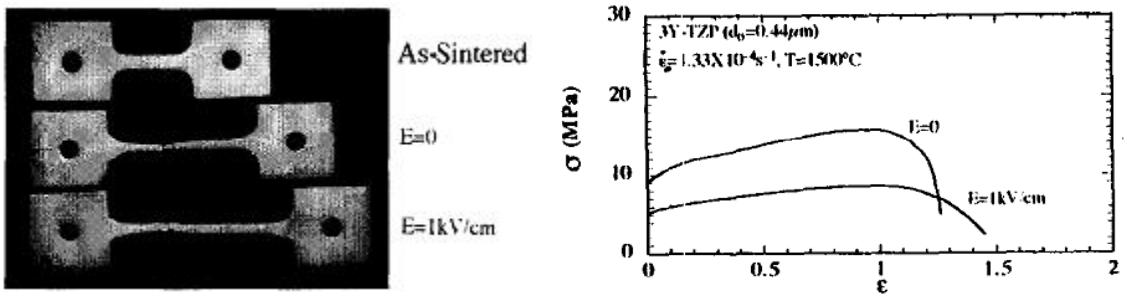

Figure 2.10: (a) shows the zirconia specimen as-sintered, and after superplastic deformation without and with applied electric field. (b) shows the true stress strain curve for a given strain-rate deformation experiment. With applied electric field, the flow stress of 3YSZ was found to be lower and more plastic deformation occurred before failure. [27]

In the follow up work on MgO, Al_2O_3 (with 400 V/cm) and 3YSZ (with 20 V/cm) [26], it was found that in a cylic on/off experiment, electric field strength had an intermediate effect on lowering the flow stress of ceramic. It was concluded that electric field creates vacancies corresponding to the slow moving specie in the space-charge region at the grain boundary that improves the diffusion of material and inhibits the grain-growth by decreasing the grain-boundary energy. Unfortunately there was no report about the current through the specimen during these experiments. It was later found by Francis and Raj [30] to have a significant affect on densification and Joule heating of sample.

2.4.2 FAST (Electric field assisted Sintering)

Based on the results of Conrad *et. al*. [26], [27], Ghosh *et. al.* [29] demonstrated with a very weak electric field of 4Vcm^{-1} the grain growth behavior in fully dense 3YSZ can be retarded. The set-up is shown in Fig. 2.11 where platinum wires are diffusion bonded to the two sides of the dense 3YSZ specimen and the expected electric field lines on the sample have been drawn below.

The field was kept ‘on’ for 10 hours of annealing at a temperature 1300 °C. On the right of Fig 2.11, one to one relation of grain-growth with strength of electric field has been shown, and a minima was observed at the highest electric field line. The field was kept too low for any appreciable current to flow to give rise to Joule heating.

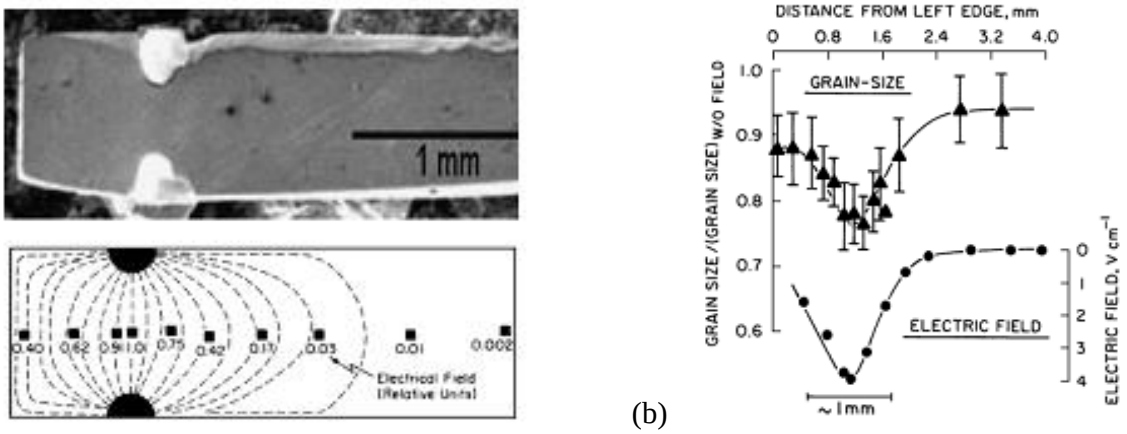

(b)

Figure 2.11: (a) Electrode position and the FEM analysis of electric field passing through the dense 3 YSZ. Specimen and (b) shows the link between the grain-size with the magnitude of electric field. [29]

This finding was also supported by the findings of Conrad *et. al* [28], [32], [33]. Experiments with Alternating field enhanced the densification rate further.. As can be seen from Fig. 2.12, for a given temperature the density is higher as we move from no electric field to Direct electric field to Alternating electric field. The explanation of the increased sintering rate has retardation of grain growth because of decrease in grain boundary energy as a result of the interaction of the field with space charge. An analytical procedure has been developed by Conrad to quantify for the space charge potential [34]

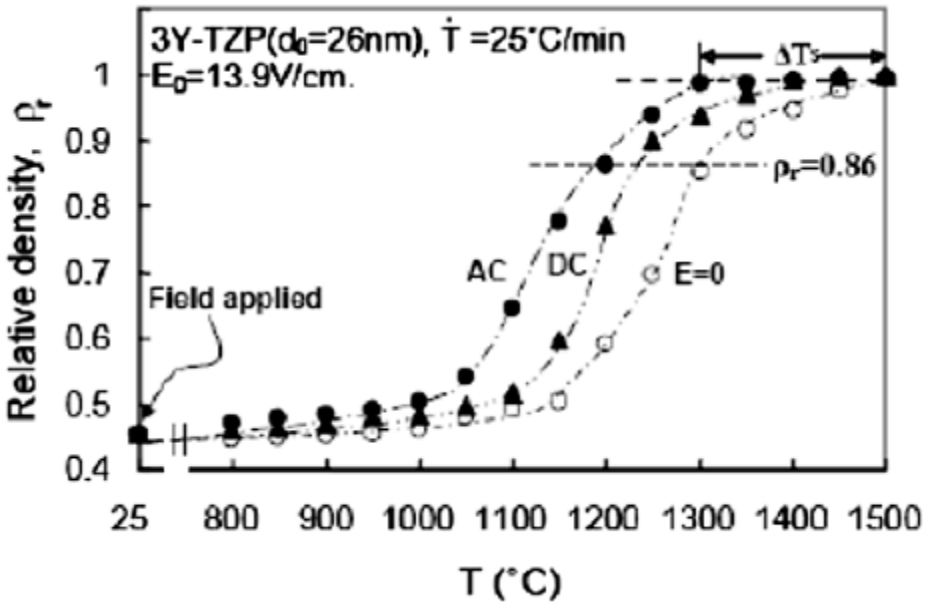

Figure 2.12: Relative density of 3Y-TZP during the constant-heating-rate (25°C/min) sintering experiments with no field, direct field (13.9 V/cm) and alternating field (13.9 V/cm rms) of 60 Hz. [35]

2.5 Flash Sintering

Flash sintering was first reported by Cologna *et al* [1] where they showed that 3 mol% yittria stabilized zirconia can be sintered to full density in few seconds at a furnace temperature of 850 °C under an applied DC field of 100 Vcm^{-1}. Fig. 2.13 shows that there is a gradual increase in the sintering rate with electric field and beyond 60V/cm instantaneous sintering occurs that has been named as Flash Sintering. The sintering temperature drops down further as higher electric field is applied. Microstructural analysis confirms that findings of FAST sintering (based on grain-growth retardation) cannot explain the flash behavior. The highly improved kinetics must be the result of enhanced diffusion of atoms beyond what is thermodynamically permitted at that

temperature. This behavior also lead to heating of specimen which has been dealt with in section 2.5.2.

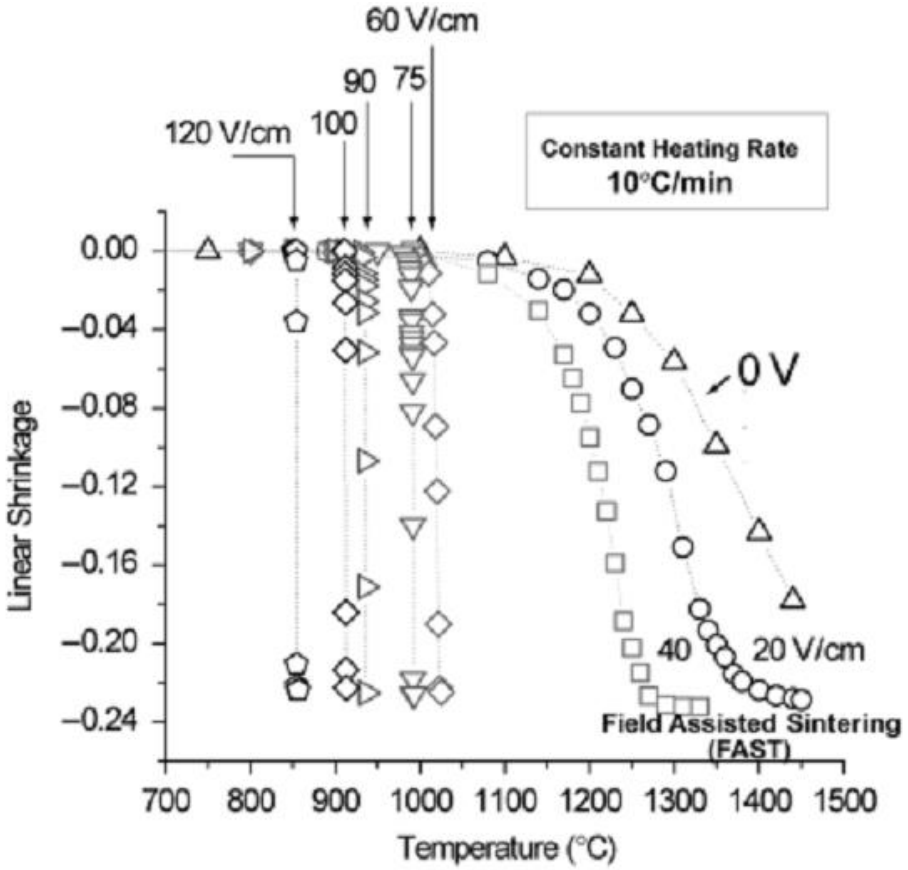

Figure 2.13: Direct current electric field enhances the sintering until an instability point is reached beyond which sintering occurs in a few seconds. [1]

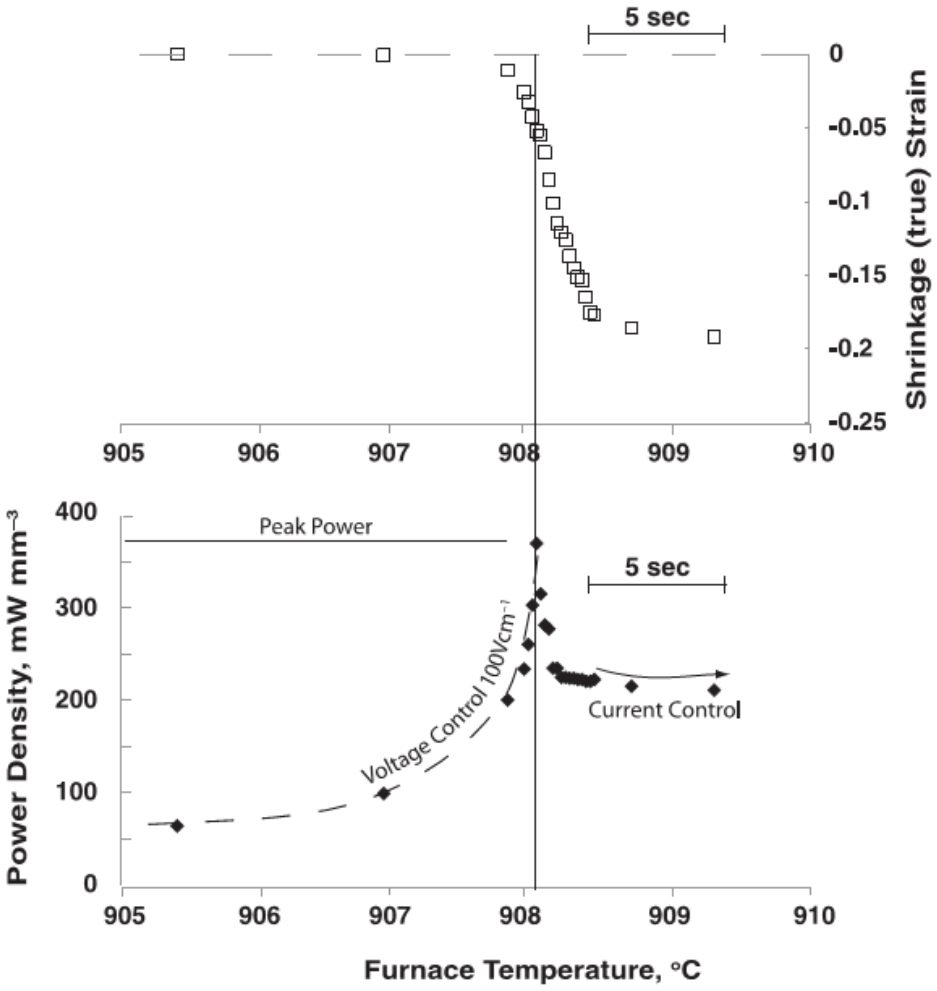

Figure 2.14 Shows the expanded view of linear shrinkage during the flash sintering and corresponding power density curve. The highest shrinkage rate matches up with power spike.[2]

To understand this extraordinary high sintering rate, it is important to understand the relation between power dissipation in the specimen because of electrical energy and the shrinkage rate. Fig. 2.14 shows on an expanded time scale that highest sintering rate was achieved at the power spike (later named as stage II). Francis [30], performed a series of isothermal flash experiments at 900° C to relate all the electrical parameter with the flash sintering, in Fig. 2.15. Unlike the FAST sintering, where electric field is constant all the time; current rises non-linearly after a short incubation time. If this runaway in current is not contained, it would lead to very high

Joule heating and eventually melt the specimen. So, an upper limit is put on the current, where, up on reaching the power-supply switches to current controlled mode and the voltage drops as determined by conductivity of the specimen and set current limit. Since power dissipation is the product of voltage and current, a spike is observed in the power density when the power supply switches from voltage controlled to current controlled mode. In voltage controlled regime, power is given by E^2/R (where R is resistance of specimen which continues to drop with higher temperature and E is applied electric field, Vcm^{-1}) and in current controlled (stage III) regime power is given by $j^{2}.R$ which drops as the R drops (j is current density, $mAmm^{-2}$). The peak of the power is determined by the applied field and current limit, however occasionally the current rises beyond the set limit before power supply switches.

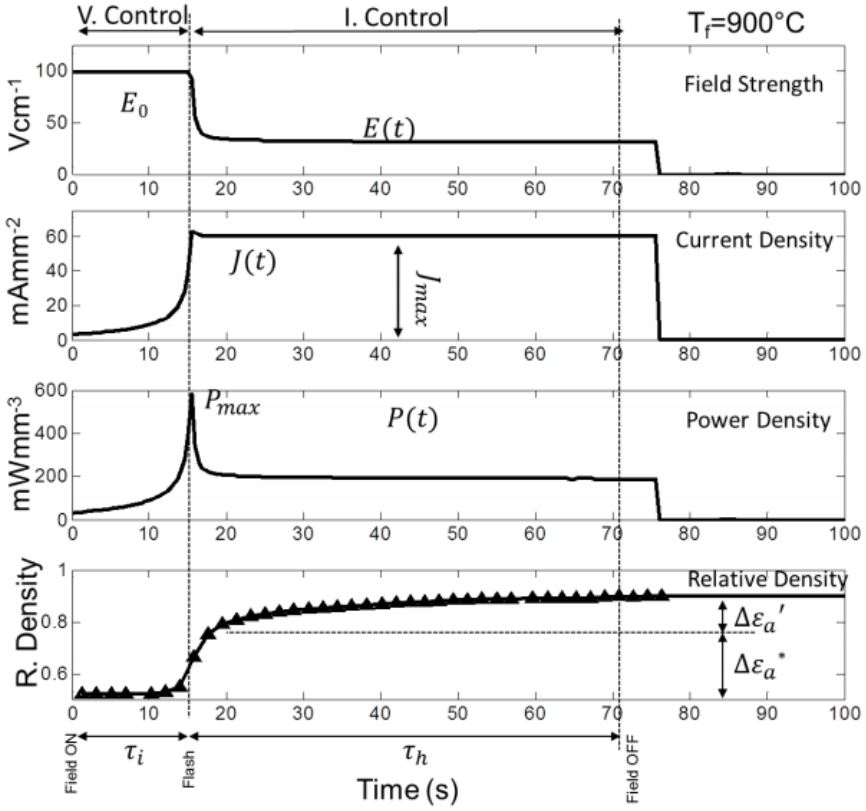

Figure 2.15 Relation of electrical parameters to densification in isothermal experiment done at 900°C. [30]

After zirconia (ionic conductor), magnesia doped alumina (insulator) was tested under the similar conditions [10] and results were compared with pure alumina as shown in Fig. 2.16. Pure alumina is so insulating in nature that no appreciable flash/FAST behavior was observed even under 1000 Vcm^{-1} whereas alumina, doped with 0.25 wt% MgO, responds to electric field higher than 500 Vcm^{-1}. The microstructural evidence shows no anisotropisity in the grains and the grain sizes are comparable to conventional sintering. It was proposed for the first time that non-linearity in conductivity during flash sintering, arises from increased defect concentration that enhances the pre-exponential term of Arrhenius equation of diffusion with inverse of temperature.

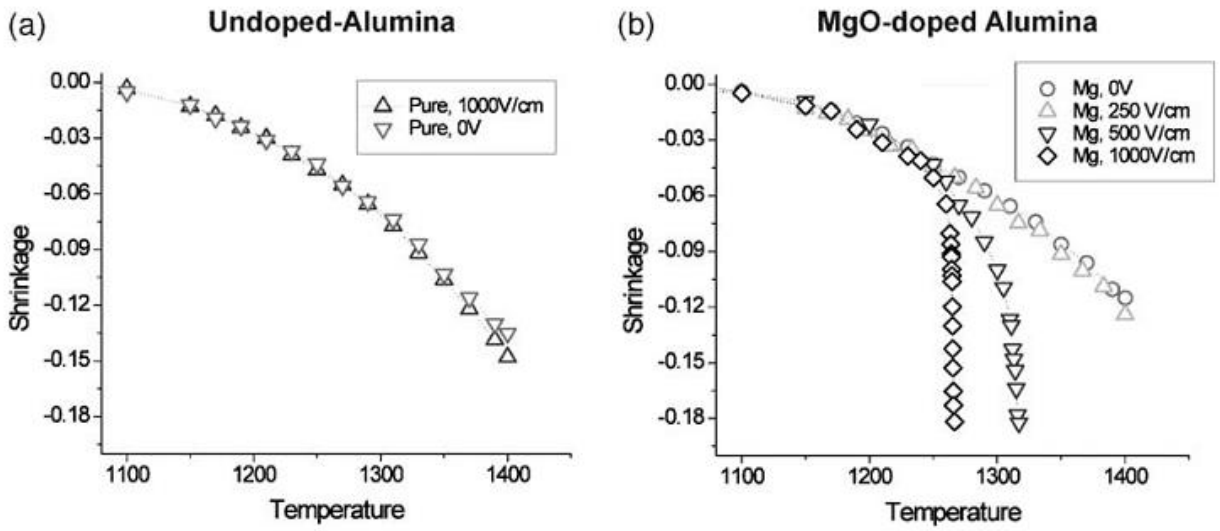

Figure 2.16: Influence of electric field on sintering behavior of (a) pure alumina and (b) MgO doped alumina, in constant heating rate experiments [10].

Later on, electric field was used to flash-sinter many other ceramics such as ZnO [36]–[38] 8 YSZ [39]–[41], LaSrCoFeO3 [42], Gd doped CeO_2 [43], $KNbO_3$ [44], TiO2 [11], Gd $BaCeO_2$ [45], SnO_2 [46], [47], $BaTiO_3$ [48], MnCo2O4 [49], yittria [50], SOFC [51], SrTiO3 [52], Co_2MnO_4 [53], Composites of 3YSZ-alumina [54] and TiO2-alumina [55] were also flash sintered. Some non-oxide ceramics have also been flash sintered ZrB2 [56] and SiC [57]. The versatility of this method to all kinds of ceramics, be it electrically conducting non-oxide ceramics (SiC), ionic conductors (3YSZ and 8YSZ), insulator (MgO doped alumina and Yittria) or mixed conductor (TiO2), is incredible. Another unexpected relation was observed in Fig. 2.17 [Raj unpublished data], all the oxide ceramics flash-sintered in a small power density window, between 10 to 100 $mWmm^{-3}$.

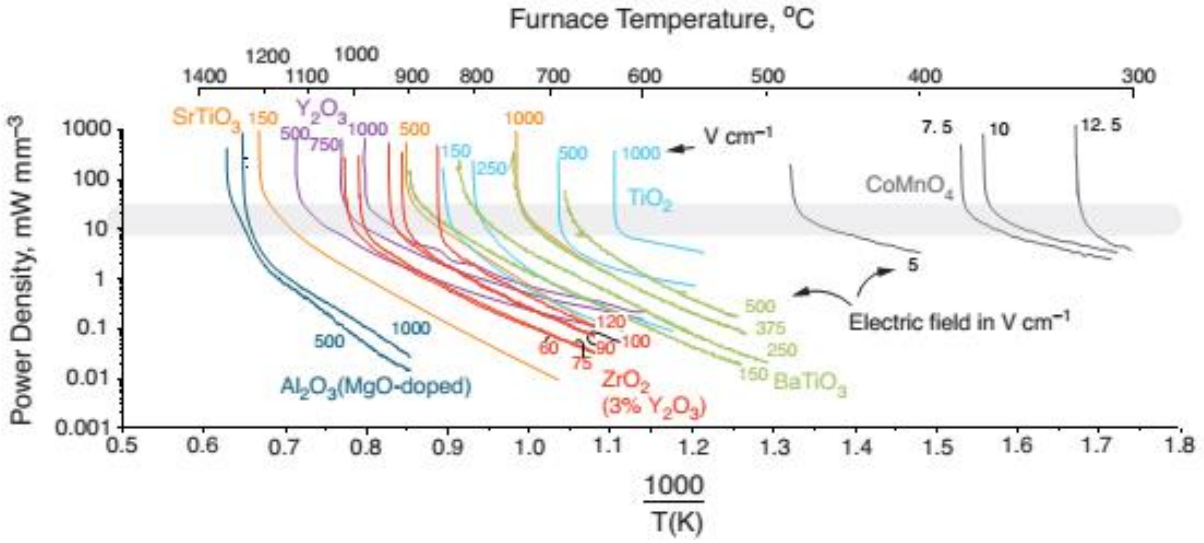

Figure 2.17: Consolidated data of various oxide ceramics showing similar values of power density for flash to occur (10 to 100 $mWmm^{-3}$). [Raj _ unpublished data].

2.5.1 Factors affecting flash sintering

In flash sintering experiment, be it isothermal (furnace temperature fixed) or constant heating rate experiment (furnace temperature rising), there can be many factors such as temperature, applied electric field, current density, time of holding, particle size and other parameter, such as pressure in flash–sinter forging experiment (explained later), that determines the final outcome.

Electric field. Voltage divided by the length of specimen gives us applied electrical field which has been used as an electrical parameter to normalize specimen with different gage-length for comparison. As the applied electric field is increased, flash sintering temperature drops down [31]. The result for cubic zirconia by Down [39], [58] has been shown in Fig. 2.18. A similar study on TiO_2 is also a part of this thesis (chapter 5, Fig. 5.9). In an isothermal experiment, the effect of higher electric field is shown in shortening of incubation time (time in which the current density

reaches its set value under given electric field for different temperature) [30], as shown for 3YSZ in Fig. 2.19(a). As can be deduced from Fig. 2.17, electric field varies considerably depending on materials.

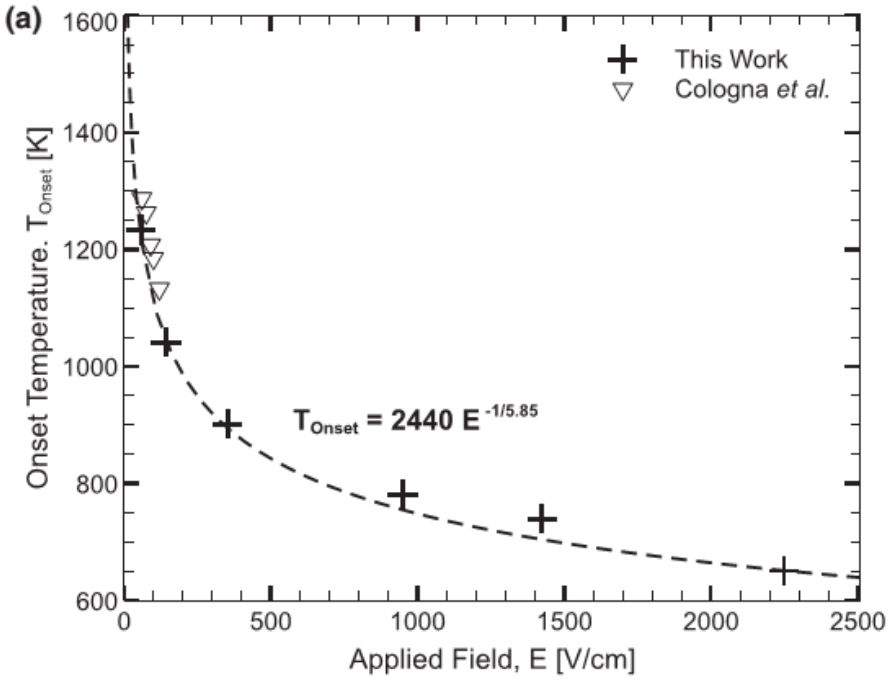

Figure 2.18. The hyperbolic curve of flash onset temperature with applied field for cubic zirconia, [39]

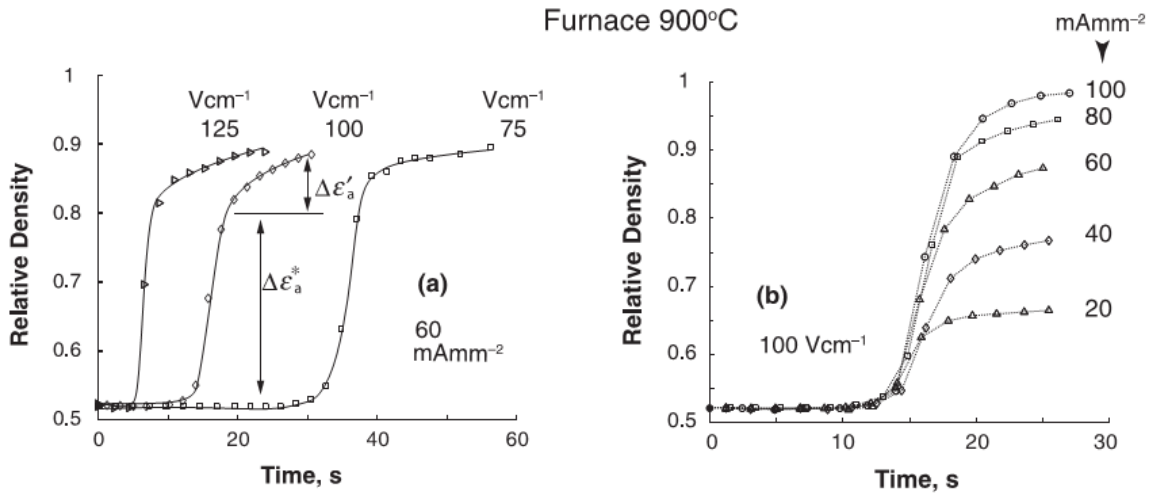

Figure 2.19 (a) Incubation time as a function of the applied electric field at 900°C (b) Effect of current density on densification. [30]

Current density. Different materials require different current densities and electric field at certain temperature for complete densification, however for a given material (for 3YSZ as shown in Fig. 2.20 (b)) there is a trend of higher final density for higher current density [30]. So, together electric field decides at which minimum temperature a given material can be flash sintered, while current density and hold time determines what would be the final density of the sample after flash sintering.

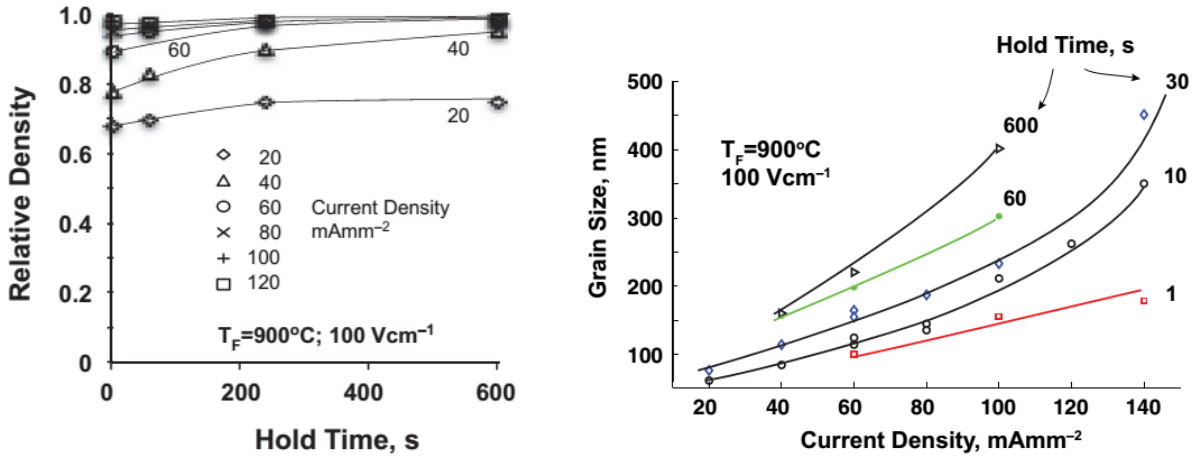

Figure 2.20 (a) Specimen for current density 40 $mAmm^{-2}$ and higher continues to sinter with time under flash until near full density is achieved, (b) Grain-growth as the function of current density and hold time.[30]

Hold time: Final density of a specimen is function of current density and time for which the specimen was held under flash (hold-time). As evident from Fig. 2.20 (b) while 100 $mAmm^{-2}$ gives full densification for 3YSZ at 900°C in 10 seconds, for 60 and 80 $mAmm^{-2}$ specimens continue to densify with time until full densification is achieved, Fig. 2.20 (a). Higher current density gives higher sintering rate (faster densification) and more grain growth for a given hold time, Fig. 2.20 (b).

Particle size: Initial particles size also influence the sintering kinetics. In terms of packing, the green density is usually smaller for bigger particles than for smaller particles. The total grain boundary area also get reduced with bigger particles which diminishes the driving force for sintering. At the same time, the diffusion distance (from middle of a grain boundary to pores) increases. Also, as pores size increase, they become stable and that leads to difficulty in further pore removal. All these factors result into lower densification. Similar effect of particle size is also observed in flash sintering [59], Fig. 2.21, where bigger particle specimen densifies less, compared

to smaller particle sized specimen for same conditions of flash. However, it should be noted that specimens with same particle sizes still densify more in flash sintering than conventional. It was also observed that the shrinkage rate is strong function of particle size, shown in Fig. 2.21 (b), which is intuitive as the sintering pressure reduces with higher particle sizes. The power density and temperature measured by pyrometer was found to be same for all experiments, irrespective of the particle sizes.

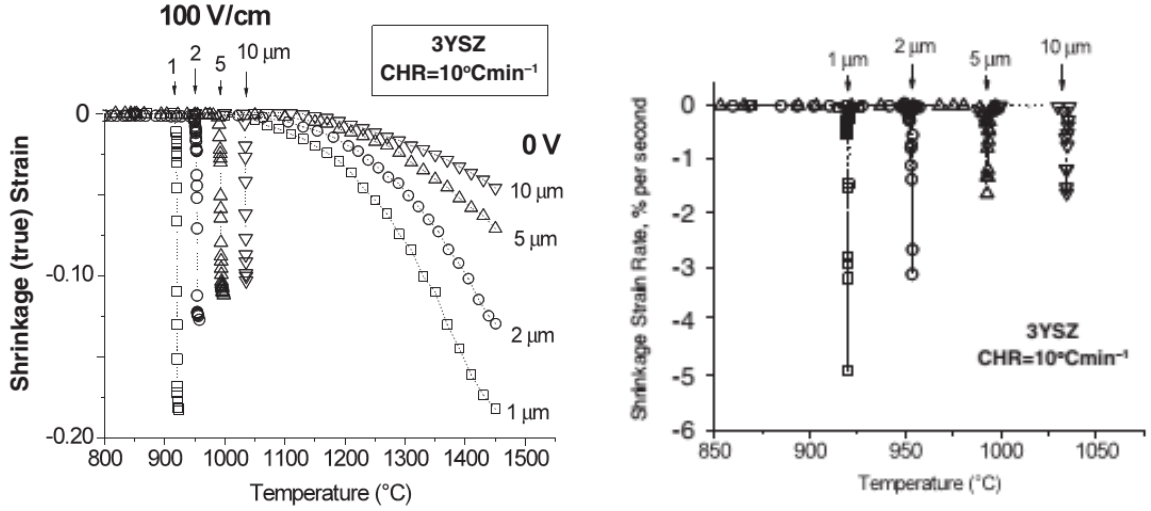

Figure 2.21: (a) Linear shrinkage for various particle size specimen with applied field (100 V/cm) and without (b) sintering rate for different particle sizes during flash sintering. [59]

Pressure: Applied pressure has been known to expedite the sintering process [21]. In sinter forging experiments, shear component of the sinter-forging experiment helps to eliminate the pore-formation and avoid grain growth. Pressure has a similar effect on lowering the threshold flash-sintering temperature, as shown in Fig. 2.22 [31]. As the applied uniaxial stress (and so the shear stress) was increased the temperature for onset of flash sintering dropped. Axial strain was found to be higher than radial strain as the applied pressure was increased but on calculation of volumetric strain (densification strain) it was nearly the same for all the experiments.

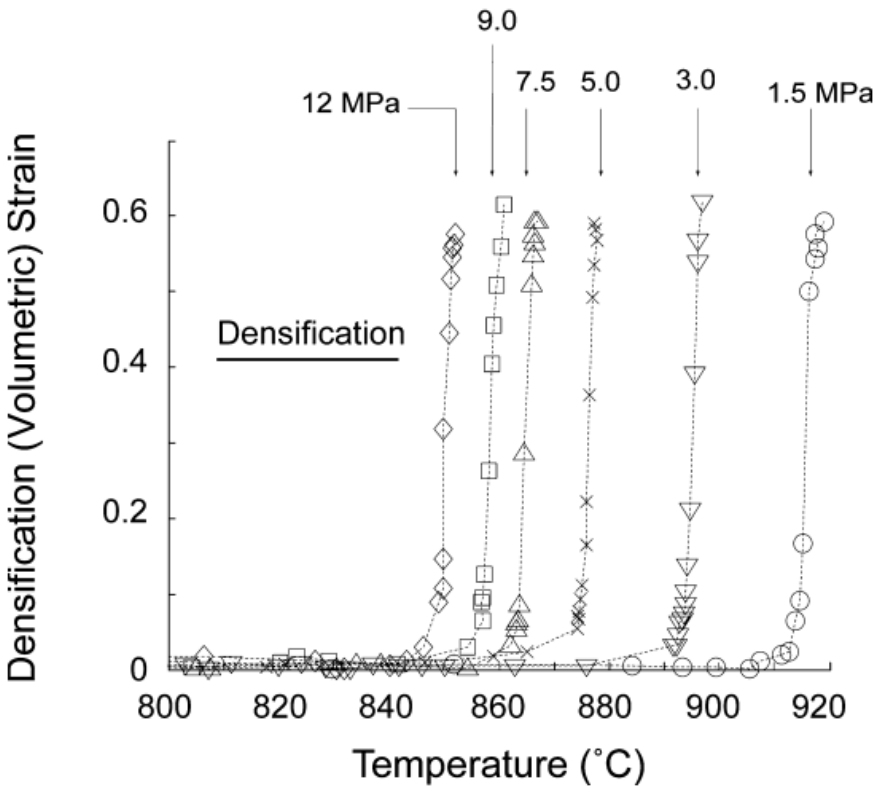

Figure 2.22. For the same flash conditions (Electric field, 100 V/cm) the threshold temperature for flash sintering drops with higher applied pressure. [31]

2.5.2 Joule Heating during flash

During flash sintering, the specimen also heats up due to the electrical heating (Joule heating). So, suspicion was raised that Joule heating is the reason for this extra-ordinary sintering rate seen. Chen and Park [40] suggested that electrical conductivity, as measured in in-situ impedance spectroscopy, can be compared with the extrapolated conductivity of specimen in to the flash regime to calculate the specimen temperature. They claimed that estimated temperature for 3YSZ falls in between 2100°C to 2500°C. However, it should be taken into account that this calculation is based on two assumptions that the transport number (number of ions for conduction) do not change under flash and there is no change in activation energy of conduction.

Later on, the claim of preferential grain-boundary heating and eventually melting [60] to facilitate the densification was negated by Holland *et al*, [61] where they showed that thermal diffusivity is so high that such kind of temperature gradient across 100 nm of grains is not possible. Steil *et al* [62] also reported, based on microstructure, that there is transient rise in temperature during the power spike of flash sintering, however power density for their experiment was much higher than what is necessary for full densification as seen in the work of Francis *et al* [30]. Of course, we admit that higher voltage and current density could lead to melting of ceramic.

Facing the incongruity in the community about the cause behind flash sintering, it was incumbent to measure the specimen temperature. Although, given the transient nature of this effect, it has been really difficult to exactly determine the temperature, especially in stage II (where the power spikes and the sintering rate is highest). The temperature of specimen rises because of joule heating and there are 3 ways of how this heat can be dissipated: (a) Conduction (b) Convection and (c) Radiation. At such a temperature (800°C and higher) and in the given set-up (two electrode sintering) conductions and convection are considered negligible compared to the radiation. A simple equation of black-body-radiation, equation 2.3, was used to calculate the temperature [2].

$$\frac{\delta T}{T} = \frac{\delta W}{4A\sigma T^4} \qquad (2.3)$$

T is the ambient temperature, δT is rise in temperature of specimen because of electrical energy (W) heat dissipation, A is the surface area for radiation and σ (= 5.67 x 10^{-8} Wm^2K^{-4}) is the Stefan Boltzmann constant. On integrating temperature from T_o (furnace temperature) to T (actual specimen temperature) and electrical energy from 0 to W_v, power dissipated per volume in units of $mWmm^{-3}$, it gives,

$$\frac{T}{T_o} = \left[1 + \frac{1000.W_v}{e_m \sigma T_o^4}\left(\frac{V}{A}\right)\right]^{\frac{1}{4}} \qquad (2.4)$$

where (V/A) is the volume to surface area ratio which changes with change in shape. This whole calculation was based on the assumption that specimen acts like black body and radiates all the electrical energy in heat. To accommodate that, a factor, e_m = 0.9, is introduced as emissivity of oxides [55]. If the heat energy because of Joule heating is more than heat radiated, the specimen temperature continues to rise until a quasi-state -equilibrium is reached. For a typical value of power density in stage III, 150 mWmm^{-3} , the specimen temperature was calculated to be about 1100 – 1150 °C by black body radiation. This value has been in good agreement with the pyrometric temperature measurement, as shown in Fig. 2.23.

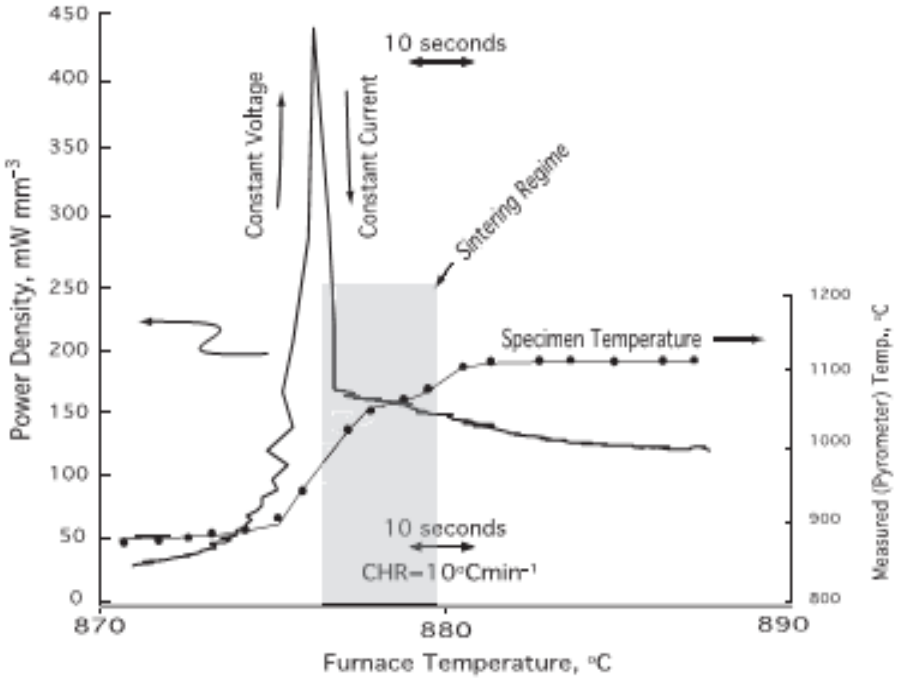

Figure 2.23: Relation between the power density and the specimen temperature. [2]

No spike was observed in the pyrometric measurement. It is reasoned that power spike should be absorbed by specimen as specific heat since it will act as adiabatic heating in such a short time interval and a calculation by Raj [2] to show that it was not enough for melting. This temperature profile obtained by pyrometer was substantiated by synchrotron data ([63] and ongoing work). An in-situ experiment was set-up to observe the change in the lattice parameter by Bragg's equation during flash sintering and the shift in the peak was used to calculate the exact temperature. This was X ray transmission experiment, Fig. 2.24 (a), where the peak shift was recorded under flash, Fig. 2.24 (b). To make sure the correctness of specimen temperature, a sliver of platinum was painted on one of the sides to acts as internal calibration. The results were in close agreement with the prior estimates calculation done with black body radiation and pyrometric measurements, as evident in Fig. 2.25. It is important to notice that usual flash sintering needs between 150 to 500 $mWmm^{-3}$ for full densification which corresponds to temperature rise by 200 to 300°C.

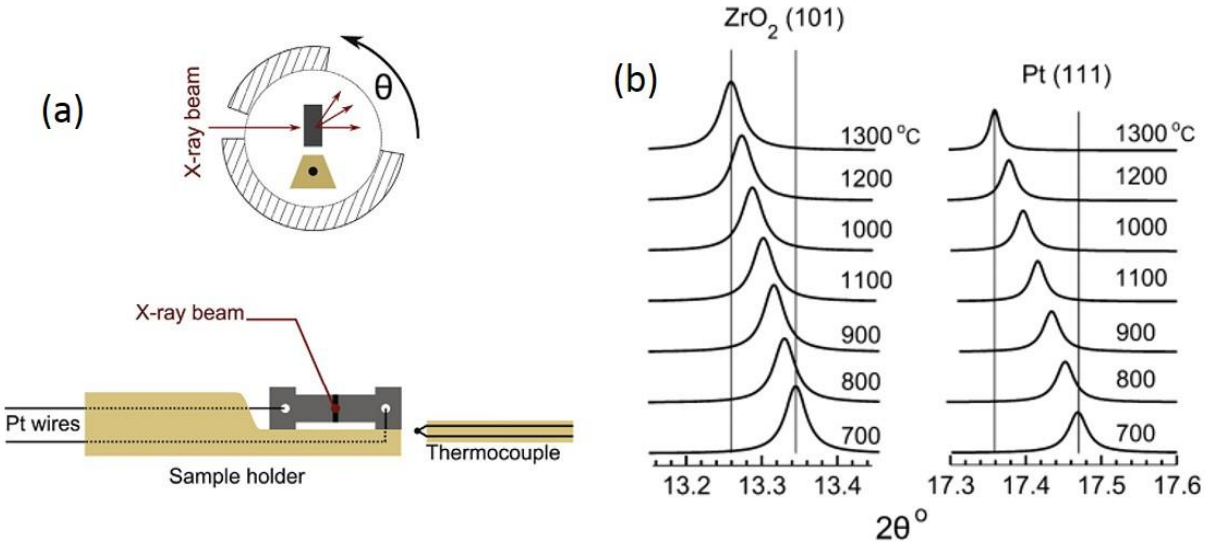

Figure 2.24: (a) shows the set up, where x-ray beam enters through the sample and diffracts. Bottom shows the connection and a black line which is sliver of Pt. paste as internal calibration. (b) Thermal expansion in 3YSZ and in Pt, calibrated againsted the furnace temperature. At higher temperature the peak shifts towards lower angle (2θ). [63]

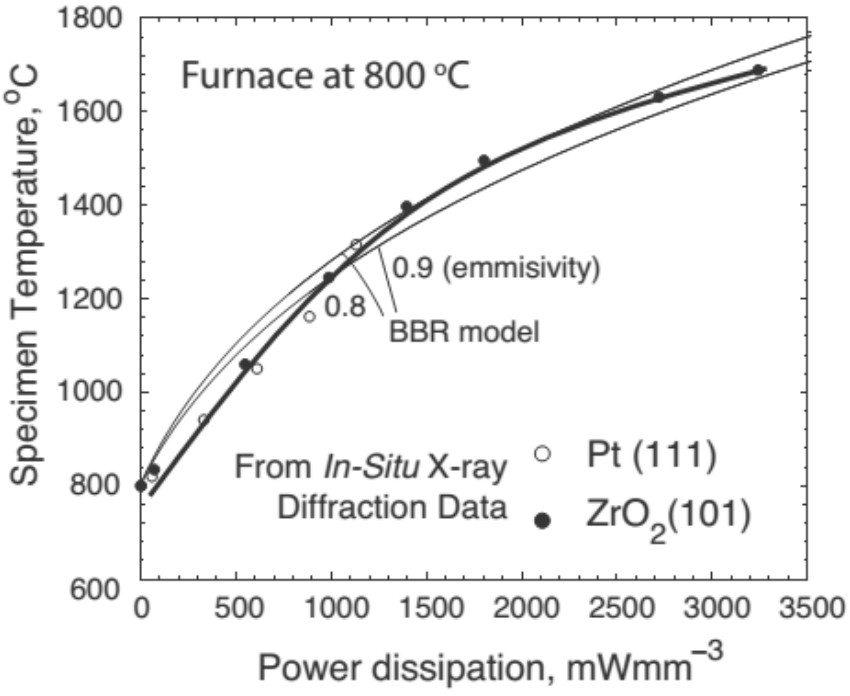

Figure 2.25: Specimen temperature plotted against power dissipation. Dots are the measured value from peak shifts and the two thin lines are the temperature estimates from black body radiation model. [63]

Baraki *et. al.* [36] also measured the volumetric strain during the On-Off flash experiment to quantify the thermal expansion with laser as a parameter to compute the specimen temperature and concluded that rise in temperature is not enough to explain the high rate of sintering.

Extrapolation from conventional sintering:

The sintering rate during flash sintering was found to be three to four orders of magnitude higher than in conventional sintering. Assuming that the acceleration in sintering occurs because of joule heating of the specimen, Raj [2] made an attempt to estimate the temperature required to attain such high rate using equation 2.5,

$$\log_{10}\frac{Rate_2}{Rate_1}=\frac{Q}{2.3R}\left(\frac{1}{T_1}-\frac{1}{T_2}\right) \qquad (2.5)$$

where the script 1 refers to conventional sintering and 2 refers to flash sintering. The graph for three values of Q, which is the activation energy for the sintering of zirconia, is shown in Fig. 2.26. To explain it further, assuming Q to be 500 $kJmol^{-1}$ [64], 3YSZ requires 1 hour to sinter at 1450°C would require 1900°C to sinter within 3.6 seconds, while the black body radiation model and synchrotron experiments estimate the specimen temperature to be ~ 1250°C for a the power density of 400$mWmm^{-3}$ at the furnace temperature of 900°C.

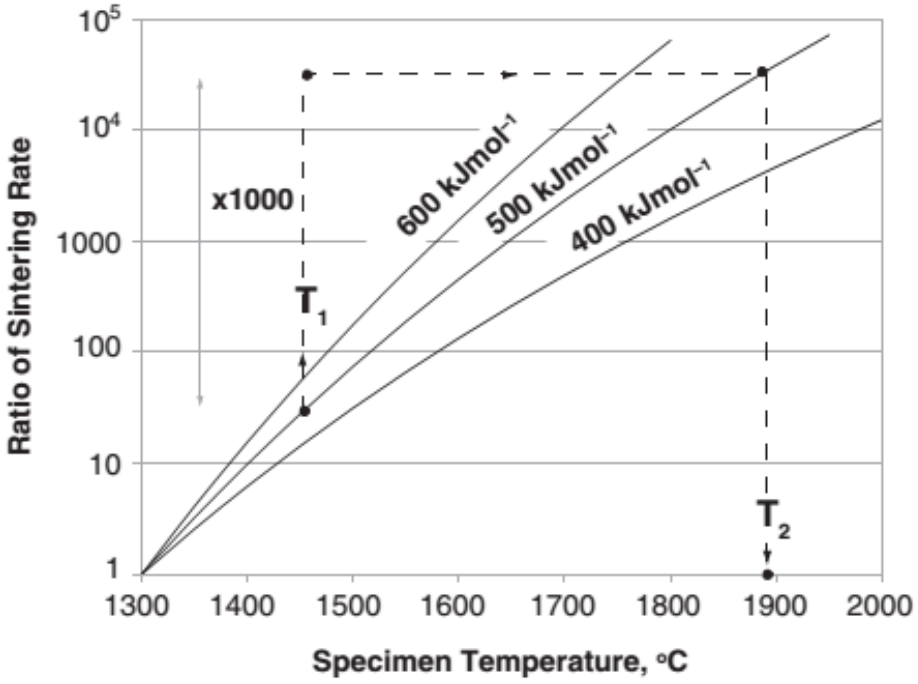

Figure 2.26: The relation between specimen temperature and sintering rate for three different activation energies to allow the diffusion. [2]

Non-linear rise in conductivity and photo-luminescence during flash:

There are two more features of the flash behavior which should be paid attention to understand it properly. First, flash occurs when the current (or conductivity, since voltage is constant) starts to rise non-linearly under the electric field. It is important to note that while conductivity depends on the fastest moving ion, sintering is controlled by slowest moving ion. But sintering and rise in conductivity coincides with each other and both of them rise by three orders of margnitude. Just joule heating cannot explain this link.

Second, flash is accompanied by optical luminescence. On a closer analysis by Terauds [63] it was found with the help of emission spectroscopy peaks of a particular wavelengths under flash which do not change with temperature unlike black body radiation, where peak shifts towards lower wavelength with higher temperature, as shown in Fig. 2.27.

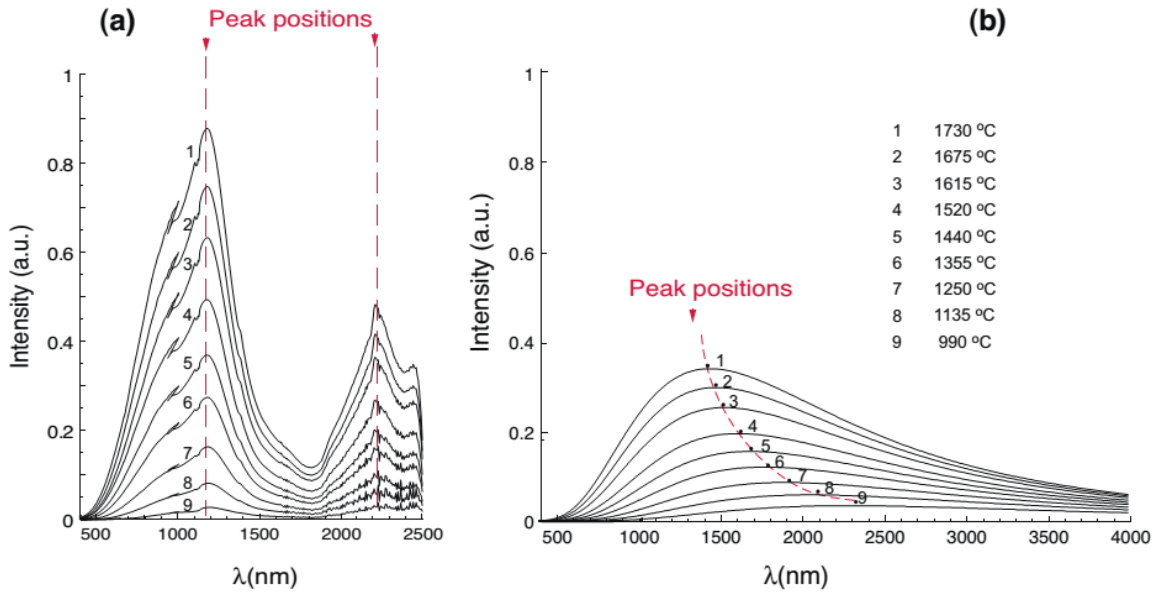

Figure 2.27: (a) Electroluminescence from specimen under flash state. The emission increases with higher current (and higher temperature) without changing the peak position (b) Black body radiation at different temperatures. [63]

In another work by Lebrun *et. al.* [65], the authors showed that the optical emission is a function of conductivity of the sample. It was also pointed out that relaxation time of optical emission is different than time taken for sample temperature to fall to furnace temperature. These two results suggest that the source of optical emission cannot be temperature.

2.5.3 Mechanism

Flash sintering has shown to densify a wide variety of ceramics within 5 seconds at much lower temperature than conventionally required. This is an extraordinary result and many authors have tried to put forth their own explanation. Measurement of temperature has been a major source of controversy. While Chen [40] claimed it is joule heating alone, Kim *et al* [66] proposed mechanism of pore migration under electric field where a bias was found at the cathode side,

suggesting that pores migrate from cathode to anode-air interface in the DC flash sintering. Narayan [60], [67] proposed that avalanche of defect generation is reason for this sintering which is possible only if liquid phase forms at the grain boundaries.

A mechanism put forth by Raj and Coworkers [2], [9], [65] has been able to explain all the observations such as high sintering rate, non-linear rise in conductivity and optical luminescence at the same time. According to this theory, under the electric field at appropriate temperature Frenkel pairs (a vacancy and a corresponding interstitial) are generated. These entities then lose their charge to form holes and electrons which migrate toward opposite electrode and result in electronic conduction. Occasionally they recombine with each other and give optical luminescence of fixed wavelengths. The two uncharged defects (interstitials and vacancies) are now free to move within the lattice. Under the effect of curvature, the vacancy then moves towards the grain boundary and interstitial migrates to the pores. On the whole it is same as movement of matter from grain boundary to pore, thus giving densification. Under the flash conditions, avalanche of these defect generation happens which cause quick sintering, since the entities of the ionic compound (Zr and O, in case of ZrO_2) no longer have to move together.

Apart from what happens during the flash sintering, there has been debate on whether the flash sintering is nucleation and growth phenomena [68] or whether it is instigated by Joule heating [69] [38], but since they are not directly related to the work presented here (they deal with initiation of flash), the detailed discussion will be avoided.

This thesis is an attempt to establish the theory of defect avalanche with new findings such as electronic conduction during flash, evolution of a texture in grain orientation, overcoming constrained sintering with electric field and improved chemical reaction kinetics.

3. Thesis objective

The prime goal of this thesis is to understand the phenomenological behavior of flash sintering and elucidate the mechanism behind the flash sintering. Material used for the experiments are titania, TiO_2 and composites of titania with alumina, TiO_2-Al_2O_3. The work has been divided in four parts, each one of which will present different findings and one theory of flash sintering, defect avalanche, has been used to explain all the results. A short abstract of them are given below:

- **Flash sintering of titania** The effect of DC electric field on sintering, and on the electrical conductivity of undoped rutile, TiO_2 (99.99%), has been investigated at fields ranging from 0V to 1000Vcm^{-1}. The sintering behavior has been divided in 2 parts, Type A (field assisted sintering) and Type B (flash sintering) Arrhenius plots of conductivity yield an activation energy of 1.6eV in Type A and 0.6eV in Type B behavior. The high rate of sintering and different activation energy of conduction during flash has been explained on the basis of defect generation.

- **Evolution of texture in titania under flash** In-situ flash experiments were performed on pure titania at the Advanced Photon Source (APS). (211) diffraction peaks was observed to gain while (110) and (111) peaks weaken in titanium oxide under the influence of the electric field. The effect is reversible, appearing and vanishing when the field is turned on and off. Furthermore the development of this texture is immediate suggesting a cooperative displacive motion of atoms in crystallites, in contrast to earlier work on 3mol% yttria stabilized zirconia [70] where the phase transformation was discovered to be diffusion controlled. Together, these results suggest that the electric field can provide a thermodynamic driving force for phase change and the induced phase is proposed to have a polar character so that it can sustain an interaction energy with the applied field.

- **Flash overcomes constrained sintering.** The phenomenon of constrained sintering, where large rigid inclusions of alumina have been shown to significantly reduce the rate of sintering of titania [71], is shown to subside nearly completely during flash sintering carried out under modest electrical fields. The result is explained by a different mechanism for volumetric and shear deformation under electric fields. It is proposed that vacancy and interstitials generated *within* the grains migrate to grain boundaries and pores to produce both volumetric and shear strain at equal rates, since, in this way, the diffusion distance for both modes of deformation becomes the same. In conventional sintering, where transport occurs from one interface to another, the diffusion distance for shear is twice as far as for densification, which retards sintering should it become controlled by shear deformation, as in constrained sintering.

- **Chemical reaction of titania-alumina under flash:** The effect of current density and hold time on chemical reaction of titania-alumina was investigated. Region of densification and phase transformation under flash have been distinguished. All the experiments are done isothermally and chemical reaction is studied under stage III of the flash where current through the specimen is stable. The electric field was found to have altered the thermodynamic transformation line of phase diagram and also enhanced the kinetics of reaction. Enhanced volumetric diffusion because of defect generation under flash has been used to explain the results.

The scope of this thesis is to cover the background and recent work done in the field of flash sintering, describe the experimental methods used and explain the results above mentioned in the frame work of defect generation.

4. Experimental Methods

4.1 Materials

4.1.1 Powders

This thesis focuses on the flash sintering behavior of Titania (TiO2) and its composite with alumina (Al_2O_3).

Nanopowder of titania (rutile) was purchased from MTI corporation. The product name was NP –TiO2-R-20 that stands for nano-powder of titania (rutile) with average particle size of 20 nm. Chemical analysis of the powder (performed by x-ray fluorescence spectroscopy) is shown in table 4.1. The purity of titania was claimed to be 99.99%. Specific surface area of the powder is > 30 m^2/g and morphology of particles are spherical. The theoretical density of rutile is 4.23 g/cm^3.

Table 4.1. Chemical analysis of titania (rutile)

Components	Ca	Hg	Mg	Nb	Pb	Si	Rutile
Contents (ppm)	75	0.01	65	119	0.2	102	Rest

Alumina (Al_2O_3): Two kinds of alumina particles were used. To analyze the constrained sintering, large rigid fully dense α-alumina particles were needed. 99 % pure alumina inclusion were obtained from Darmann Abrasive products under the product name WA600. The average particle size were 10 μm. For analyzing the effect of current density for chemical reaction between α-alumina and titania (rutile), dried powder of de-agglomerate alumina suspension from Allied High tech Products, inc., CA were used. The average particle size of the powder was 300 nm.

4.2 Sample preparation

Two kinds of sample preparation were required. Other than the synchrotron work, dog-bone shaped samples were used, as shown in figure 4.1.

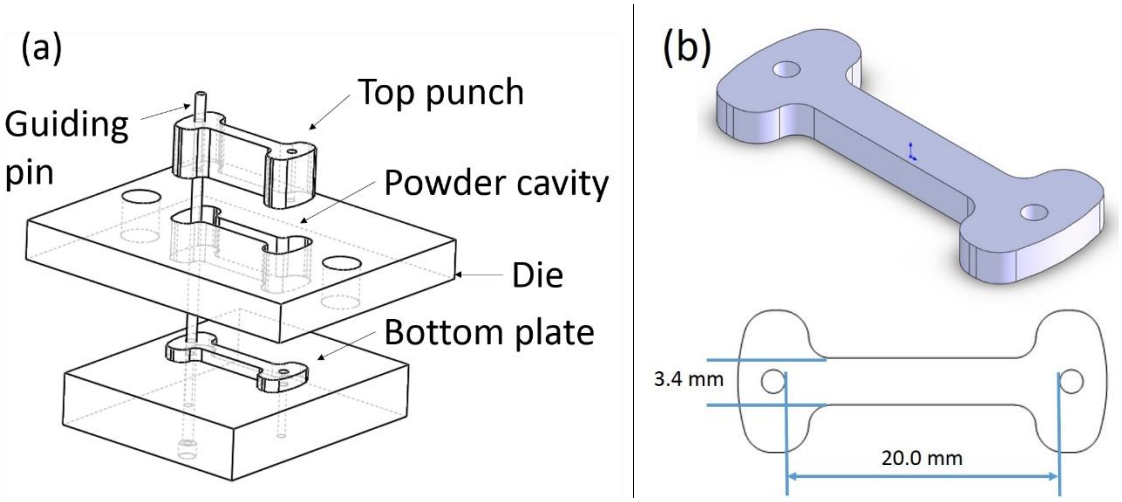

Figure 4.1 (a) Dog-bone Die design (b) dog bone sample dimensions. [72]

4.2.1 Flash sintering of titania

Nano powders of titania (particle size 20 nm) were uniaxially pressed into dog bone-shaped specimen under the load 130 MPa yielding a relative density of ~ 47%. The length and breadth of the gage-section are 20 mm and 3.4 mm respectively. The thickness of the green compact depends

on the packing powder in the cavity. On an average over total of 12 specimens, thickness was measured to be 1.5 mm.

4.2.2 Texture evolution

This work involved an X-ray in-situ flash experiment at Argonne National Laboratory, Chicago on Beamline 33BMC. Powders were pressed into rectangular bars under a pressure of 130 MPa, leading to specimens having a green density of ~ 48%. They were then conventionally sintered to 1200 °C for 3 hours which yielded dense samples with a grain size of 3-5 μm. After wrapping the platinum thin wires over the specimen for applying the electric field, the effective gage length of sintered specimens was measured to be 3.72 mm with a cross-section area of 1.33 mm x 0.55mm.

4.2.3 Constrained sintering

Rutile powders of particle size 20 nm (the matrix) were dispersed with rigid inclusions of α-Al_2O_3 of 10 μm. The procedure of mixing titania with alumina and analysis are described here. The titania powder is called A and the alumina powder is called B. The powder mixtures were prepared by mixing measured weights of TiO_2 powder, w_A, with Al_2O_3 powder, w_B. The true volume fraction of B in A, f_B, is then given by

$$f_B = \frac{w_B}{w_B + w_A \frac{\rho_B}{\rho_A}} \qquad (4.1)$$

where the densities are ρ_A = 4.23 gcm^{-3} for alumina and ρ_B = 3.95 gcm^{-3} for titania. In this way specimens containing f_B = 0%, 4.8%, 9.6% and 19% were prepared.

The method of preparation consisted of making a slurry containing 50 % by weight TiO_2 and 5% by volume of glycerol (to slow down the drying rate) in water. Al_2O_3 powder was then added to the slurry. 25mmolL^{-1} of NH_4Cl was added to compress the double layer so as to make solid loading easier. Next a few drops of HNO_3 were added to change the pH of solution in order to avoid the isoelectric point of TiO_2 which occurs at pH 5.0 [71], [73]. 5 wt% P.V.A. (polyvinyl alcohol) in water was added as binder. A magnetic stirrer was used to mix the slurry, followed by ultrasonication in Branson 5510 (ultrasonic cleaner) in order to de-agglomerate the powder. The slurry was kept in drying furnace at 80 ^oC for 1 day. The dried slurry was then crushed into fine powder using an alumina mortar and pestle and sieved through mesh size of 80 with an opening of 0.177 mm.

Powders were uniaxially pressed into dog-bone shape, Fig 4.1, [10], [30] at 105 MPa. All specimens were prepared in this way. On the average, the dog-bone specimens had gage length of 19.8 mm, and a rectangular cross section of 3.4 mm x 1.1 mm.

4.2.4 Chemical reaction

. Titania (rutile) nano-powders were mixed with 20 vol% (18 wt %) of alumina of particle size 300 nm. The method of powder preparation is same as for section 4.2.4. Two kinds of experiments were performed: in-house and at synchrotron. For in-house experiments powders were compacted in usual dog-bone shape as mentioned in previous section and for synchrotron rectangular bar specimen are pressured under 100 MPa to the size of 4.6 x 1.5 x 0.9 mm^3.

4.3 Sintering equipment and experiments

Vertical tubular furnace was used for flash sintering and conventional sintering experiments, shown in Fig. 4.2. The furnace, manufactured by Deltech Inc. (Denver, CO), has a 5 cm diameter alumina tube in the middle surrounded by six molybdenum discilicide heating elements. B-type thermocouple is used with Eurotherm 2404 PID temperature controller.

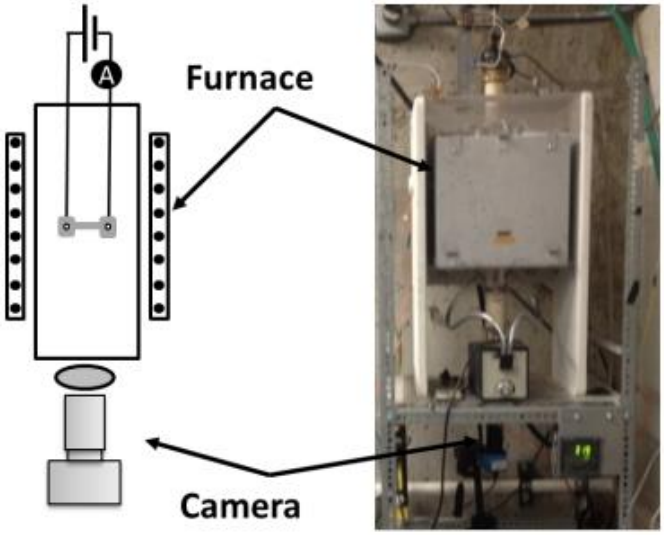

Figure 4.2 Sintering furnace with schematic diagram. [18]

The specimen was suspended into the furnace with a pair of platinum wires, which also served as the electrodes for applying the electric field across the gage section. Platinum paste was applied over to holes to provide better electric contact between platinum wires and the specimen during the flash sintering. A CCD camera (Imaging Source DMK 41-AUO2), placed underneath the furnace, records the synchronized shrinkage with the electrical parameter and temperature of furnace as the sample sinters. Two kinds of power supplies were used for flash experiments, (a) 2000 V with 1.5 A current limit - 3000 Watt power supply, manufactured by Glassman high

Voltage Inc. and (b) Sorensen 300V with 2A current limit (Ametek, San Diego CA). To accurately measure the current passing through the sample, a digital multimeter (Keithly 2000, Keithley Instruments, Cleveland, OH) is connected in series with the electric circuit. A GUI (graphical user interface), developed in-house by Francis and Lebrun [74], that runs on MATLAB program was used to acquire data form instruments at the sampling rate of 2 per second.

All the green compacts were first pre-sintered at 550°C for 1 hour to burn off the binders (5 wt. % P.V.A. in water). Two kinds of sintering experiments were done (a) constant heating rate experiment and (b) Isothermal experiments. The temperature profile for respective experiments have been shown in Fig. 4.3.

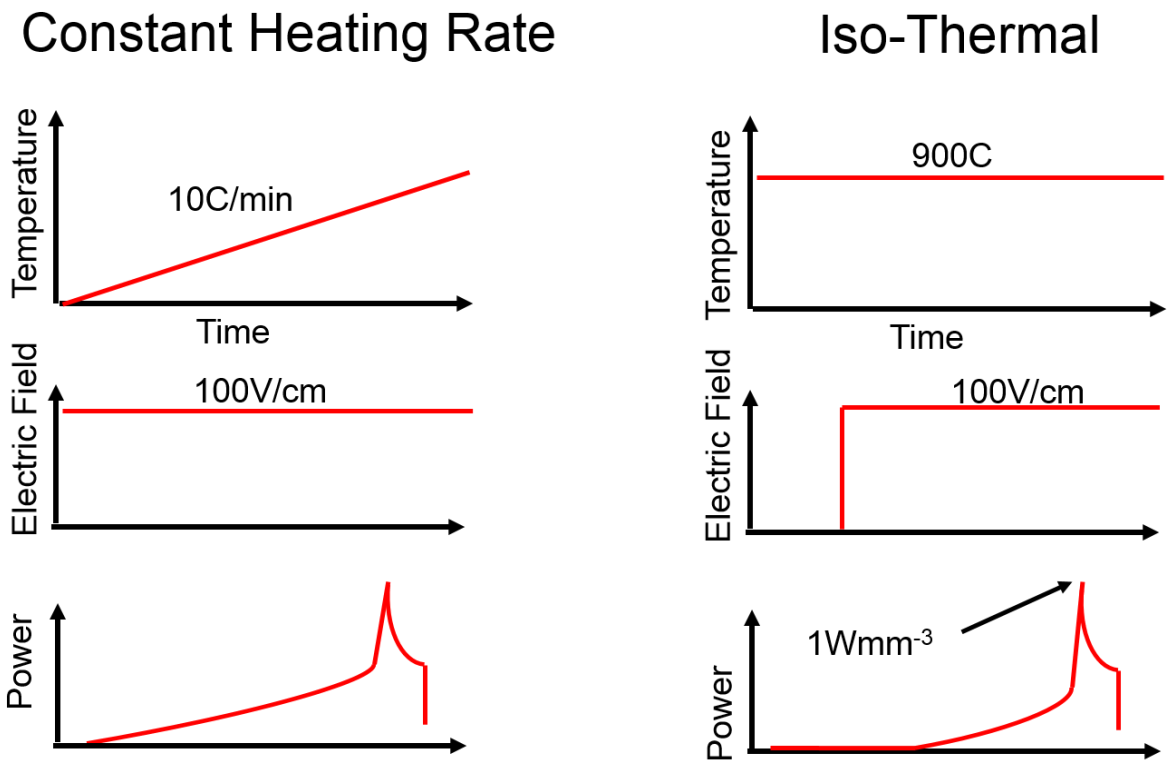

Figure 4.3 (a) Constant heating rate experiments (b) Isothermal experiments [18]

4.3.1 Flash sintering of titania

Samples were pre-sintered at 550 °C to burn off the binders for 1 hour and then heated at the rate of 10 °C/min until it sintered to full density (in case of conventional and FAST sintering) or the flash occurred. Glassman 2000V-1.5A was used as the power supply.

The phenomenon of flash sintering is characterized by a highly non-linear rise in electrical conductivity. Under voltage control, this effect produces a sudden rise in power dissipation which is limited experimentally by switching the power supply from voltage to current control. Under current control, the sample stabilizes to a steady state voltage, determined by the intrinsic conductivity of the specimen in the flash-state. The conductivity in this activated state was obtained by dividing the current density by the electric field. The baseline data for the temperature dependent conductivity of TiO_2 was obtained from the four-probe method on conventionally sintered titania. A field of 5 Vcm^{-1} was used for these measurements.

4.3.2 Texture evolution

Electric field was applied to the specimens with platinum wires that were wrapped around the ends of the specimens as shown in Fig. 4.4. As shown in the same configuration, diffraction peaks were measured with an angle to the beam transmitted through the specimen. A DC power supply (Sorensen 300-2, Sorensen San Diago, CA) was used to apply the field. The power supply was switch to current control after the onset of the flash and this switching time is specified to be 20 ms. by the manufacturer.

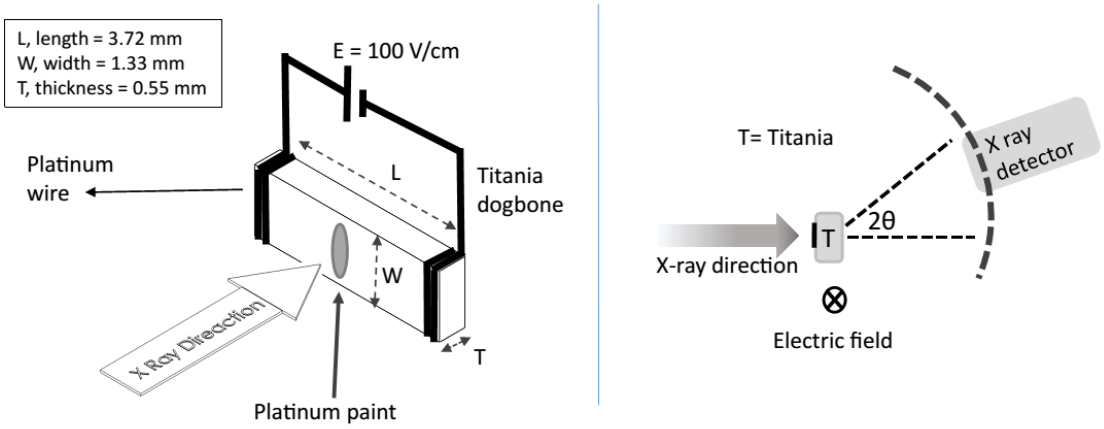

Figure 4.4. (a) Electrical connection of rutile rectangular bar under applied electric field. A thin coat of platinum paint has been placed as internal temperature reference. (b) shows configuration and X-ray beam coming in and transmitted to the other side to the X ray detector. Direction of electric field is perpendicular to the direction of X ray beam.

A quadrupole Lamp Furnace [75] was used for the *in-situ* experiments. All experiments were carried out at a constant furnace temperature of 800 ^{o}C. In all experiments, a field of 100 V cm^{-1} was applied as a step function. The current limit for the experiments was set at 25 mAmm $^{-2}$. The field was turned on and off at 100 s intervals. The experiments were carried out over several on-off cycles. The electric field, the current density, and the power density, calculated as the product of the two normalized for the specimen volume, are shown in Fig. 4.5. At this value of the applied field, the incubation time for the onset of the flash in dense sample of titania is negligible; i.e. the specimen flashes immediately upon the application of the field.

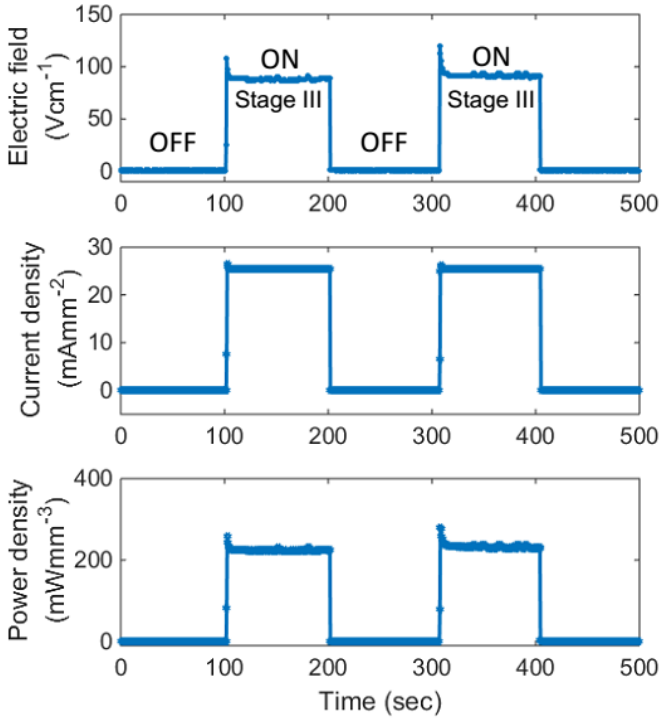

Figure 4.5. A typical ON-OFF flash experiments

4.3.3 Constrained sintering

The weight and dimensions of the specimens were measured after the binder burn off. The experiments were carried out in two ways (i) applying the field and then heating the furnace at a constant rate, or CHR (10 ^{o}Cmin^{-1}), and (ii) holding the furnace at a constant temperature, called isothermal or IST, and applying the field as a step function. All experiments were carried out at an applied field of 250 Vcm^{-1}, with the current limit set to a density of 18 mAmm^{-2} after the onset of the flash. In the isothermal flash experiments, the specimens were held at 850 ^{o}C for 100 seconds before the field was applied as a step function to allow the temperature to equilibrate. The current quickly rose and reached its preset limit within a few seconds (called incubation time). The specimen was held at constant current for 10 s and then the power was switched off.

In conventional sintering, the CHR (constant heating rate) experiments were carried out at 10 $^{o}Cmin^{-1}$, with the temperature allowed to rise up to 1150°C which is considered to be enough for full densification of titania [11]. The isothermal experiments were carried out at 850°C for 0.5 hour. The experimental parameters for the specimens are summarized in Tables 4.2 and 4.3.

Table 4.2. Details of conventional constrained sintering experiments.

Conventional Sintering (CS)			
Sample	Type of experiment	Maximum Temperature (CHR) Hold Time (IST)	Rel. Density %
CHR-CS-0	Constant heating rate at 10 ^{o}C/min (CHR)	1150^{o}C	100
CHR-CS-4.8			80
CHR-CS-9.6			75
CHR-CS-19			67
IST-CS-0	Isothermal holding at 850 ^{o}C (IST)	0.5 h	65
IST-CS-4.8			56
IST-CS-9.6			55
IST-CS-19			55

Table 4.3 Details of flash sintering experiments subjected to constrained sintering

Flash Sintering (FS)										
Sample	Type of experiment	Incubation Time, s	Flash Temp, ^{o}C	Electric Field Vcm^{-1}	Current Limit $mAmm^{-2}$	Hold Time (sec) in Stage III	Total Energy in Stage II (Jmm^{-3})	Power Density in Stage III ($mWmm^{-3}$)	Rel. Density %	Black body radiation expected temp (^{o}C)
CHR-FS-0	Constant heating rate at 10 ^{o}C/min	n/a	827	250	18	10	1.5	195	98	1095
CHR-FS-4.8			835	250	18	10	1.7	230	99	1125
CHR-FS-9.6			842	250	18	10	2.56	275	96	1165
CHR-FS-19			850	250	18	10	3.16	280	88	1170
IST-FS-0	Isothermal holding at 850 ^{o}C	6	n/a	250	18	10	0.88	175	96	1075
IST-FS-4.8		10		250	18	10	0.97	175	97	1075
IST-FS-9.6		15		250	18	10	2.19	225	92	1122
IST-FS-19		19		250	18	10	2.36	250	90	1144

4.3.4 Chemical reaction

In-house experiments used 3000 W DC power supply and a multimeter in series with the connection to measure the current passing through the sample. Samples were pre-heated at 550°C for 1 hour to burn off the binders and then taken to 830°C at 10°C/min and held isothermally for 100 seconds, before an electric field of 500 Vcm^{-1} as a step function was applied. Electric field was kept constant through all the experiments while current densities and hold times were altered. The experimental map of variables has been shown in Fig 4.6.

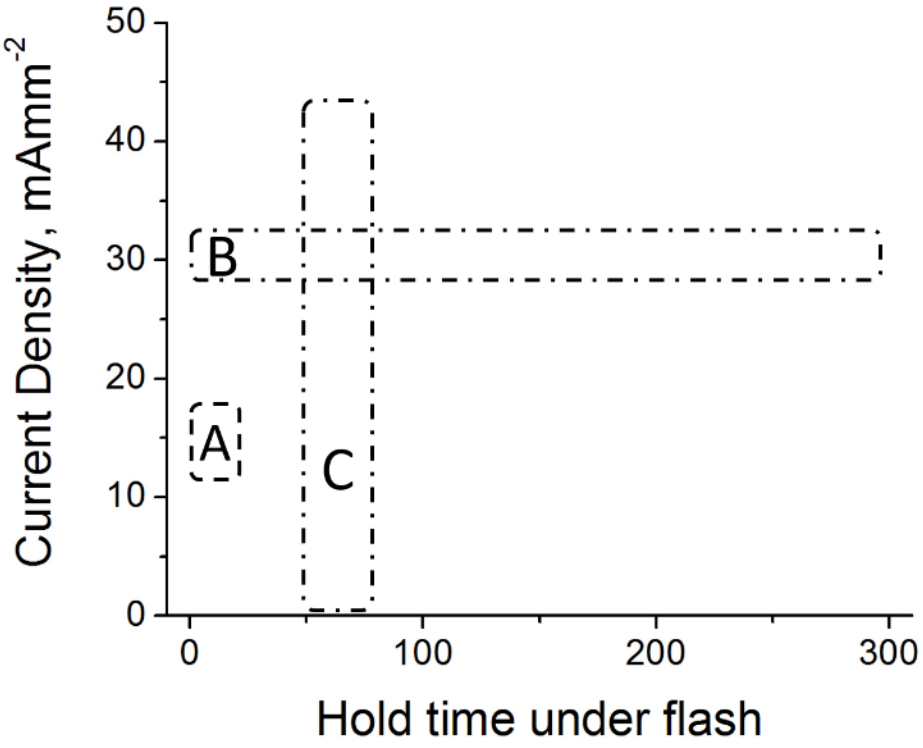

Figure 4.6 Schematic representation of the area of investigation of the current density v/s hold time experiments.

In-situ flash experiments were conducted at Argonne National Laboratory to establish the temperature of flash and observe the evolution of third peak with time and current density. The

X-Ray Beamline used for the purpose was 33 BMC with the radiation wavelength of 0.59 °A. The details of the apparatus setting has been detailed in section 4.3.2. Samples were brought up to the temperature of 900°C before applying the field of 500Vcm^{-1}. Diffraction data were obtained in local scan mode, where 2θ (bragg angle for diffraction) range was fixed from 12.2 to 16.4. The acquisition time for each scan was 1 sec.

4.4. Characterization: X ray diffraction

X ray diffraction has been used for different purposes in three different chapters. In sixth chapter, we study the effect of electric field on titania in terms of evolution of texture in grain orientation. XRD spectra was used to quantify how one peak intensity changes with respect to others. Chapter seven usages X ray diffraction pattern to identify the phases present while chapter eight usages X-Ray diffraction extensively to quantify the depletion of one phase which is a parameter of measuring chemical reaction.

4.4.1 Texture evolution

The *in-situ* experiments were carried out at the APS at the Argonne National Laboratory on beamline 33BMC. The X-ray beam used had wavelength of 0.59 Å. The diffraction spectra were measured with a Pilatus 100K 2D image plate detector (DECTRIS Ltd, Villigen, Switzerland). Diffraction data were obtained by two methods: in the full scan mode, and the local scan mode. In the full scan mode the detector moved from 2θ = 7° to 22° in 75 steps with an exposure time of 1 sec at every step; thus the full scan took 1:15 min. For the local scan mode experiments the detector remained stationary covering the range 2θ from 17° to 30°, within which the (211) peak from rutile resides. These XRD data sets were acquired once every of 0.5 s, that is at the rate of 2 Hz.

4.4.2 Constrained sintering

X ray diffraction of the samples containing 19 vol % alumina were compared for flash sintered and conventionally sintered. CuKα radiation (λ = 1.5406 A^o) was employed in Phillips X'pert MPD operated at 45kV and 40 mA, in the range of 2θ=20-40^o. For reference, XRD scans of pure titania and alumina were also done.

4.4.3 Chemical reaction

To quantify the extent of reaction between alumina and titania to form Aluminum titanate, ($TiAl_2O_5$), the X ray diffraction (XRD) relative intensity ratio (RIR) technique was employed [76]. As an internal reference, silicon powder of equal weight was mixed in with powder of specimen and ground together. The reason for choosing silicon is that its prime peak, (111), does not overlap with titania, alumina, aluminum titanate or any of the other secondary phases of the two. CuK_α radiation (λ = 1.5406 A°) was used on D2 PHASER 2nd GEN (Bruker AXS GmbH, Karlsruhe, Germany) for this purpose. The scan was done in 2θ range of 20° - 50° with a step size of 0.01° and integration time of 1 s per step. Bruker Diffract Suite Eva software was used to fit a Gaussian curve to the XRD spectra and to remove the background noise before comparing the peaks. The intensity of silicon (111) peak was compared with that of alumina (104).

For calibrating the alumina content in the composite with RIR method [76], Silicon peak (2θ = 28.5°) was calibrated with respect to alumina (2θ = 24.65°), for λ = 1.54 °A (Cu Kα), as shown in Fig. 4.7. Alumina in different fractions, from 5% to 20% by weight, were added to silicon and ground together. The intensity of X-ray-diffraction peak was measured and a linear relation between weight fraction of alumina and intensity ratio was derived as Eq. (4.2). The precision of the measurement depends on the peak ratio of alumina and silicon. When alumina content

decreases the peak ratio is also becomes very small, which account for lower errors in measurement. To estimate the error in measurement, two lines, each one touching upper limits and lower limits are drawn and the difference between these two sets of line is considered as the range of probable error in measurement. This error range is given by Eq. (4.3). Although peak of $TiAl_2O_5$ appears in the XRD spectrum with the advent of reaction, it is not used as parameter of chemical reaction since unlike alumina, no standard was available to evaluate its relative intensity ratio (I/Ic) of titanate.

$$Y = 19.7*X - 24.9 \qquad (4.2)$$

$$\Delta Y = 4.8*X - 5.21 \qquad (4.2)$$

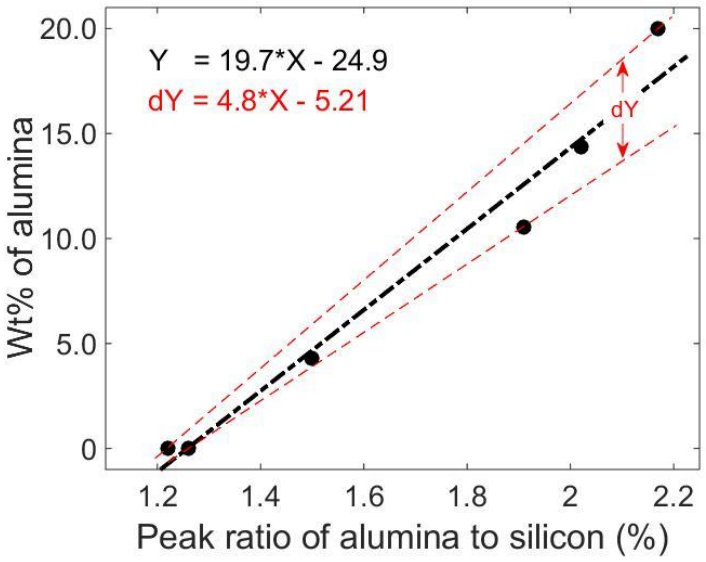

Figure 4.7. Linear relation of content of alumina with peak intensity ratio of alumina to silicon in %.

4.5 Data analysis

4. 5.1 Flash sintering of titania

During sintering, specimen shrinks. This true linear shrinkage strain is given by equation 4.3,

$$e = \ln(l / l_o) \qquad (4.3)$$

where l_o is the initial gage length and l is instantaneous gage-length. Final density, ρ, can be calculated from the linear shrinkage using the following equation,

$$r = r_g e^{3e} \qquad (4.4)$$

where r_g is the normalized green density. Note that since $l < l_o$, the strain, e, has a negative value. Therefore, in Eq. (4.4), $r > r_g$. The green density values were obtained after pre-sintering the samples (varying from 0.468 to 0.476) and were assumed to be 0.472 for all the experiments. This equation is based on the assumption of isotropic shrinkage in all the directions of specimen, which was confirmed from geometric calculation of density of rectangular section of sintered sample and Archimedes method [77]. All three methods of density measurements were in close agreement with each other.

4.5.2. Texture evolution

Since we did the flash experiment on dense sample, there was no densification during the flash experiments. The extent of grain orientation (development of texture) in the specimen was quantified in the terms on texture coefficient, TC, as described in Barrent and Massalski [78] ,

where the strength of individual peak is measured relative to the average number of specific peaks according to

$$TC = \left(\frac{I(hkl)}{\Sigma_0^n I(hkl)} \right) \Big/ \left(\frac{I_o(hkl)}{\Sigma_0^n I_o(hkl)} \right) \qquad (4.5)$$

here $I(hkl)$ and $I_o(hkl)$ are the intensities of the peak corresponding to the (hkl) plane. I_o are the intensities measured without the electrical field.

4.5.3. Constrained sintering

The shrinkage in length during sintering experiments was converted to true linear shrinkage strain from Eq. 4.3 and the volumetric shrinkage is the then given by Eq. 4.4.

We are, however, interested in calculating the sintering rate of the titania matrix alone in the composite. The following analysis was used for this purpose. The specimen density, ρ_S is given by

$$\rho_s = \frac{v_A^o + v_B^o}{v_A^o + v_{pores} + v_B^o} \qquad (4.6)$$

where v_A^o and v_B^o represent the true volume of dense A and dense B, and v_{pore} is the volume of the pores in the specimen. The density of the titania matrix is given by

$$\rho_A = \frac{v_A^o}{v_A^o + v_{pores}} \qquad (4.7)$$

Combining (4.6) and (4.7) we obtain

$$\rho_A = \frac{\rho_S}{1+\alpha\left(1-\rho_S\right)} \qquad (4.8)$$

where

$$\alpha = \frac{v_B^o}{v_A^o} \qquad (4.9)$$

It now remains to relate α to f_B, the volume fraction of alumina in the specimen, which is as follows

$$\alpha = \frac{f_B}{1-f_B} \qquad (4.10)$$

In summary, the experimental measurements of ρ_S are converted to the densification in the titania matrix, ρ_A from Eq. (4.7), where α is related to the volume fraction of alumina, f_B calculated from the weight fractions of the powders as given by Eq. (4.1), and inserting that into Eq. (4.10).

It remains to calculate the green density of specimen, ρ_s^g, from the measurements of the weight and the volume of the sample. If the volume of the sample (that is the gage section of the dog-bone samples) is V_S, then

$$\rho_S^g = \frac{v_A^o + v_B^o}{V_S} \qquad (4.11)$$

The measured weight of specimen is given by,

$$W_S = v_A^o \rho_A + v_B^o \rho_B \qquad (4.12)$$

It is easily shown that

$$\left.\begin{aligned} v_A^o &= \frac{W_S}{\rho_A + \alpha\rho_B} \\ v_B^o &= \frac{\alpha.W_S}{\rho_A + \alpha\rho_B} \end{aligned}\right\} \qquad (4.13)$$

Combining Eqs (4.12) and (4.13) and substituting into (4.9) gives the experimental value for the green density of the samples, which are reported in Table 4.4.

Table 4.4 : Green density of specimens in constrained sintering experiments

Relative density after compaction				
	Volume % of alumina	$\alpha = \frac{v_B^o}{v_A^o}$	Composite relative green density	Titania relative green density in composite
CHR-CS	0	0	0.46	0.46
	4.8	5.0	0.49	0.48
	9.6	10.6	0.51	0.49
	19	23.4	0.54	0.48
CHR-FS	0	0	0.45	0.45
	4.8	5.0	0.48	0.47
	9.6	10.6	0.51	0.49
	19	23.4	0.53	0.48
IST-CS	0	0	0.47	0.47
	4.8	5.0	0.49	0.47
	9.6	10.6	0.49	0.47
	19	23.4	0.53	0.48
IST-FS	0	0	0.46	0.46
	4.8	5.0	0.49	0.48
	9.6	10.6	0.50	0.48
	19	23.4	0.56	0.50

4.6 Measurement of specimen temperature

4.6.1 Flash sintering of titania

The nature of field assisted sintering falls into two regimes:

(i) The low field regime where the conductivity of the specimen continues to follow the nominal Arrhenius behavior determined by ionic diffusion. In this regime sintering is somewhat enhanced but the effect is minor and does not change in mechanism of conductivity. At the same time, heating of the specimen is insignificant [79]. We call this Type A behavior.

(ii) In the high field regime where "flash sintering" is accompanied by a highly non-linear increase in the conductivity of the specimen. We call this Type B behavior. The non-linear rise is conductivity is limited experimentally by switching the power supply from voltage to current control. Under current control the specimen settles to a steady state power input into the specimen. In this state, the temperature of the specimen is measured directly with a pyrometer. The specimen temperature is also estimated from a black body radiation model [1], [2], [28] where the power dissipation is equated to increased radiation (which scales as the fourth power of the temperature) to determine the steady state temperature. Since other losses such as convection and conduction are neglected the model gives an upper bound for the temperature. According to this model the specimen temperature, T^*, is related to the furnace temperature, T_o, by the following equation [28]:

$$\frac{T}{T_o} = \left[1 + \frac{1000.W_v}{e_m \sigma T_o^4}\left(\frac{V}{A}\right)\right]^{\frac{1}{4}} \qquad (4.14)$$

where the temperatures are expressed in K. The power dissipation per unit volume of the specimen is given by W_V, in units of mWmm^{-3}. The volume to surface area of the specimen is (V/A) written in units of mm (for our samples it value is equal to 0.5mm). σ is black body radiation constant, being equal to 5.67 × 10^{-8} Wm^{-2}K^{-4}. The equation assumes the emissivity, e_m, to be ~ 0.9 for oxides. The validity of Eq. (4.14) had been established against experimental data where the temperature of specimens in the flash-state was measured exactly through thermal expansion for various levels of power dissipation [36]. Further discussion of Joule heating of the specimen is given in Appendix A.

4.6.2 Texture evolution

On top of black body radiation estimate, the specimen temperature was also measured with a platinum standard, as has been done on 3YSZ as well by Terauds [63]. A thin layer of platinum paste was applied to the surface of the specimen as shown in Fig. 4.4(a). The shift in the (111) peak of platinum was used to estimate the specimen temperature. Standard handbook value for the thermal expansion of Pt. [80] was used for this purpose. The calibration curve for the peak shifts is given in Fig. 4.8. Under the conditions of Stage III flash, described in Fig. 4.5, the specimen temperature is measured to be 925 °C, at 2θ = 14.775° for the Pt. peak. The application of the black body radiation model [2],[55] to the conditions of power dissipation and specimen surface-to-volume ration, and assuming the emissivity to be equal to 0.9, yields the estimate of the specimen temperature to be 920 °C ± 20°C, in good agreement with the measurement using the platinum standard.

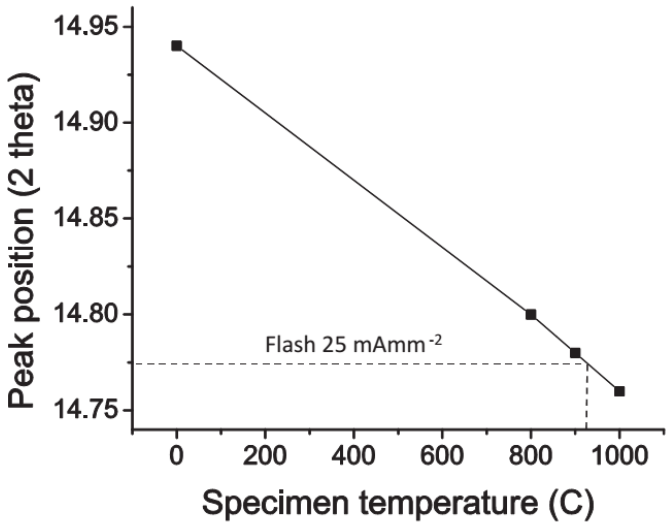

Figure 4.8 Calibration of platinum peak (110) used as internal temperature reference to determine the specimen temperature under flash.

4.6.3 Constrained sintering

Black body radiation model alone was used to estimate the specimen temperature, which is detailed in previous section 4.6.1.

4.6.4 Chemical reaction

Both black body radiation model and shift in pt. peak at synchrotron was used to determine the specimen temperature during flash. For synchrotron experiments, a sliver of platinum was applied on one of the surface of the specimen and the temperature was estimated from the shift of the (111) peak of Pt, that can be predicted from tabulated values of thermal expansion (Fig. 4.9). This calibration curve was obtained by conventionally heating a specimen with Pt. paste on it at regular interval of temperature. Point A and B on the curve shows the shift in peak position of

platinum at room temperature and 900°C respectively. The temperature estimated from black body radiation is also compared. It is important to keep in mind that the dimension of the specimens used at the synchrotron was 4.6 x 1.5 x 0.9 mm^3 with a volume to surface area ratio of 0.25, significantly smaller than that of regular dog-bone specimen (0.45). The temperature estimate with different methods for different experiment has given in table 4.5.

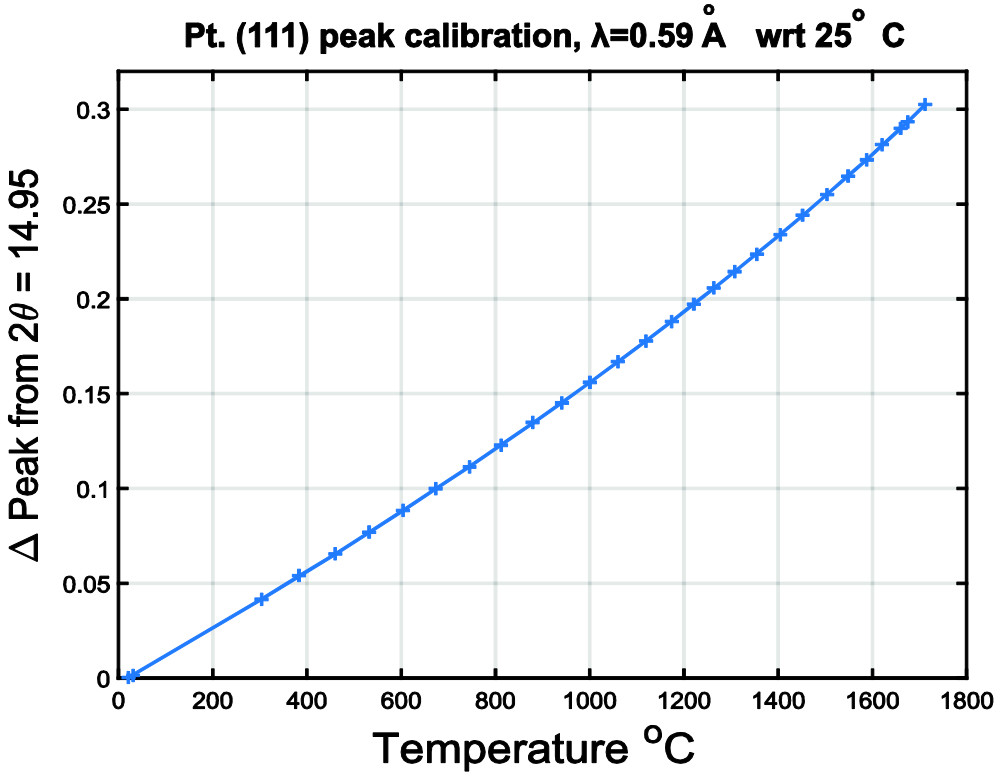

Figure 4.9: Calibration curve for temperature of platinum paint with shift in (111) peak.

Table 4.5 Temperature estimates by peak shift and black body radiation in chemical reaction work.

	Flash parameters		Furnace temp. (°C)	Estimated specimen temperature	
	Electric field	Current density		BBR (°C)	In situ (°C)
In house	500 V/cm	20 $mAmm^{-2}$	830 °C	1110 ± 20	----
	500 V/cm	30 $mAmm^{-2}$	830 °C	1250 ± 25	
	500 V/cm	40 $mAmm^{-2}$	830 °C	1275 ± 30	
Synchrotron	500 V/cm	20 $mAmm^{-2}$	900 °C	1150 ± 10	1180 ± 30
	500 V/cm	25 $mAmm^{-2}$	900 °C	1310 ± 15	1340 ± 30

4.7 Microstructural analysis

To look at the microstructure, for grain size analysis (chapter 5) or to see the distribution of different phases (chapter 7), samples are need to be polished and etched properly, which is called sample preparation.

4.7.1 Sample preparation

Dog-bone samples were first potted in epoxy resin, sectioned using sectioning saw and then ground up to 600 grit of silicon carbide papers. They were further polished with diamond

slurries down to 1 μm finish. Polished samples were then removed from the mount and then thermally etched at 900°C for 1 hour (for titania and composite of titania). All the specimen were plated to 3 nm layer of gold-palladium to avoid charging of ceramic surface during SEM (scanning electron Microscope) observations. JOEL (JSM-7401F JOEL, Tokyo, Japan) field emission scanning microscope was used for taking the micrographs.

4.7.2 Microstructural Image processing

The average grain size in a microstructure is measured by the linear intercept method and then multiplied by 1.56 to obtain 3-dimentional size, based on the model suggested by Mendelson[81]. Another GUI (graphical user interface) was developed on MATLAB ® , by Francis [18] to analyze the microstructural-images. The software draws randomly oriented lines across the micrograph and counted the grain-boundaries it intersected and then averages it out. It also provides the grain size distribution. An example of it has been shown in Fig. 4.10, where (a) shows a micrograph of flash sintered titania under 150 Vcm^{-1} and its grain-size distribution.

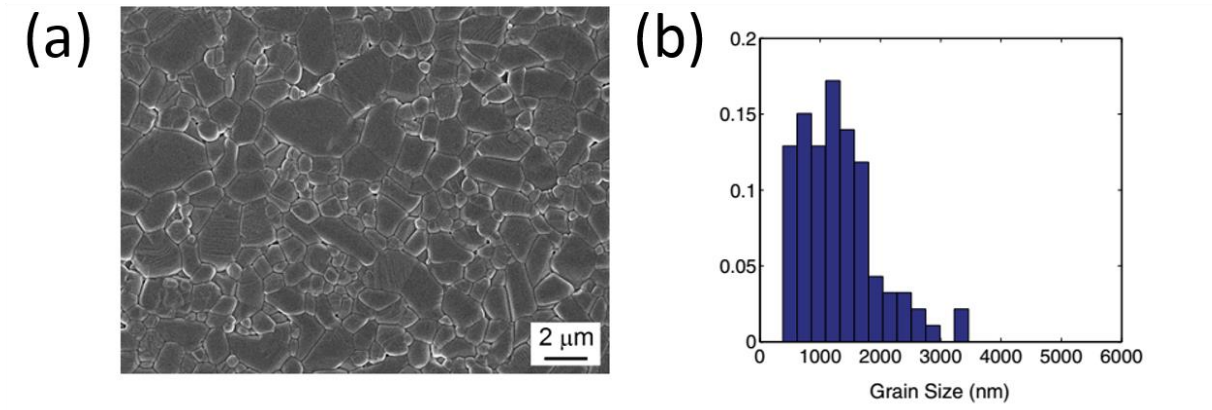

Figure 4.10 (a) SEM micrograph for flash sintered pure titania under 150 Vcm^{-1} and (b) shows the grain-size distribution. .

5. Flash sintering of titania

5.1 Disclaimer

This work has been published in Journal of American Ceramic society [11]. The research was supported by the Basic Science Division of the Department of Energy under Grant No: DE-FG02-07ER46403.

5.2 Introduction

TiO2, in its two commonly known forms, anatase and rutile, have shown promise for applications such as dye sensitized solar cells [82], [83], sensors [84], and capacitors [85], [86]. In other work, the effect of rapid cooling and annealing temperature on the transition from ionic to electronic conductivity in undoped TiO2 has been reported[87]. Quenching TiO_2 sample from a gradually increasing dwell temperature changes the nature of conductivity from insulator to semiconductor, which has been attributed to freezing of oxygen vacancies in the structure. The effect of atmosphere (with different partial pressure of oxygen) on the conductivity of sample at room temperature has also been evaluated[87]. Doping with pentavalent oxides, such as V_2O_5,

Nb_2O_5 which act as donors, raises the dielectric constant, the breakdown strength and the exponent of nonlinearity for the I-V plot in varistor applications [88].

The above properties depend on the sintering treatment, which determines the grain size and the defect concentration. While large grained TiO_2 shows higher electrical conductivity, homogeneously distributed finer grain structures have been reported to have the highest breakdown strength. Getting a finer grain size is not an easy task because grain size increases rapidly above ~1000 ^oC [85]. Thus, long hours of sintering at 800 ^oC are needed to avoid grain growth, and still full densification may not be realized. Pure titania has been reported to sinter to full density at 1000 ^oC for 20 hours [89]**.** Two step sintering methods [8], [90] have achieved fine grain sizes with little grain growth but at the expense of very long hold time. A ramp up experiment at 10 $^oC\ min^{-1}$ reduces the time required for sintering but the temperature needs to go up to 1150 ^oC to achieve full densification along with some grain-growth. Doping with aliovalent oxides have shown to enhance sintering but they promote grain growth as well [88].

Recently, field assisted sintering methods, where the electric field is applied directly to the specimen with a pair of electrodes, have been reported to have advantages over conventional and spark-plasma sintering. In the earliest work on flash sintering, the sintering temperature for 3YSZ [1] was reduced from 1400 ^oC to 850 ^oC in constant heating rate experiments with a mere field of 120 Vcm^{-1}. In these experiments sintering was accompanied by an abrupt increase in the conductivity of the specimen. Sintering occurred in a few seconds, as if in a flash, which led to it being called flash sintering. Initially this phenomenon was ascribed to Joule heating [1], but in a later Raj et. al [9] have considered defect avalanche as another possible explanation for this unusual behavior. Baraki et. al. [36] have reported careful measurements of the specimen temperature in the flash-state (by the measurement of thermal expansion), which suggest that Joule heating is not

high enough to yield temperatures that can produce sintering in a few seconds [Appendix A]. They have also proposed the effect of flash on grain growth [36].

Flash sintering as a technique has found applications in different fields such as SOFC [41], [91],[92] and tape casting [92]. Application of AC instead of DC fields on field assisted sintering behavior remains an open question[93]. In the experiments with yttria doped zirconia Muccillo et al. [45],[94] and M'Peko [79] have reported an increase in the grain boundary conductivity under the effect of flash.

With this background, we attempt to understand the effect of the electric field on the sintering behavior and the electrical conductivity of TiO_2. The influence of the sintering protocol on grain size is studied.

5.3. Experimental Methods

The experimental section has been described in great details in chapter 4. Here is a very short recap of the steps involved. Rutile nanopowders were uniaxially pressed into dog bone-shaped specimen under the load 130 MPa. All the samples were heated at the rate of 10 $^{o}Cmin^{-1}$ up to 1150 ^{o}C or less depending on the temperature needed for flash to occur.

Linear shrinkage during the sintering process were used as a parameter to calculate the densification using eqn. 5.1 and 5.2

$$e = \ln(l / l_o) \qquad (5.1)$$

$$r = r_g e^{-3e} \qquad (5.2)$$

where l_o is the initial gage length and l is instantaneous gage-length. Final density, ρ, is calculated from the linear shrinkage equation 5.1 and green density ρ_g [95]. Since the specimen shrinks (negative θ) the final density ρ is higher than green density. Final density was also verified by geometrical calculations and Archimedes method.

Once sintered, samples were polished and thermally etched and analyzed under FESEM (Field Emission Scanning Electron Microscope). The average grain size and grain-size distribution was measured using linear intercept method with an in-house-developed program by Francis [18].

To realize the effect of flash on the conductivity of TiO_2, the baseline data for temperature dependent conductivity was obtained from four-probe method on a conventionally sintered sample (with grain size ~ 1.7 μm) under 5 Vcm^{-1}

The specimen temperature during flash sintering was estimated using black body radiation equation, as detailed in section section 4.6.1.

5.4 Results

5.4.1 Sintering Behavior at low and high fields

The linear shrinkage strain plots with applied field ranging from 0 Vcm^{-1} to 1000 Vcm^{-1} are shown in Fig. 5.1. For fields of less than 50 Vcm^{-1} the shrinkage coincides with conventional sintering data (0V). At fields of up to 150Vcm^{-1} sintering rate is enhanced but the character of the sintering curves continues to behave as in conventional sintering, that is, sintering occurs gradually with time. At higher fields sintering occurs abruptly, in mere seconds, which we have called flash sintering. The behavior at low fields is classified at Type A behavior, while flash sintering at the

higher fields is being called Type B behavior. The transition from the Type A to Type B behavior is gradual. For example at 150 Vcm^{-1} sintering appears to be a combination of A and B, with the abrupt increase in sintering taking place after a shrinkage of about 0.12. In the next section we describe a formal procedure for separating the sintering strain into Type A and Type B.

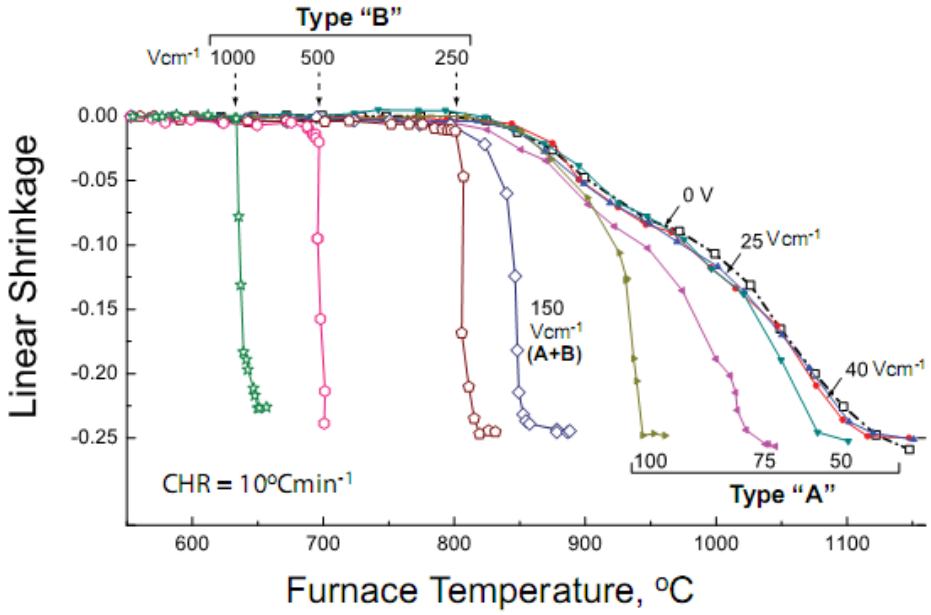

Figure 5.1 Sintering curves for the linear shrinkage measured at different applied DC fields in experiments carried out at constant heating rate.

The procedure recognizes that the TiO_2 specimens exhibit a non-linear rise in electrical conductivity at a threshold temperature in a constant heating rate experiment. This phenomenon is shown by the results in Fig.5.2, where a non-linear increase in power density is seen at fields of 50 Vcm^{-1} or greater. These data show two important features of the experiments: (i) the rise in power dissipation is limited by switching the power supply from voltage to current control, which leads to a decline in power dissipation towards a steady state, and (ii) the non-linear increase is conductivity is not necessarily coupled to sintering: in Type A behavior sintering occurs before

the onset of the non-linearity while in Type B behavior the non-linearity and sintering occur together in what has been called flash sintering.

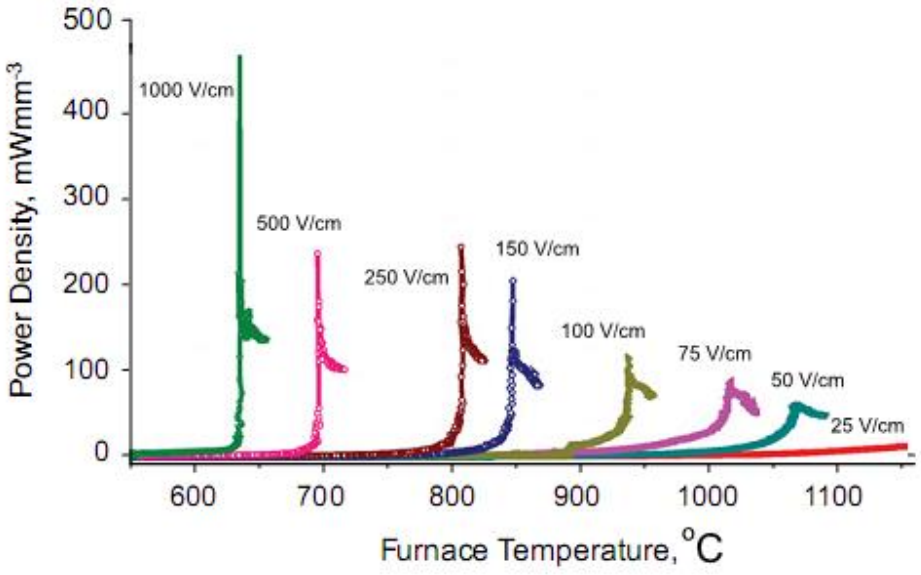

Figure 5.2 Power dissipation plots near the "flash" temperature for various DC fields.

Point (ii) above is explained by the data in Fig.5.3 where the shrinkage data and the electrical behavior are plotted synchronously. Two situations, one at an applied field of 100 Vcm^{-1}, and the other at 500 Vcm^{-1} are shown. The electrical non-linearity occurs at ~935°C at the low field and at ~700°C at the higher field. The shrinkage strain is given by the y-axis on the left: at high field all the shrinkage strain occurs in the flash-state, but at the lower field one half of the densification strain has occurred before the onset of the flash. This procedure was repeated at different fields to separate the densification into Type A (before flash) and Type B (after flash) regimes. The results of this exercise are given in Fig.5.4, which shows that the mechanism of field assisted sintering changes from one to the other as the field is increased.

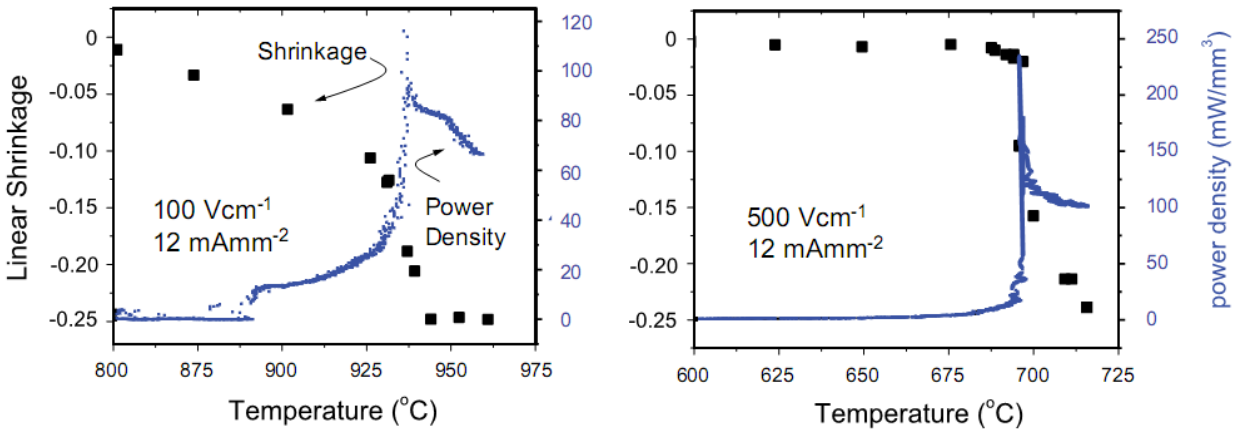

Figure 5.3. The synchronization between sintering and the nonlinear increase in conductivity (the flash event) at two different applied fields.

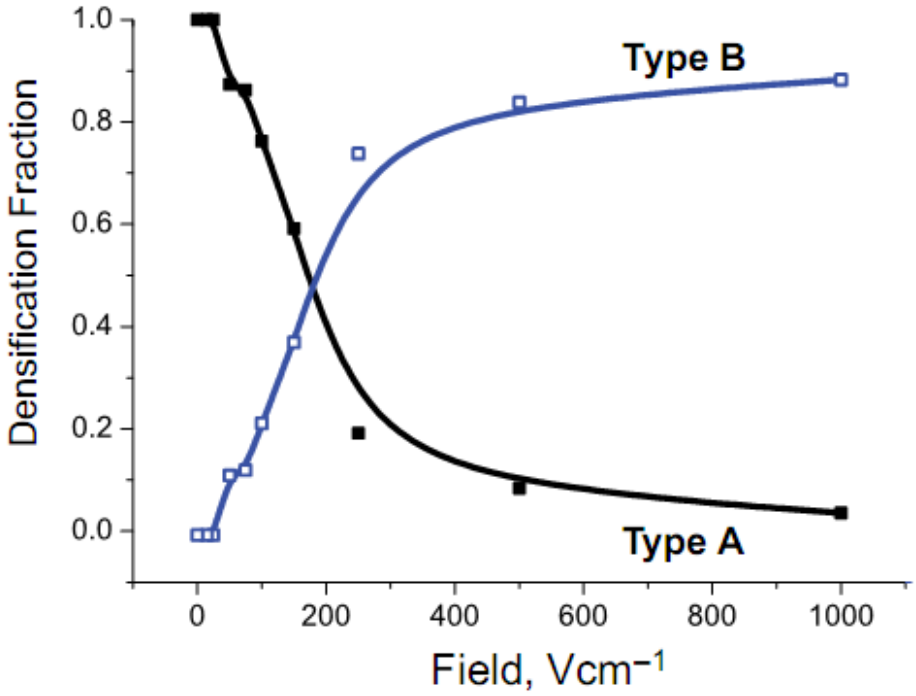

Figure 5.4. Partitioning of densification strain attributed to Type A and Type B behaviors.

5.4.2 Density as a function of the electric field

The final density of the specimens, estimated by the three methods (linear strain, Archimedes and physical), are given in Fig.5.5. The density calculated from the shrinkage is consistently somewhat higher than from the other two methods. Most likely this can be attributed to slight differences in the shrinkage in the thickness and width directions than in the longitudinal direction because of anisotropic packing of particles as the green samples were prepared by uniaxial pressing.

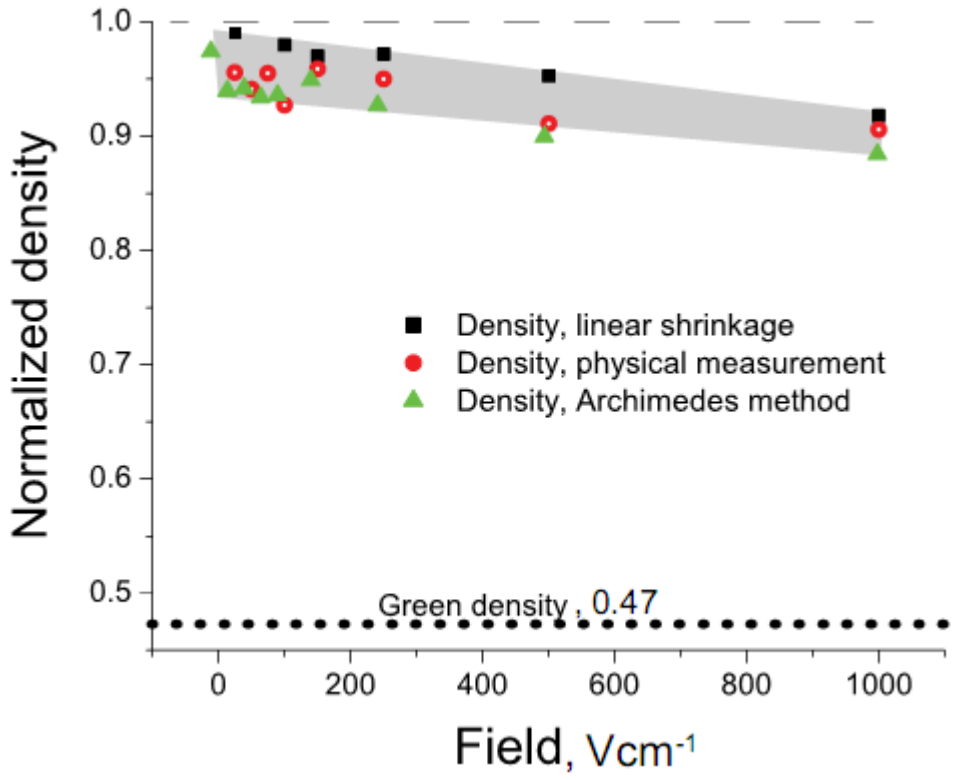

Figure 5.5. The density of the sintered specimens as a function of the applied field under which they were sintered.

5.4.3 Electrical conductivity

The baseline values for the electrical conductivity of dense TiO_2 made by conventional sintering was measured by the four probe technique under a field of 5 Vcm^{-1} at temperatures up to

1200ºC. The results are shown by the solid black line in Fig.5.6. As was expected the behavior is Arrhenius with an activation energy of 1.6 eV, which is in good agreement with literature values[96].

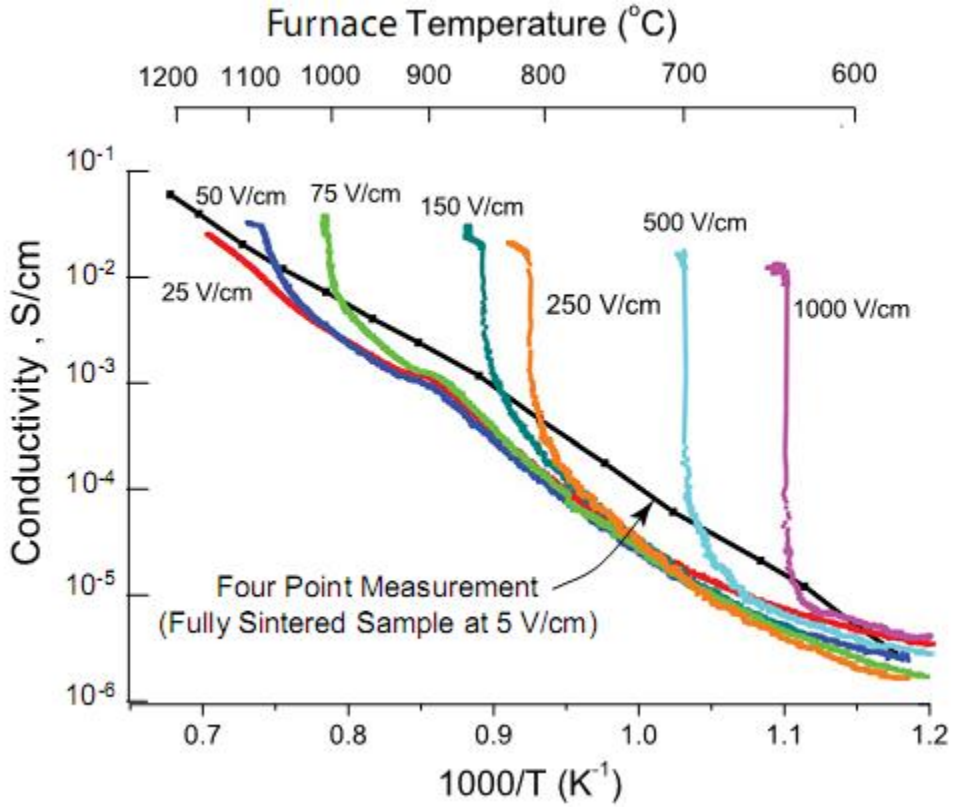

Figure 5.6. The change in the conductivity of the specimens as they sinter. The abrupt increase in the conductivity is a signature of the flash event. The black line gives the baseline ionic conductivity of conventional sintered specimens.

The conductivities from the flash experiments at different levels of electrical fields are given in various colors in Fig. 5.6. Note that while the conductivities are below the conductivity of the dense specimen, most likely due to the porous nature of the specimens, they rise precipitously at the onset of the non-linearity.

The conductivity measurements, therefore, show two regimes of behavior. Before the flash the conductivities are in reasonable agreement with the ionic conductivity of dense specimens, but after the flash the conductivities are much higher. It was possible to calculate the conductivities in the flash regime because under current control the specimens relax to a steady state as seen by the plateaus just after the peaks in Fig.5.2. The conductivities obtained in this manner just after the flash temperature are plotted in in Fig. 5.7, which also contains the data from the four probe measurements of fully sintered specimens at 5 Vcm^{-1}. The activation energy for the "flash-state" is 0.59 eV far below the activation energy for ionic diffusion. Note that the temperatures given in Fig. 5.7 for the flash-state refer to the specimen temperatures as estimated from the black body radiation model.

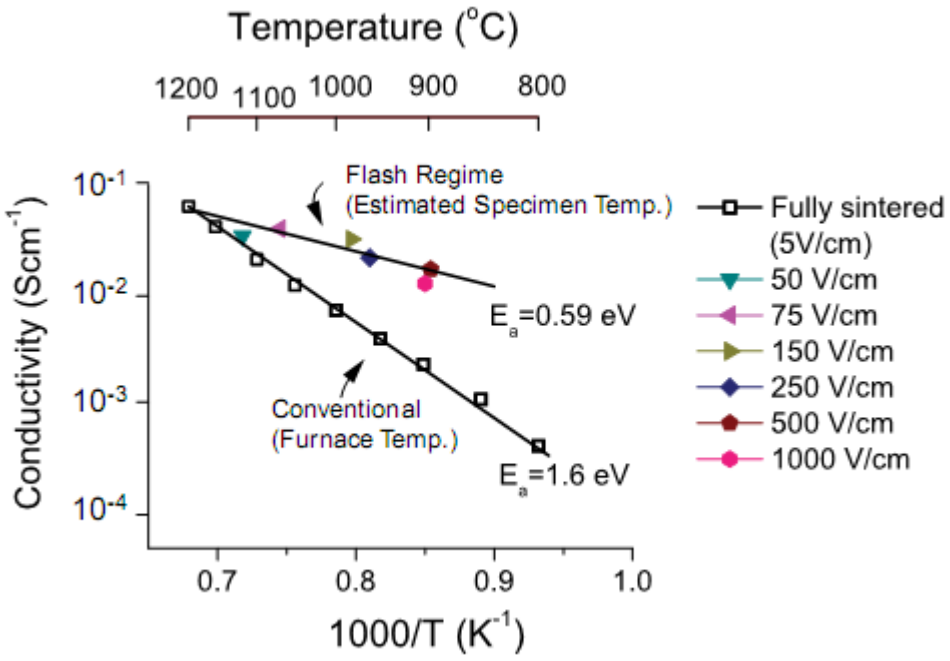

Figure 5.7 An Arrhenius plot of the conductivity of the specimen in the flash regime. It gives a much lower activation energy than the conductivity measured for a dense specimen at weak fields, where the conduction is predominantly ionic.

5.4.4. Joule heating

In the flash regime the specimens operate under current control and develop a steady state voltage as determined by the conductivity in this activated state. This phenomenon is explained in Fig. 5.8, where the power input into the specimen is plotted against the specimen temperature. The current supplied to the specimen is held constant; therefore, if the specimen temperature were to rise the power dissipated within it would fall. On the other hand the power needed to raise the specimen temperature increases with temperature because black body radiation increases with the fourth power of temperature. Thus an equilibrium is established where the power dissipation required to maintain the specimen temperature is equal to what the current can supply. The specimen heats if it is below, and cools if it is above this temperature.

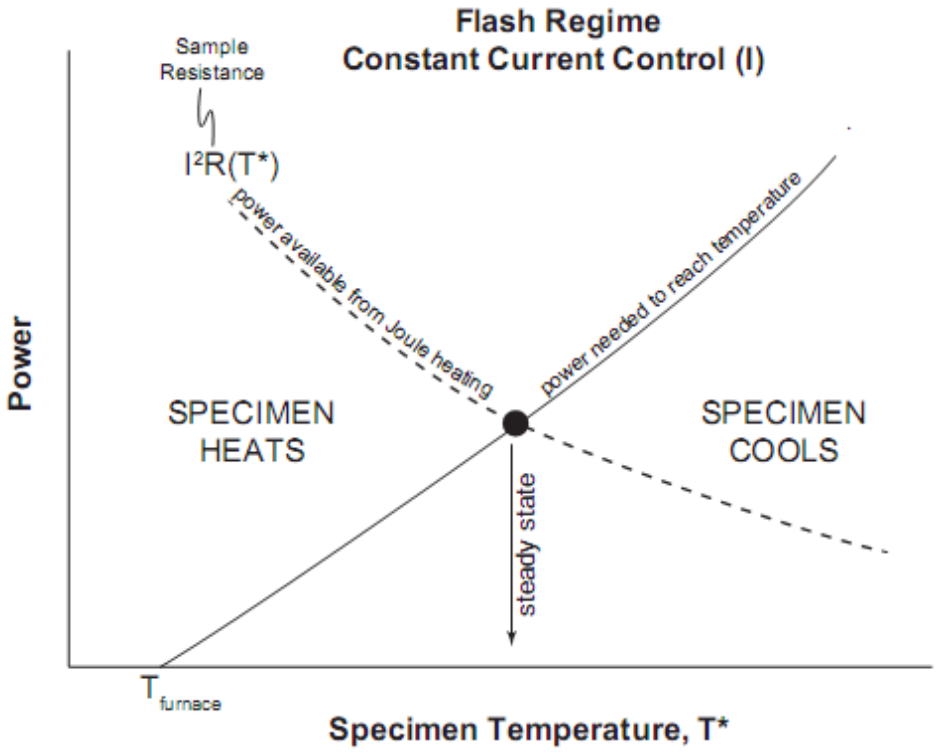

Figure 5.8. The specimen reaches a steady-state temperature in the flash regime by finding the balance between its change in resistance, which controls electrical dissipation and blackbody radiation. Both are function of temperature, both in opposite ways.

These results that give the furnace temperature, the specimen temperature and the power dissipation are given in Table 5.1. The sample temperature and the furnace temperature are plotted in Fig. 5.9. The error bars in the former include the uncertainty arising from the fluctuation in the voltage measurement and as well as 0.9-1.0 in the value of the emissivity of the sample. The flash regime occupies the high fields (above ~200 Vcm^{-1}) where the sample temperature is in the 800-950^{o}C range. These temperatures are far below the temperatures that would be required to sinter TiO_2 in just a few seconds (conventional sintering requires ~1100^{o}C for a few hours).

Table 5.1: Listing of experimental parameters, and from them the derivation of the specimen conductivity in the flash (Type B) regime for flash sintering of titania.

Applied field, Pre-flash, Vcm^{-1} (under voltage control)	Post flash field, Vcm^{-1} (under current control)	Current density during stage III, $mAmm^{-2}$	Conductance, Scm^{-1}	Power density, $mWmm^{-3}$	Furnace temperature, ^{o}C	Sample temperature, ^{o}C
0	n/a (voltage control)	0	0.027	0	1150	1150
15		2.4	0.027	3.6	1150	1152±1
25		5	0.019	10	1150	1158±2
40		9.7	0.026	39	1150	1178±4
50	47	12 (current control)	0.033	52	1077	1121±6
75	45		0.026	60	1100	1060±12
100	59		0.019	75	930	1015±10
150	60		0.021	95	840	968±23
250	87		0.015	118	780	984±16
500	100		0.012	110	700	896±21
1000	105		0.011	149	640	917±25

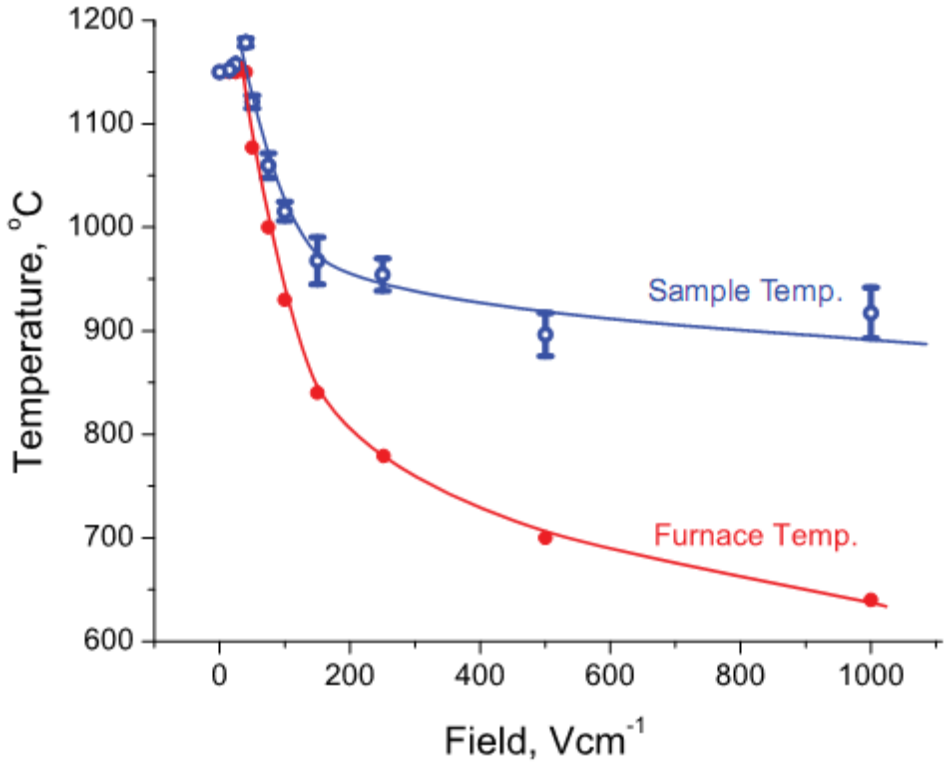

Figure 5.9. The divergence between the furnace and the specimen temperature. The full data, including the power dissipation are given in Table 5.1.

5.4.5 Microstructure

The grain size of all samples sintered under the electric field was measured. Micrographs for three cases along with the grain size distributions are shown in Fig. 5.10, and the values from all experiments are plotted in Fig. 5.11. The grain size clearly decreases in Type A sintering and increases slightly unchanged in Type B behavior. Curiously at small fields (less that 40 Vcm^{-1}) there is a rapid increase in the grain size with the applied field. While the reason for this behavior is unclear, it explains why these low fields do not show enhanced sintering (Fig. 5.1): we speculate that the increase in grain size overrides the benefit of the electric field to the sintering rate when the fields are small.

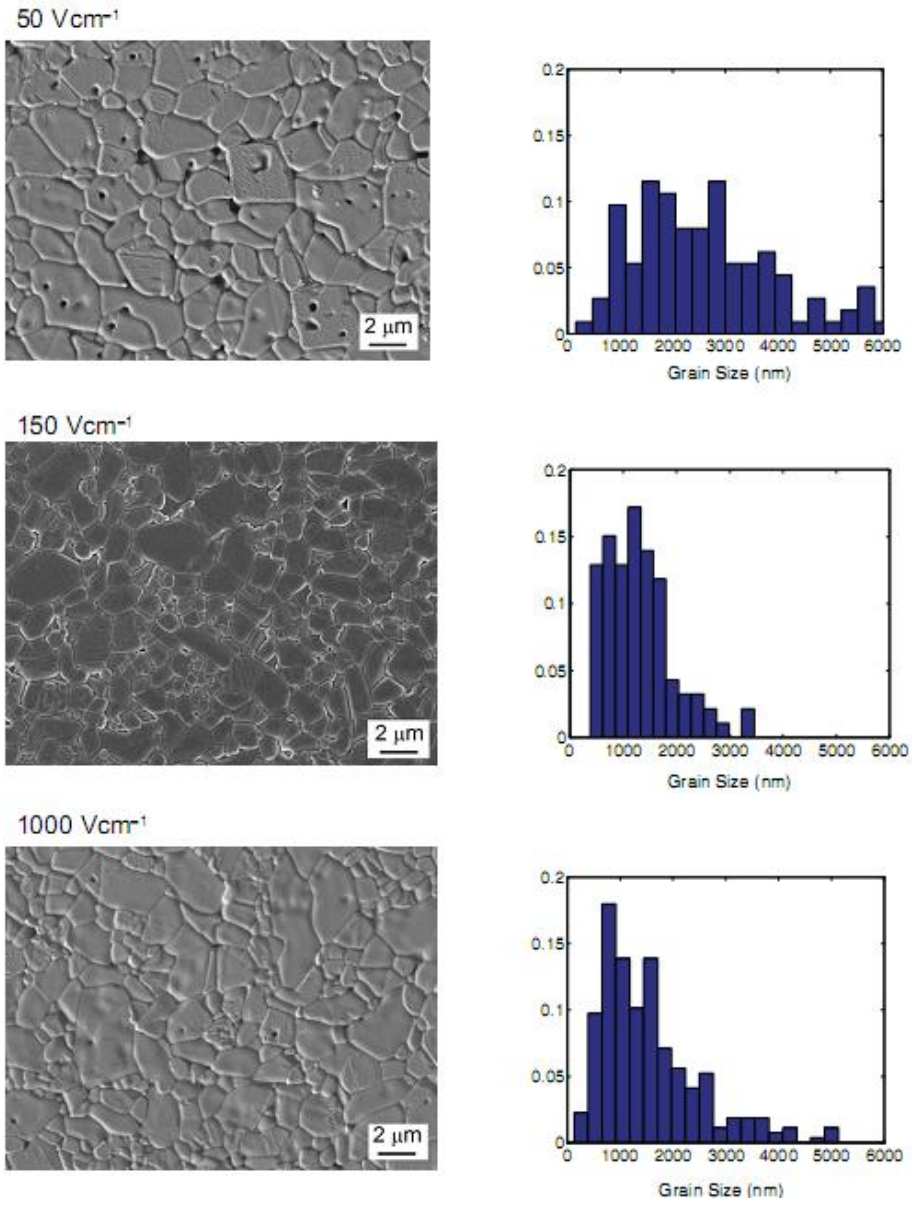

Figure 5.10. SEM micrographs of specimens showing the grain microstructure of specimens sintered under different electric fields. The distribution of the grain size is included on the right.

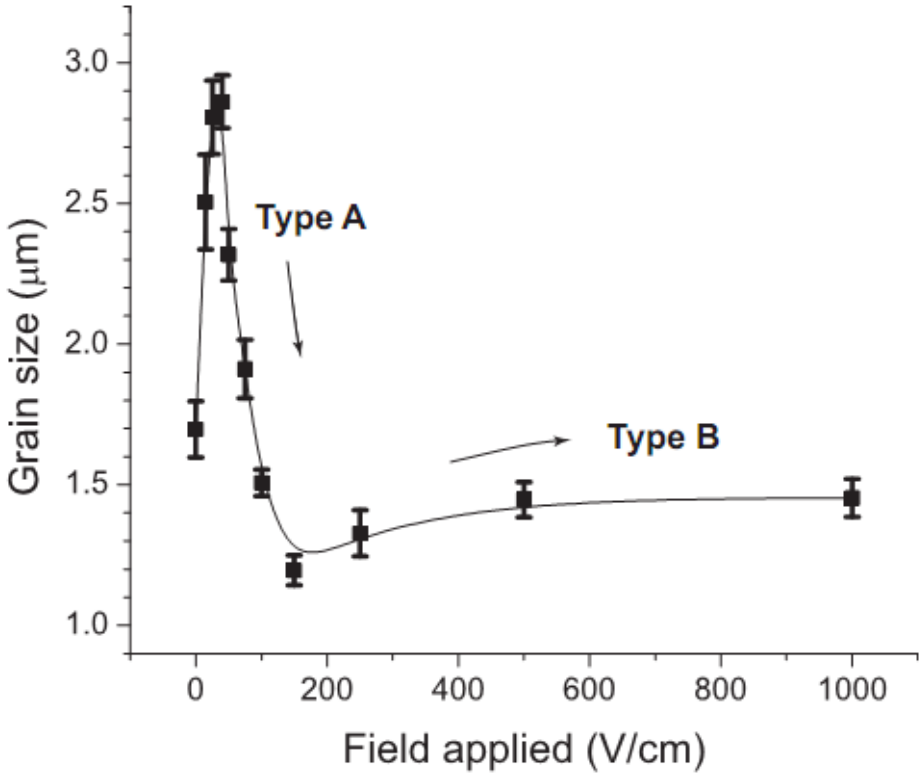

Figure 5.11 Measurements of the grain size in the specimens sintered at different applied fields. A decline in the grain size under Type A and a small increase under Type B sintered are consistent with earlier work on Yttria-stabilized zirconia, but grain growth at very low fields for the present experiments on titania has not been seen before

The grain microstructure in the flash sintered samples was isotropic and equiaxed, even though the experiments were carried out under a DC field. Furthermore we were unable to identify any differences in the grain size and the density across the gage section of the specimens; this was probably because the specimen geometry had been designed to achieve a uniform current density through the gage section, assured by placing the electrode contacts at the large handles of the dog-bone shaped specimens.

5.5. Discussion

5.5.1 Mechanisms of field assisted sintering and conductivity

The influence of electrical fields on mass transport and electrical conductivity in ceramics, particularly the oxides, can have various outcomes, depending on the temperature and the electrical control parameters. Just as the dominant mechanisms underlying the mechanical response of materials can change with temperature, the applied stress, the microstructure and the duration of the test, so can the response of ceramics to applied fields vary with temperature, the strength of the electrical field and the time dependent shape of the power cycle and the microstructure (for example the effect of particle size [59]). In mechanical experiments, one can control either the applied stress or the strain rate, not both, so it is in the present experiments where it is possible to control either the voltage or the current.

The results presented here show that at least two different mechanisms in field assisted sintering can operate. At low fields (Type A) sintering is enhanced but without a non-linear increase in the electrical conductivity, while at high fields sintering occurs as if in a flash (Type B) with the effect being invariably accompanied by a highly non-linear increase in electrical current. The power dissipation in the sample is given by the voltage times the current; thus the ever increasing current can lead to unbounded Joule heating of the specimen. Control is exercised by limiting the current flowing through the specimen after the onset of the flash. The specimen then finds its own electrical steady state in temperature and conductivity, dictated by a balance between black body radiation and the change in conductivity with temperature (Fig. 5.8). The design of the electrical parameters at the power supply has been germane to obtaining a well-controlled and reproducible effect of sintering in the flash regime. It is important to recognize that

different mechanisms of field assisted sintering and electrical conductivity can be invoked by changing the strength of the electrical field and the temperature.

5.5.2 The Experimental Space: AC/DC Power, Voltage - Current Control and Joule Heating

Preliminary results from our laboratory with AC fields are revealing that in addition to the voltage and current the frequency of the electrical fields has a strong influence on the outcome of the experiment. It important to recognize the magnitude of the electric field, the current setting, the frequency and the temperature can lead to different results, reflecting many different mechanisms for field assisted sintering. This point is often overlooked leading to unnecessary controversy when comparing results from different laboratories.

The role of Joule heating in flash sintering is an example of such a controversy. Surely a sample left under voltage control in the flash regime would continue to heat up, become unstable, and eventually melt [appendix]. Recent results from Park and Chen [40] where they estimate the sample to reach a temperature of 2500 ^{o}C under voltage control is an example of this disconnect with the current controlled experiments conducted in our laboratory. The 300 kHz fields used by Park and Chen [40] stand in contrast to the DC fields in our experiments which throw further uncertainty into this comparison. Furthermore, we are also dubious about the method used by Park and Chen to estimate the sample temperature: they extrapolate the low-field Arrhenius ionic conductivity data obtained up to ~1400 ^{o}C, to 2500 ^{o}C (well beyond 1400 ^{o}C), which lies in the flash regime where the mechanism of conductivity changes. The results in Fig. 5.9 show that the activation energy for conductivities in the flash regime is very different from the low-field ionic

regime, which raises serious questions about the Park and Chen[25] approach for estimating the sample temperature.

Recently, Steil et al [62] have reported systematic experiments on the effect of current density after the initiation of the flash on densification behavior of 8 mol% YSZ. Their finding that the density increases with the current setting is in agreement with the work from this laboratory [30] . However, their final densities are somewhat lower, even though the steady state power levels achieved in current control were higher than our experiments. It is possible that this difference reflects the use of 1000Hz AC electrical fields as opposed to the DC fields. They also estimate an upper bound value for the specimen temperature of 1710^{o}C based upon adiabatic heating during the power spike which occurs when switching from voltage to current control. While this estimate is likely to be a significant overestimate of the specimen temperature (due to conduction losses through the electrodes and black body radiation losses that increase as the fourth power of temperature), it still would not explain the sintering of YSZ in one or two seconds (the theoretical estimate for sintering in ~3 seconds is approximately 1910^{o}C [2]

To our knowledge the only direct estimates of the specimen temperature in the flash regime are from the measurement of thermal expansion[36], and the measurements with two different pyrometers in this laboratory. These estimates are self-consistent and in good agreement with predictions from a black body radiation model. Collectively these results show that flash sintering occurs at temperatures that are hundreds of degree Centigrade below the temperature that would be required to sinter YSZ in just a few seconds. Given such a large discrepancy it is difficult to conceive that localized melting, at grain boundaries for example, can instigate flash sintering (it is not credible to assume that hundreds of degrees differential between the grain boundary and grain matrix temperature is sustainable [61].

The specimen geometry also plays in these experiments. We use dog-bone specimens hung into the furnace with platinum wires hooked through holes in the handles of these specimens. Platinum paste is used to spread the current flowing into the specimen. In this design the conduction losses are negligible. The dog-bone shape assures that the current flow is uniform through the narrower cross section of the gage length. Uniformity of the grain size across the gage length confirms this effect. This specimen design also helps to isolate the near-electrode effects (where the current is non-uniform) from the gage section. It is of note that experiments from the literature discussed above were carried out on penny shaped specimens with the field applied with large area electrodes in contact with its opposing surfaces.

5.5.3 Grain Growth under Electric Field

Type A behavior, which was first reported in the sintering of 3mol% yttria stabilized zirconia at low fields [1], was explained by the reduced rate of grain growth under weak electrical fields. Since sintering rate increases (inversely) with the fourth power of the grain size, even a modest reduction in grain size can produce a significant increase in the rate of sintering. The convergence between the reduced rate of grain growth and higher rates of sintering has successfully explained Type A behavior in yttria stabilized zirconia[95], [29].

As in YSZ we find that grain growth is retarded in the low field regime, marked as Type A behavior in Fig. 5.11, for fields ranging from 40 Vcm^{-1} to 150 Vcm^{-1}. However, the results given by the two points to the left, showing an increase in the grain size with the field are anomalous. These experiments were repeated to ascertain their reproducibility. We do not have a reasonable explanation for these two points.

The results for Type B regime stand in contrast to Type A behavior: we find that in the flash-regime, the grain size exhibits a tendency to increase, which is opposite to the low field behavior.

The spectrum of results in Fig. 5.11 illustrates the complex influence of electric fields on the grain size, of which we understand very little. Even the clear result in work of Ghosh et. al.[29], where weak electrical fields applied to fully sintered polycrystals of zirconia were shown to retard grain growth are enigmatic since enhanced sintering and superplastic deformation of oxides under electric fields implies faster diffusion kinetics, which would be expected to enhance grain growth as well. The explanations for the reduced rate of grain growth under electric fields have centered on a change in the interfacial energy with applied field, either because of some degree of local heating at grain boundaries, which lowers the energy due to the entropy [29], or due to an interaction between electric field and the space charge at the boundaries [34]. The influence of electrical fields on grain growth in the Type B (Flash regime) is variable and remains unpredictable in case of titania.

6. Texture evolution in titania under flash

6.1 Disclaimer

This work has been submitted to the Journal of Applied Physics Letters [97]. Author has performed the experiments and written the draft. Dr. J. M. Lebrun helped to plan the experiments and contributed critical inputs on the draft. Prof. Raj is the principle investigator of the work and Prof. Waltraud M. Kriven and her group has provided their expertise on the furnace set-up at Synchrotron. The experiments have been supported by the Basic Energy Sciences Division of the Department of Energy under grant number DE-FG02-07ER46403.

6.2 Introduction

The phenomenon of flash sintering [1] was first observed in 2010, where sintering occurs at unusually low furnace temperatures in mere seconds. The surge in conductivity which accompanies sintering is a signature of the flash event [10]. When the experiments are carried out at a constant furnace temperature, and the field is applied as a step function, the flash occurs after an incubation time. This time delay has been called Stage I. The non-linear increase in conductivity is controlled by limiting the current through the specimen, known as Stage II. The specimen may then be held in a constant state of flash under current control, which is Stage III of the flash

experiment. Since most of the sintering occurs during Stage II, the sample is often dense and stable during the Stage III experiments.

Recent experiments in Stage III with yttria stablilized zirconia have revealed new physics: the oxide exhibits intense optical luminescence [63]. In these experiments the specimen temperature is measured from lattice expansion during *in-situ* experiments to account for Joule heating. The optical luminescence was compared with the radiation spectrum that would be expected from black body radiation. The shape and nature of the radiation spectrum was consistent with electroluminescence rather than black body radiation. The spectrum showed two distinct peaks that remained at the same wavelengths when the specimen temperature was increased consistent with recombination of electron-hole pairs or excitons [65] Furthermore, the emission peaks were at shorter wavelengths than would have been expected from black body radiation. Measurements of optical luminescence have been confirmed in the literature [98]

In another set of experiments, also conducted at the synchrotron, we have observed the emergence of a new phase in 3mol% yttria stabilized zirconia (3YSZ), which was identified to have a pseudo cubic structure [70] The phase emerged and then dissolved when the field was turned on and then off. The experiments could be repeated in several on-off cycles, and therefore could be attributed to a thermodynamic force induced by the electric field. There was, however, a time lag between the appearance and the dissolution of the new phase relative to the moment that the field was switched, showing that the phase transformation was diffusion controlled.

In this article, we present results of field induced texture in titania during flash experiments. As was the case of 3YSZ, these experiments were also carried out in Stage III. However, we discover that in this instance the change in structure is like a martensitic transformation, appearing

and disappearing nearly instantaneously when the field is turned on and off. It is concluded that the effect is a result of cooperative movements of atoms in the crystallites such that they develop a polar character, which couples with the electric field through electrostatic interactions. These experiments build on earlier results on flash sintering and measurements of electrical conductivity of titania in the state of flash [11]

6.3 Experimental set up

Refer to chapter 4 for experimental set up in all details. A short summery is as follows. Powders of titania is uniaxially pressed into rectangular bar shape and conventionally sintered to full densification. The gage-length of specimen is 3.72 mm with 1.33 mm x 0.55 mm cross-section area. *In-situ* experiments were carried out at the Synchrotron source, Argonne National Lab. Specimen were heated to temperature of 800°C and an electric field of 100 Vcm^{-1} was applied in a cyclic On-Off pattern. The electrical parameters is shown in Fig. 4. 5.

Two kinds of XRD scans were done using synchrotron: (i) In Full-scans, $2\theta = 7° - 22°$ is covered in 75 steps with an integration time of 1 sec at every step (many peaks were covered with higher accuracy). (ii) For the local-scan mode experiments, the detector remained stationary covering the range $2\theta = 18.5° \pm 1.5°$ (response of selected peaks were monitored with time) with acquisition time of 0.5 sec, within which the (211) peak from rutile resides.

The shift in the (111) peak from platinum was used to estimate the specimen temperature. Under the conditions of Stage III flash, described in Fig. 4.5, the specimen temperature is measured to be 925 °C, at $2\theta = 14.775°$ for the platinum peak. The application of the black body radiation model [2] yields the estimate of the specimen temperature to be 920 °C ± 20°C, in good agreement with the measurement using the platinum standard.

6.4 Results

6.4.1 full scan

The results from the full scan measurements while the specimen is held under the constant state of flash in Stage III are shown in Fig. 6.1. Two on-off cycles are given. Note that (211) peak gains in strength while the (110) and (111) peaks weaken when the field is turned on. The sample recovers essentially to its original state when the field is turned off. The response repeats over several cycles. The emergence of texture and its reversal is coincident with the change in the applied field.

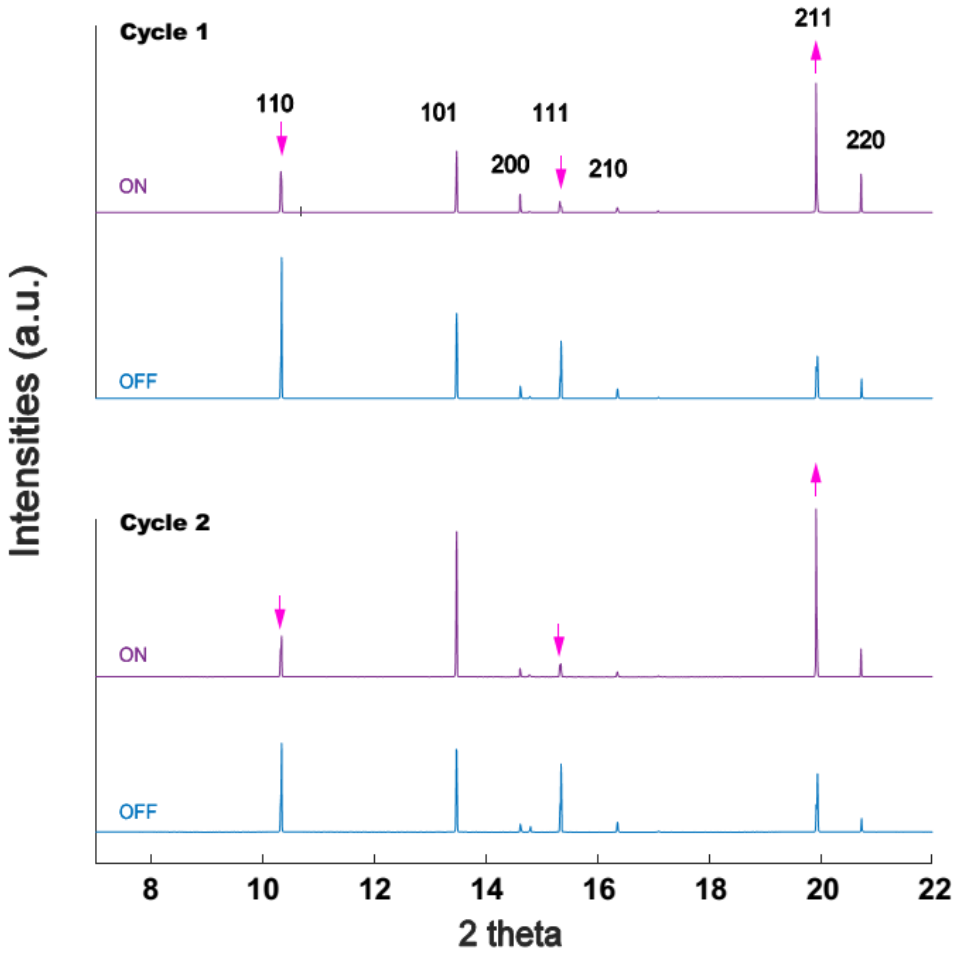

Figure 6.1 Texture along the (211), (110) and (111) planes induced by the electric field, in a martensite-like transformation.

The change in the relative strength of the peaks from different planes may be quantified in terms of a texture coefficient, TC, as described in Barret and Massalski [78] where the strength of individual peaks is measured relative to the average of a number of specific peaks, according to

$$TC = \left(\frac{I(hkl)}{\Sigma_0^n I(hkl)} \right) \Big/ \left(\frac{I_o(hkl)}{\Sigma_0^n I_o(hkl)} \right) \qquad (6.1)$$

The results from the application of Eq. (6.1) to the data are shown in Fig. 6.2, for two cycles. In both cases the denominator in Eq. (6.1) was set equal to the intensities obtained during

the first cycle. Thus we see that there is some residual texture in the second cycle when the field is turned off. However, the strong and consistent presence of texture is evident from the relative strengths of these four peaks when the field is on. Keep in mind that these data were obtained from full scans which required a time of 1:15 min. Therefore, fluctuations over this period are implicit in these data.

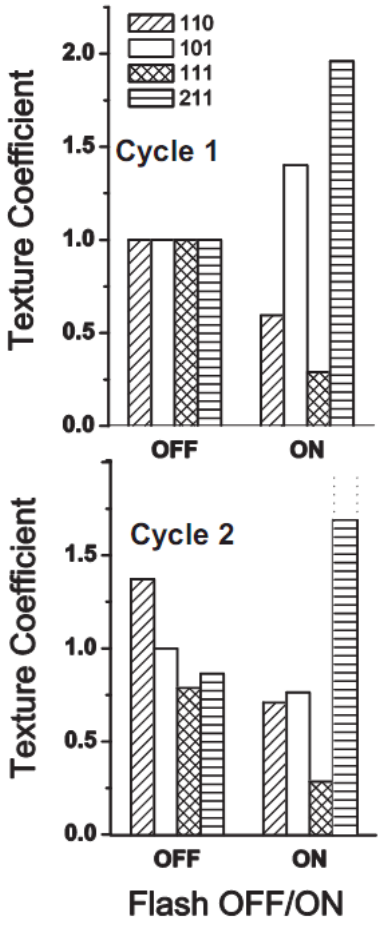

Figure 6.2. Fluctuation in the peak intensity calibrated to XRD scan at 800°C before application of electric field.

6.4.2 Local scan

We have noted that the strength of the peaks fluctuated with time even though the specimen is held in a constant state of flash. For example as seen in Fig. 6.1, the strengthening of the (101) peak is sporadic. This point is further clarified in the results from the local scan mode experiments where the detector was kept at the fixed position to record the strength of the (211) peak. These data, measured at the rate of 2 Hz, are shown in Fig. 6.3. While there is fluctuation in the strength of the (211) peak the correlation with the on-off cycles of the electric field is strong. Note, however, that the peaks are stronger when the power surges as the field is turned on. Thus it appears that the strength of the peaks may be related to power dissipation. On the other hand a momentary increase in the strength of the (211) peak also occurs when the field is switched off. Thus it appears that step changes in the field produce a transient increase in texture. It is possible the specimen serves like a capacitor which charges and discharges, and that these transients are related to texture.

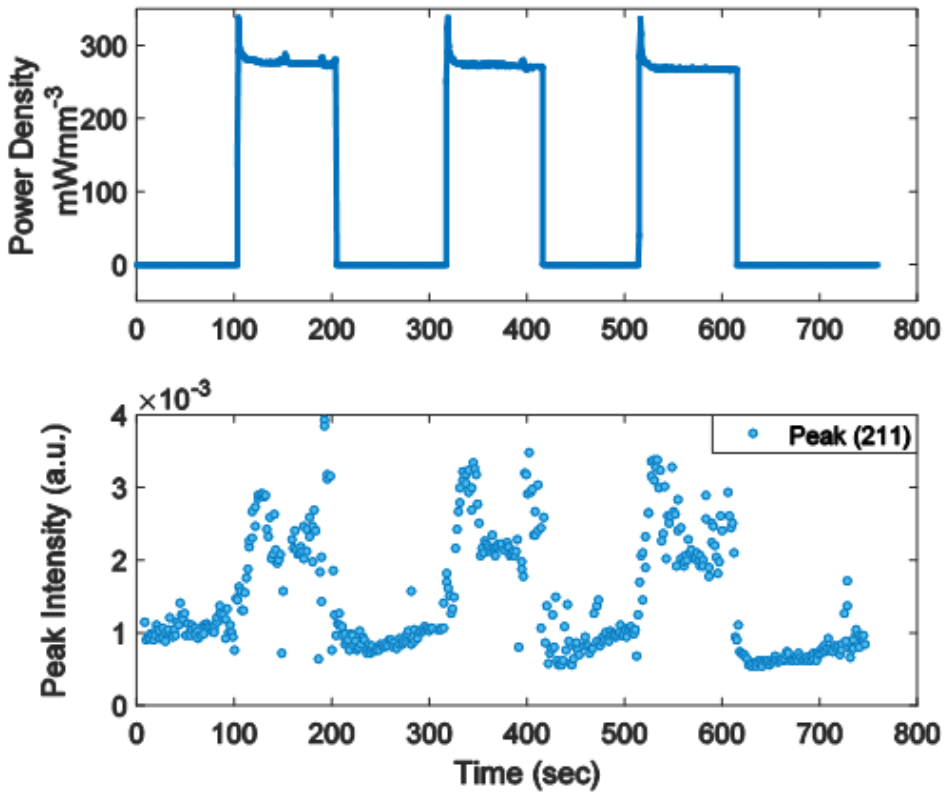

Figure 6.3: Time resolved response of (211) peak under ON-OFF flash experiments.

The first question to be answered is whether the texture may have been a result of Joule heating. Recall that the specimen temperature with the applied field was measured to be 925 ^{o}C with the platinum standard. The diffraction patterns obtained at furnace temperatures of 925 ^{o}C and 800 ^{o}C, without the applied field are similar to each other than to flash specimen as can be seen figure 6.4, thus proving that the texture was not a result of Joule heating.

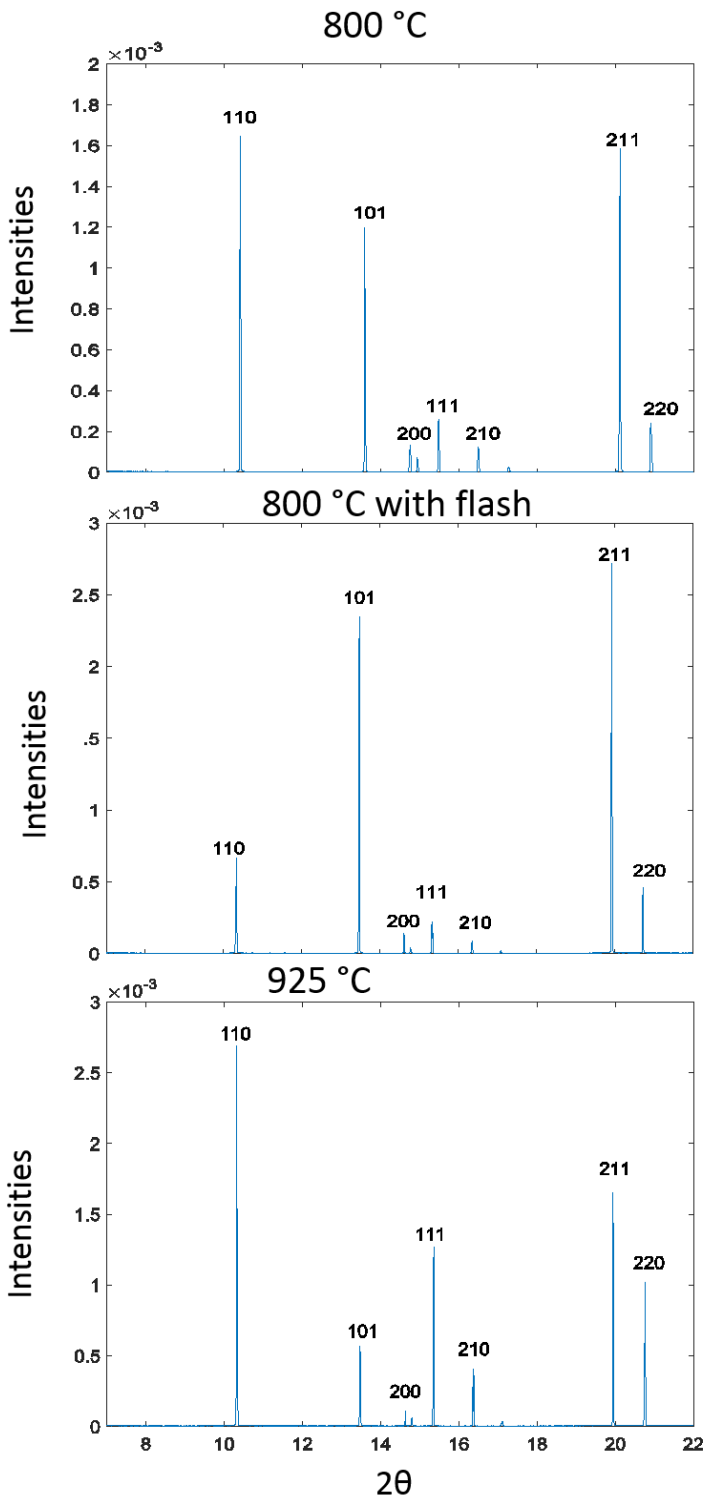

Figure 6.4 Comparison of diffraction patterns of flash with specimens kept at equivalent temperature.

The peaks from the texture fluctuated with time suggesting some type of stochastic events within the polycrystal where the orientations of the crystallite do not necessarily hold steady but fluctuate with time. Our measurements do not provide information regarding the rate of these stochastic fluctuations but given that our measurements were made at the rate of 2 Hz, we can say that they occurred at least at this rate. Experiments with AC fields can provide further insights into the frequency of these fluctuations. This knowledge can help to guide the development of mechanisms and models for this unusual phenomenon.

6.5 Discussion

This article is a second report on change in structure in polycrystals induced by the electric field. Earlier, we have shown the emergence and extinction of a new phase in 3YSZ [70]. However, in that case phase evolution was diffusion controlled and therefore probably occurs by a nucleation and growth process. In the present case, the structure change apparently occurs by cooperative displacements of atoms in crystallites, similar to martensitic transformations. Thus we find that crystals oriented along the (111) direction change to the (211) orientation. There is also evidence of (110) orientations giving way to (101) texture under the applied field, although this change seems more sporadic than the evolution of the (211) texture. In either case, the manifestation of texture appears to have a stochastic character.

The cooperative movements of atoms in the crystallites can be expected to be coupled to the propagation and dispersion of phonons in the polycrystal [99]. The underlying physics for the results reported in this work would need to explore how electric fields can couple with the phonons. This interaction must be such that the favored orientations develop a polar character, which can amass electrostatic interaction energy with the applied field. The question then arises how phonon

dispersion can be influenced by the polar nature of the crystals. It can be conjectured that the phonons would attempt to undo the texture while the electric field would attempt to restore it, which could be the origin of the stochastic behavior that we have observed.

The effect reported in this letter is different from the traditional experiments where very high electrical fields are employed to induce "poling" in piezoelectric materials. In poling experiments dipoles, which exist in the structure, are forced into alignment under the electric fields. In present experiments the fields are several orders of magnitude weaker and the structures are not intrinsically polar. It may be argued that the electrical fields induce dipoles within the structure, with whom they develop an interaction energy that serves as the driving force for the phase transformation.

7. Flash on constrained sintering

7.1 Disclaimer

This work has been published to Journal of American Ceramic Society [55]. Author did all the experiments. The experiments have been supported by the Basic Energy Sciences Division of the Department of Energy under grant number DE-FG02-07ER46403

7.2 Introduction

The phenomenon of constrained sintering is related to the generation of shear stresses when uniform volumetric shrinkage, as required in simple densification, is obstructed by physical constraints. Shear stresses imply that at least two principal stresses in the stress-state are unequal or of the opposite sign. For instance if a film is prevented from shrinking in the plane of the substrate then it develops a tensile principal stress in that direction, while the out of plane principal stress, which arises from the sintering pressure, remain compressive, generating, in this way, a shear stress [71], [100]. Unless the shear stress is relaxed sintering cannot move forward, meaning that the rate of shear relaxation rather than the rate of densification controls the sintering rate.

A similar scenario arises if the sintering body contains inclusions that are rigid. If these inclusions are much larger than the particles in the surrounding powder, then continuum mechanics can be applied. Fortunately sintering and shear rates induced by diffusion are linear in stress, so that linear elastic analysis can be used directly by replacing the shear modulus by shear viscosity, and the bulk modulus by volumetric viscosity, using the principle of equivalence. The linear elastic analysis of a sphere having a compressibility that is different than that of the matrix, when loaded in isostatic compression, will produce pure shear in the matrix surrounding it. Again if the sphere is rigid then the densification rate of the matrix becomes controlled by shear relaxation [101], [102].

The mechanism of diffusional creep and sintering in polycrystalline bodies has been well studied, theoretically and experimentally [71], [100]–[102]. The rate of both processes is sensitive to the grain size, being proportional to d^{-3} for shear and d^{-4} for densification [9]. Here densification of the body is assumed to occur under its own intrinsic sintering pressure, which being proportional to d^{-1}, adds the additional power to the grain size dependence. While the exact explanation for the power in the grain size dependence is not straightforward it is indeed related to the effective diffusion distance for mass transport, from the source to the sink that produces either shear or densification [100]. As illustrated in Fig. 7.1, this diffusion distance is proportional to the grain size, but its magnitude for shear is nearly twice that for densification. It may then be predicted that shear rate will be about ten times slower than densification rate. If sintering becomes constrained then its rate will slower by such a factor as well.

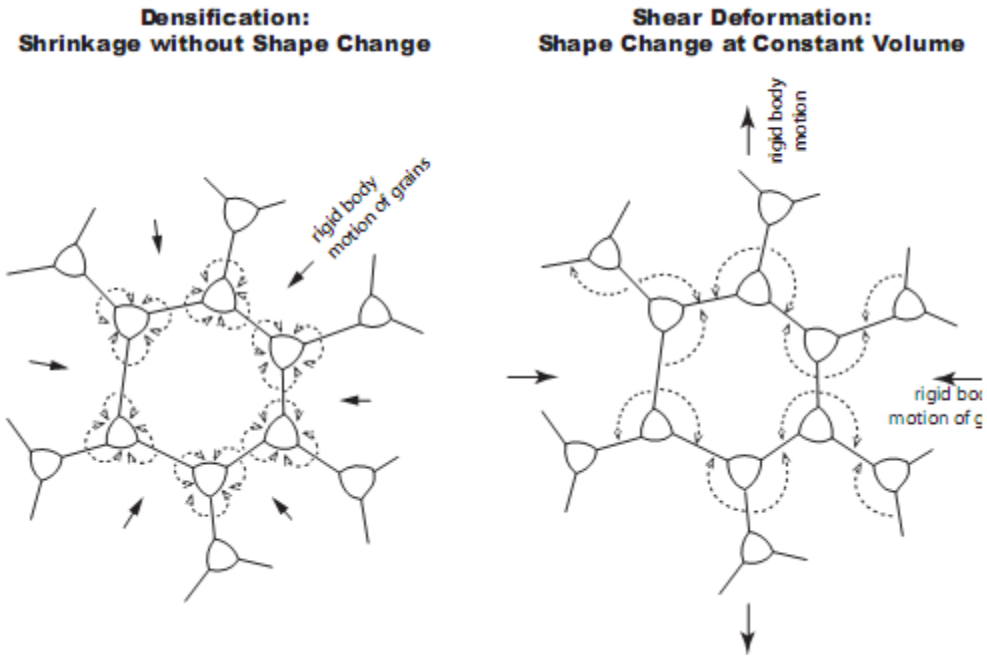

Figure 7.1 Diffusional paths for volumetric shrinkage (left) and shear deformation (right) in conventional sintering and deformation. The diffusion distance for shear deformation is twice for densification.

Given the unusual nature of flash sintering [1], [9], we were curious if the study of constrained sintering can shed some light on the underlying mechanism for the influence of electrical fields on sintering behavior. Indeed, we find that the introduction of large rigid inclusions of alumina [71] do not markedly change the rate of sintering of the titania matrix under electric fields. The implication is that shear and densification rates occur at the same pace in flash sintering. We interpret this behavior in terms of a diffusion distance scenario that is different than the traditional explanation for sintering and diffusion creep.

7.3 Experimental setup

Al_2O_3 inclusions of particle size 10μm are dispersed in the matrix of rutile nanopowders (particle size 20 nm) in different volume fractions. The volume fraction of alumina in titania were determined using Eq. (4.1) to be 0%, 4.8%, 9.6% and 19%. Detailed process of power processing is explained in section 4.2.3. Once the mixed powder was dried, they were uniaxially pressed in dog-bone shape under 105 MPa.

The compact samples were annealed at 550°C for 1 hour to burn out the binders. The experimental parameters for the specimens are summarized in table 4.2 and 4.3 . Two kinds of flash experiments were done: applying the field and then heating the furnace at a constant rate, or CHR (10 $^{o}Cmin^{-1}$), and (ii) holding the furnace at a constant temperature, called isothermal or IST, and applying the field as a step function. All experiments were carried out at an applied field of 250 Vcm^{-1}, with the current limit set to a density of 18 $mAmm^{-2}$ after the onset of the flash. In the isothermal flash experiments, the specimens were held at 850 ^{o}C for 100 seconds before the field was applied as a step function. The current quickly rose and reached its preset limit within a few seconds (called incubation time). The specimen was held at constant current for 10 s and then the power was switched off.

In conventional sintering the CHR experiments were carried out at 10 $^{o}Cmin^{-1}$ with the temperature allowed to rise to 1150°C that is necessary for sintering of pure titania. The isothermal experiments were carried out at 850^{o}C for 0.5 h.

Mathematical analysis of sintering of matrix (titania) has been derived in section 4.6.3. Specimen after sintering were analyzed using XRD to confirm that no new phase has been formed

during conventional/flash sintering. Black body radiation model is used for temperature estimation during flash sintering, presented in .table 4.3.

7.4 Results

7.4.1 Stages of flash sintering

In isothermal experiments flash sintering may be separated into three stages, as shown in Fig. 7.2. Stage I corresponds to the incubation time between the application of the field and just before the onset of the flash. In Stage II the current rises until it reaches the current limit set at the power supply, which switches from voltage to current control. The switching time was 20 ms, according to the manufacturer's specification. In this stage the conductivity of the specimen can increase by nearly three orders of magnitude [11]. Under current control the voltage drops quickly to its quasi steady state value determined by the conductivity of specimen and the current limit. This demarcates the beginning of Stage III. The sample may be maintained in Stage III for an extended period.

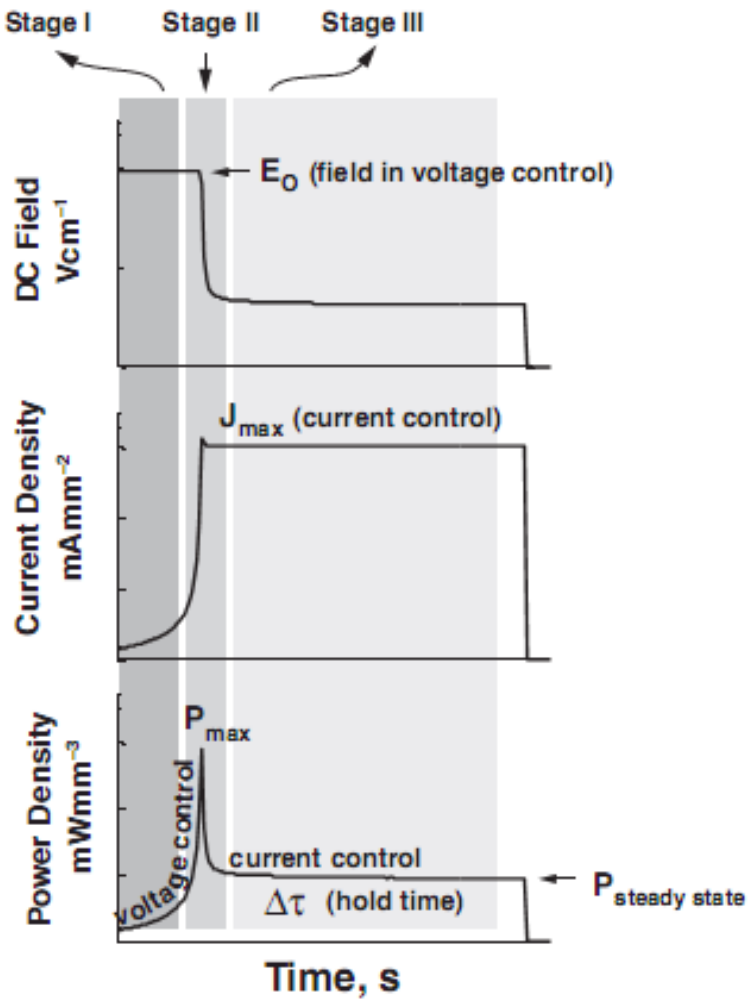

Figure 7.2 Three stages of flash sintering at constant furnace temperature. The field applied as a step function at time "zero". The current begins to rise nonlinearly after an incubation time (called Stage I). The onset of the flash during which the power supply switches from voltage controlled to current control in called Stage II. Under current control the sample remains in a stable flash activated state which is called Stage III.

The sintering rate is highest in Stage II. The power spike in this stage reaches its maximum theoretical limit, given by product of the electric field and the current limit. (The power spike in Stage II does not produce an equivalent spike in the specimen temperature, since the integrated energy expended within the spike is absorbed by the specific heat of the specimen.) We have

empirically chosen the beginning of Stage II when the current reaches 10 % of its set limit, and lasts for 2 seconds after power spike; at this point the voltage finds its quasi-steady state value in Stage III.

For experiments carried out at constant furnace temperature, the field must be adjusted to control the incubation time, since the incubation time lengthens quickly as the field is lowered. In the present experiments, 250 Vcm^{-1} was employed at furnace temperature of 850 ^{o}C. Under these conditions the incubation time was a few seconds.

7.4.2 Constant heating rate and isothermal experiments

Constant heating rate experiments for both conventional and flash sintering were carried out at a heating rate of 10 $^{o}Cmin^{-1}$. These results are shown in Fig. 3. In conventional sintering pure titania reaches full density at 1150 ^{o}C (CHR-CS-0). However, the addition of alumina slows the sintering rate. For example, the 4.9% alumina sample is able to reach a density of 85%, while the 9.6% sample sinters to 75% and the 19% sample to only 67%.

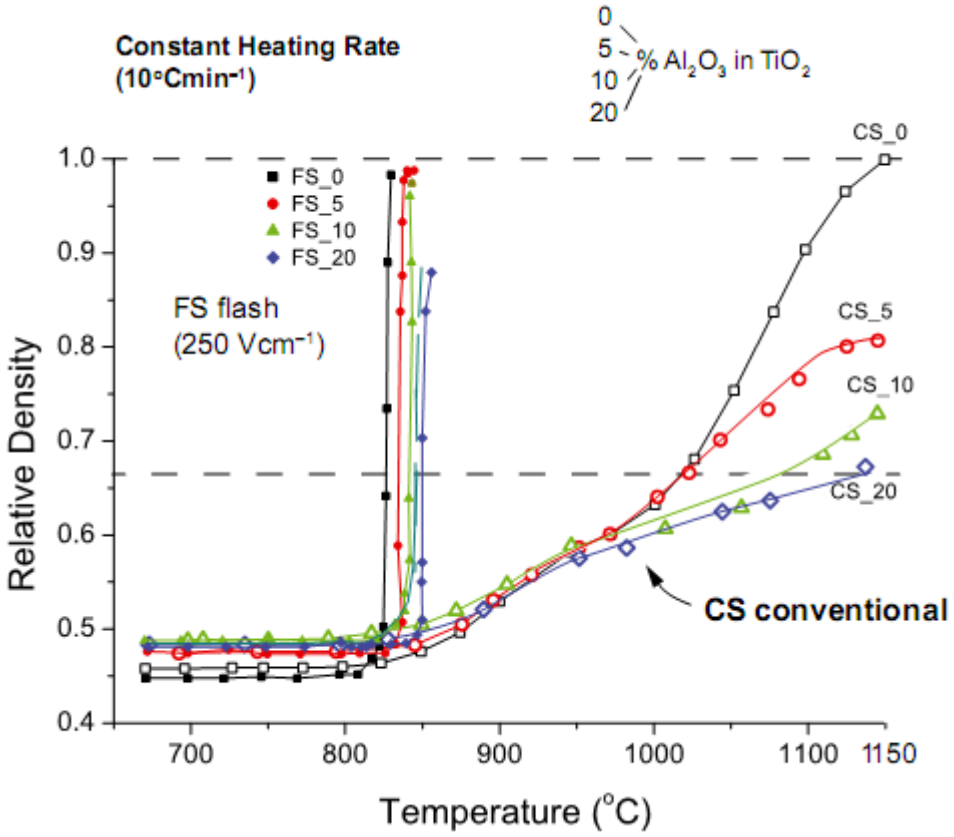

Figure 7.3 A comparison of conventional (CS) and flash (FS) sintering of composites with increasing volume fractions alumina in titania matri. Relative density of titania during conventional and flash sintering. Constant Heating Rate Experiments.

Under electrical field the specimens with and without alumina sinter in the same way. These experiments were carried out with a field of 250 Vcm^{-1} with the current limit set to 18 $mAmm^{-2}$. All samples flash-sintered within a narrow range of 825 – 850 ^{o}C. When contrasted with the results for conventional sintering, these results show that the constraining effect of alumina inclusions is abated under field assisted sintering.

The results for the isothermal experiments, at a furnace temperature of 850 ^{o}C, and an applied field of 250 Vcm^{-1}, are given in Fig. 7.4. The time scale in this figure begins after the

furnace reaches 850 ºC. The electric field is applied 100 s after the furnace reaches this temperature. The incubation time (Stage I) is counted from the moment electric field is applied to the point that the current reaches its set limit (18 $mAmm^{-2}$). These incubation times are listed in Table 4.3. They rise with the volume fraction of alumina, increasing from 5 seconds to 20 seconds. The flash sintered composites show near full densification except for the 19 vol% alumina sample which sintered to 88% - 90% density for both constant heating rate and isothermal experiments. This point, that is the lower density of 19% samples under electric field, is discussed in detail in the next section.

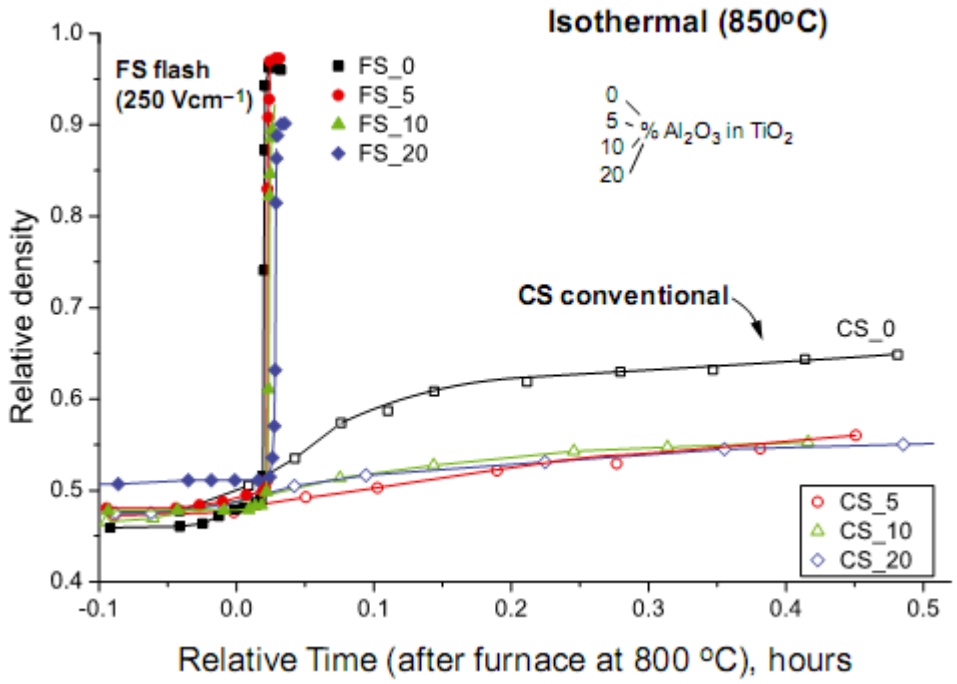

Figure 7.4 Conventional (CS) and Flash (FS) sintering experiments at constant furnace temperature of 850°C.

The link between power dissipation and densification is shown in expanded time scales in Fig. 7.5 and Fig. 7.6. . Under electric field rapid densification is achieved in less than 5 seconds at a furnace temperature of 850 ºC for all specimens.

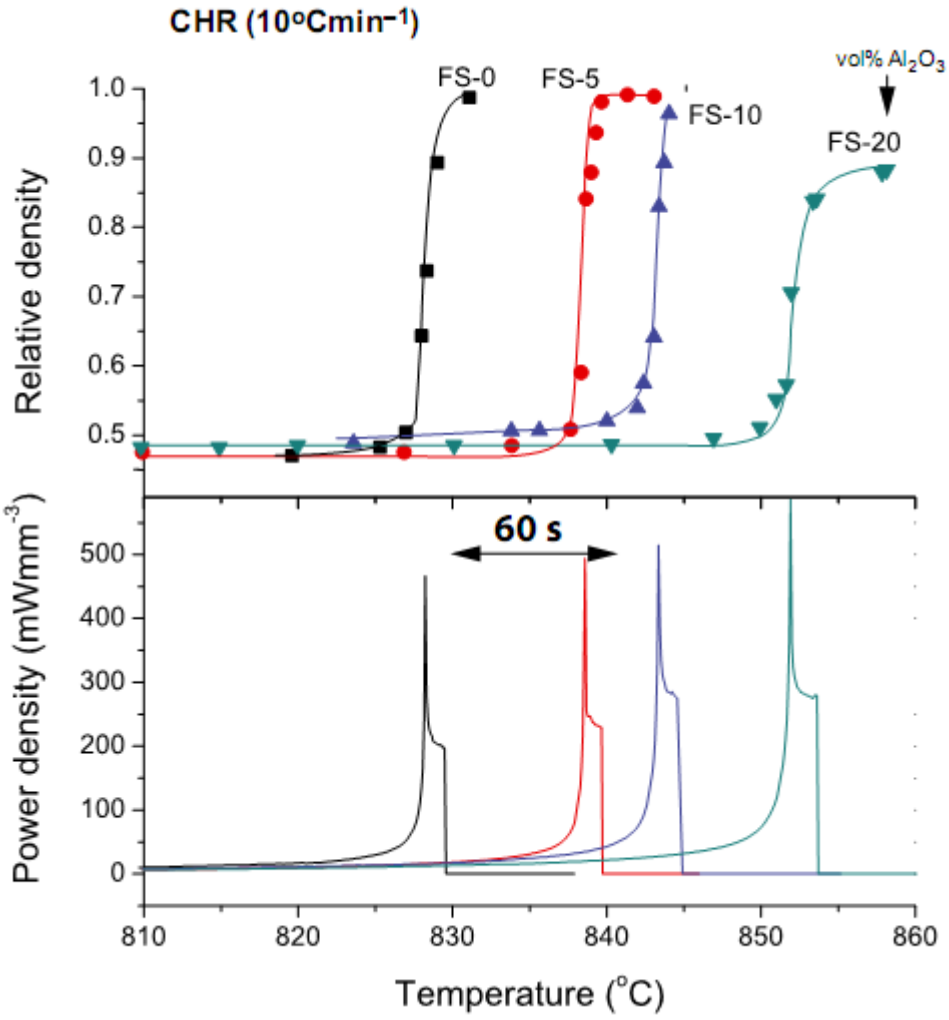

Figure 7.5. The correspondence between the shrinkage and power dissipation during flash sintering in constant heating rate experiments. In all instances, the applied field was 250 Vcm^{-1} and current limit was set at 18 $mAmm^{-2}$.

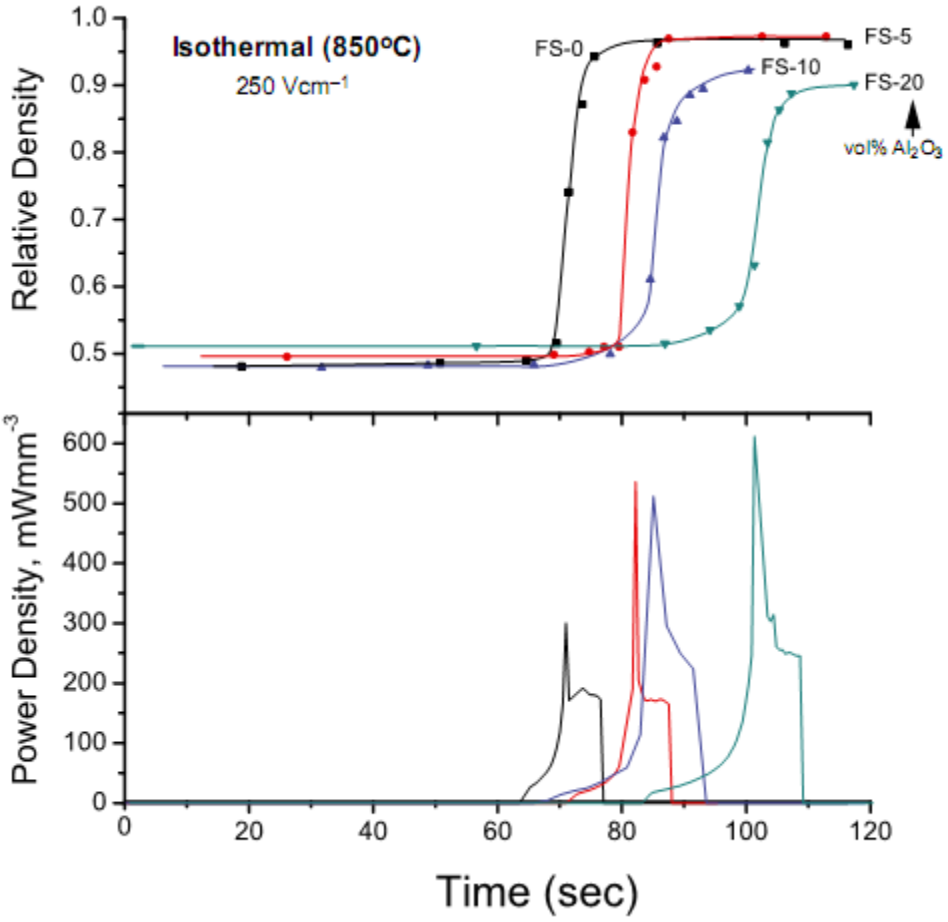

Figure 7.6. The correspondence between the shrinkage and power dissipation during flash sintering with the furnace held at a constant temperature. In all instances, the applied field was 250 Vcm^{-1} and current limit was set at 18 $mAmm^{-2}$.

7.4.3 Microstructure

We were intrigued why the specimens containing the highest volume fraction of alumina inclusions (19%) would sinter to ~90% density under electric field, while the specimens with lower inclusion fractions sintered to near full density.

The answer to this question may be evident from the microstructure of the flash-sintered, high volume fraction specimen, as shown in Fig. 7.7. In this specimen the alumina inclusions form clusters, shown by the bright areas in the micrograph on the left. The micrograph on the upper right shows that the titania matrix sinters in the neighborhood of single alumina inclusions. However, sintering remains incomplete within clusters of alumina inclusions as shown at the bottom right. This observation can be explained by the fact that the electrical current flow through the titania particles sequestered within the clusters of alumina-inclusions is prevented because they are electrically shielded by the insulating alumina inclusions. It has been definitively shown that electrical current is essential for producing field assisted sintering [30].

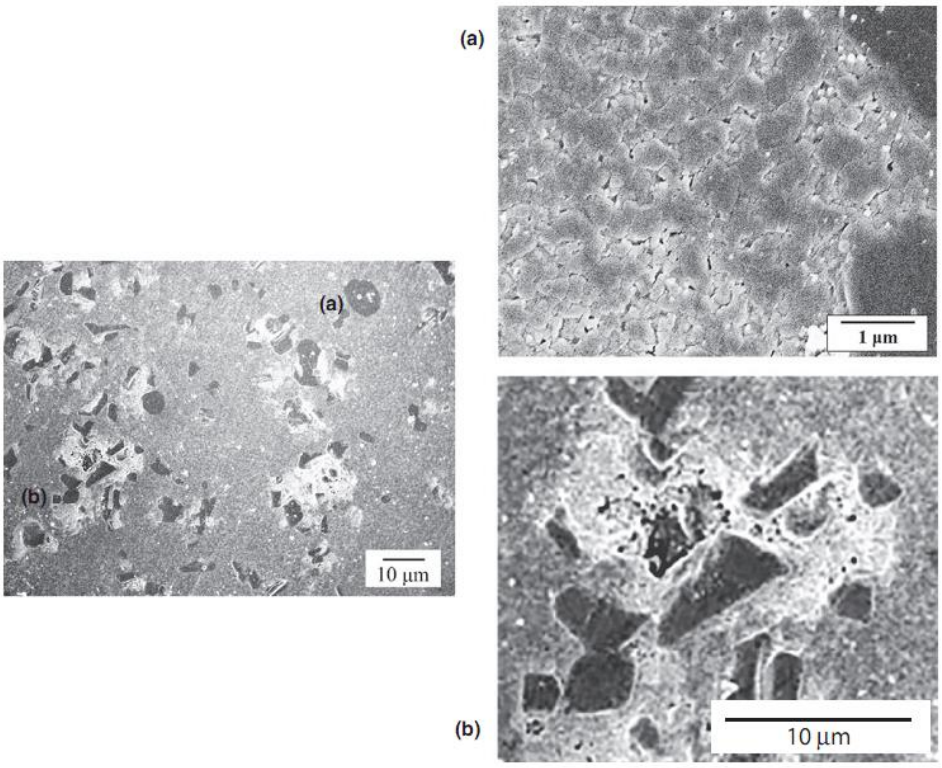

Figure 7.7 Micrographs from flash-sintered 19 vol% Al_2O_3 specimen showing good densification in the neighborhood in single alumina inclusion (a), and low densification in regions where alumina inclusions are clustered (b).

It may also be argued that the titania particles within the cluster remain porous because of the mechanical rigidity of the alumina clusters within which they are embedded. The counter argument is that if these titania particles would have sintered then they would have left behind large pores. Instead we see porosity that resembles the porosity in the green samples.

7.4.4 X-ray diffraction

The diffraction data are shown in Fig. 7.8. Diffraction spectra for pure Al_2O_3 and pure titania (CHR-FS-0) are shown as the baseline. Isothermal sintering with and without flash shows only the presence of alumina and rutile (titania). We do not find the presence of any new phase

under flash sintering, such as $TiAl_2O_5$ which according literature, starts to form beyond 1280 ^oC and becomes kinetically favorable beyond 1350 ^oC [103], [104].

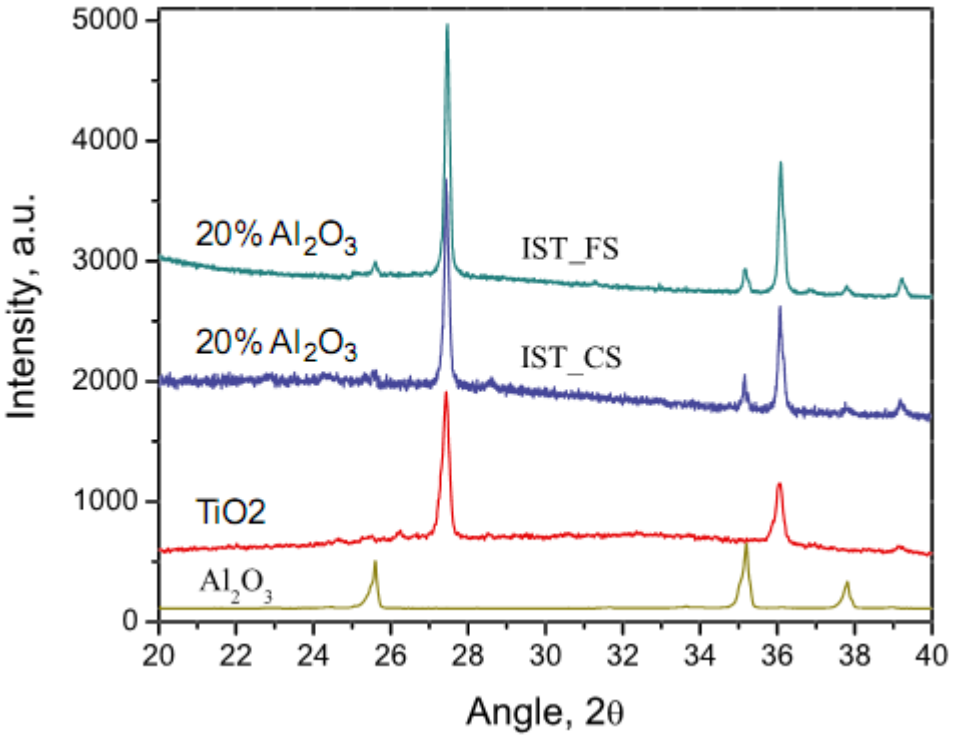

Figure 7.8. Diffraction pattern from FS and CS specimens obtained at constant furnace temperature compared with the spectra from single phase titania and alumina.

7.5. Discussion

The objective of this work had been to determine the difference in constrained sintering behavior with and without electric fields. Earlier work on pure titania with alumina inclusions [71] served as the baseline for the present study. In pure titania it had been shown that flash sintering occurs at 250 Vcm^{-1} at a furnace temperature of ~ 825 ^oC [11].

In conventional sintering, pure titania sinters to full density at 1150 ^oC, but the composite with 19 volume % alumina-inclusions shows the titania matrix to sinter to only 67% (Fig. 7.3).

Under electrical field, all samples, with and without alumina inclusions, sinter at 825 - 850^{o}C, proving that the phenomenon of constrained sintering, prevalent in conventional processing, is abated under flash conditions. As shown in Figs 7.5 and 7.6, full densification is reached within within 5 seconds of reaching the peak in the power density (Stage II).

It is notable that the power dissipation in Stage III increases with the alumina content (Table 4.3). The power supply in Stage III is current-controlled; therefore the power dissipation is given by I^2R, where I is the current and R, is the resistance. An increase in the resistance of the specimen due to alumina-inclusions increases power dissipation.

As explained in introduction, the uniform volumetric shrinkage is impeded by the shear stress generated in the matrix by the presence of rigid inclusions. In conventional experiments, shear deformation involves longer diffusion distance than densification (Fig. 7.1), which can result in the rate of shear deformation to be significantly slower than the rate of densification. Under constraining conditions, the sintering rate slows because it becomes controlled by shear relaxation.

In the present work we see that the addition of large and rigid alumina inclusions does not affect flash sintering of the titania matrix. Such abatement of constrained sintering is possible only if the shear stresses can relax as quickly as they are produced by densification of the matrix. We explain this behavior by a different mechanism, whereby vacancies and interstitials are generated within the grain matrix under the influence of the electric field. Densification is achieved by the interstitials migrating to the pores and the vacancies to the grain boundaries, which effectively transports mass from the grain boundaries to the pores. Shear deformation is similarly achieved the interstitials moving to the boundaries under tension and the vacancies to the boundaries under compression. The great difference from the conventional mechanism is that the diffusion distance

for both shear deformation and densification are now equal, as illustrated in Fig. 7.9. Since shear deformation can now occur at the same rate as densification the phenomenon of constrained sintering is obviated.

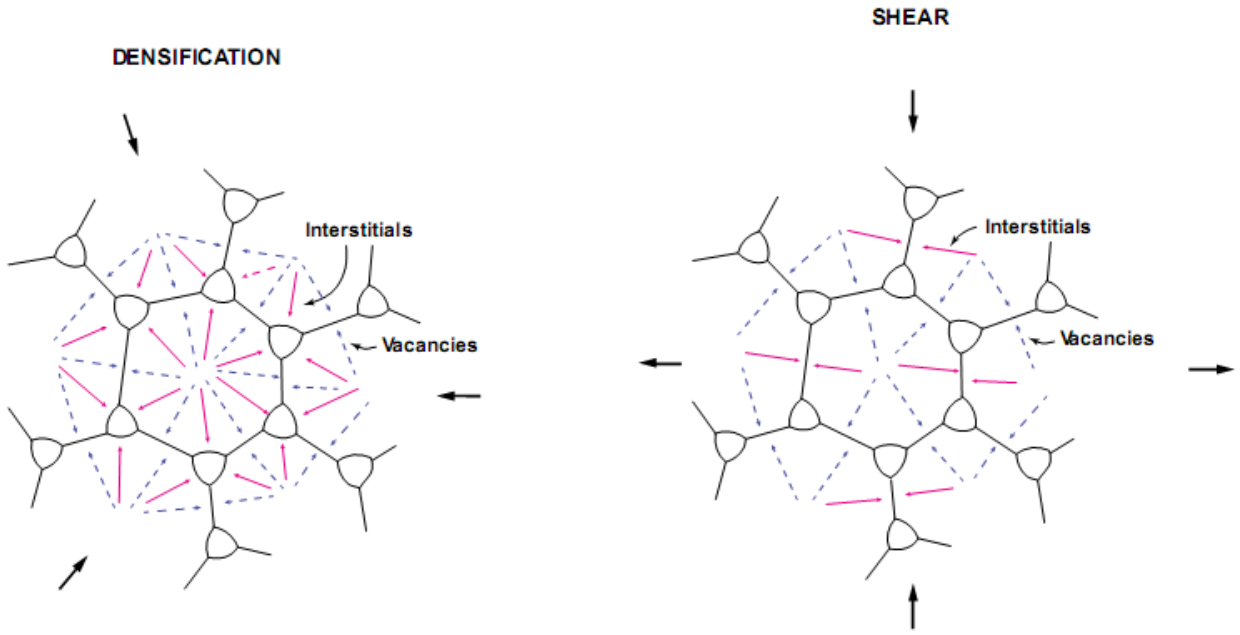

Figure 7.9 Shear deformation and densification under flash. Diffusion distance is same for both the processes, which explains the suppression of constrained sintering.

It can be argued that the higher temperature of the specimens containing alumina particles, during the flash, as listed in Table 4. 3, could have assisted in the sintering of the composites. The specimen temperature is shown to increase with the volume content of alumina, with the value being 1170 ^{o}C in constant heating rate experiments, and 1144 ^{o}C in the isothermal experiments. These temperatures are certainly not high enough to produce sintering in the composites. For instance, the highest volume fraction sample reached a density of only 67% at 1150 ^{o}C in conventional sintering. Also the nature of the data for flash sintering for samples of various volume fractions of alumina is remarkably consistent, that is the onset of the flash occurs at essentially the

same point. If the specimen temperature because of Joule heating had been playing a significant role, there would have been a systematic shift in the sintering behavior with increasing volume fractions of the alumina inclusions. But, we do not see such things.

It is noteworthy that the sintering of multilayers, made with layers that sinter at different rates, is also abated in flash sintering [51], a result that is consistent with the present experiments.

8. Chemical reaction under flash

8.1 Disclaimer

This was a collaborative effort with Dr. J. M. Lebrun and will be submitted for publication in Journal of American ceramic society [105]. The author was responsible for the experiments. Co-author Dr. Lebrun helped in the synchrotron experiments and gave critical inputs on the draft preparation and analysis of some of the data. Dr. W. M. Kriven's expertize helped us in setting up the experiment at Synchrotron source. The experiments have been supported by the Basic Energy Sciences Division of the Department of Energy under grant number DE-FG02-07ER46403

8.2 Introduction

Al_2TiO_5, Aluminum titante is a well-known material for high temperature applications such as furnace lining owing to its very low thermal coefficient of expansion and high melting point. According to the phase diagram, alumina and titania react together to form spinel aluminum titanate at 1280°C as per the reaction Eq. 8.1.

$$\alpha - Al_2O_3 + TiO_2 \Leftrightarrow \beta - Al_2TiO_5 \qquad (8.1)$$

Over the years many formulation methods have been implemented or studied, such as hot pressing [104], combustion synthesis [103], solid state reaction with fine powder and single crystals [106] [107], ball milling [108], reaction sintering [109], chemical route [110]. Doping with MgO, SiO2, ZrO2, Fe2O3 [111]–[113] [114] has also been used to reduce the transformation temperature of AT synthesis. In this work, we present another method for synthesis of Aluminum titanate at 830°C furnace temperature with the help of electric energy and the process named as“flash”.

Flash sintering is a process of sintering ceramics with electric energy in addition to thermal energy, which gives full densification within few seconds at a much lower temperature than conventionally needed [1]. The method has been successfully used to sinter many ceramics [10], [11], [38], [46], [52], [115], [116] [57], [56]and composites, such as zirconia, titania-alumina [55]and zirconia-alumina [54]. For the first time, we have tried to observe the effect of electric field-current on chemical kinetics, which has shed light on the mechanism of flash itself.

8.3 Experimental set up

Titania nanopoweder of particle size 20 nm were mixed in with 20 vol % (18 wt. %) of alumina power with average particle size 300 nm. The method of preparation is same as that of section 4.2.3. Two kinds of experiment were done, one in-house experiments with regular dog-bones as shown in Fig. 4.1 and another kind at synchrotron with bar shaped samples. Powders were uniaxially pressed under 105 MPa into respective shapes.

Only isothermal tests were performed with flash experiments at 830°C (in-house) and 900° C (synchrotron) respectively. The specimen temperatures were estimated by black body radiation models, section 4.6.1, Eq. (4.14) and verified with peak shift of Pt. (111) (for *in-situ* experiments

only) as a result of lattice expansion during flash. Green composites were also conventionally heated at equivalent temperature, obtained by black body radiation, to be compared with flash results.

To quantify the extent of chemical reaction between alumina and titania to form aluminum titanate, according to Eq. 4.2, XRD RIR technique [76] was employed (section 4.4.3). Silicon was used as internal reference. Powder of silicon was mixed in with equal amount of specimen powder by weight and diffraction pattern is obtained. On comparing the peak intensity of alumina with that of Silicon (111) peak, it gives us an estimate of amount of alumina present in the specimen. A calibration curve was obtained between the peak intensity ration and alumina present by mixing a known amount of alumina with silicon, Fig. 4.7. Equations relating the peak ratio with alumina were also derived along with an idea about possible error in our estimate.

8.4 Results

8.4.1 The guiding map

The experimental map is shown in figure 8.1 (a) with two variables: current density and hold-time under flash. The region A corresponds to low current density and low holding time. An example is shown in figure 8.1 (b), with a current density 15 $mAmm^{-2}$ and flash hold time 20 seconds. The linear shrinkage shows full densification in less than ten seconds with no detectible chemical reaction.

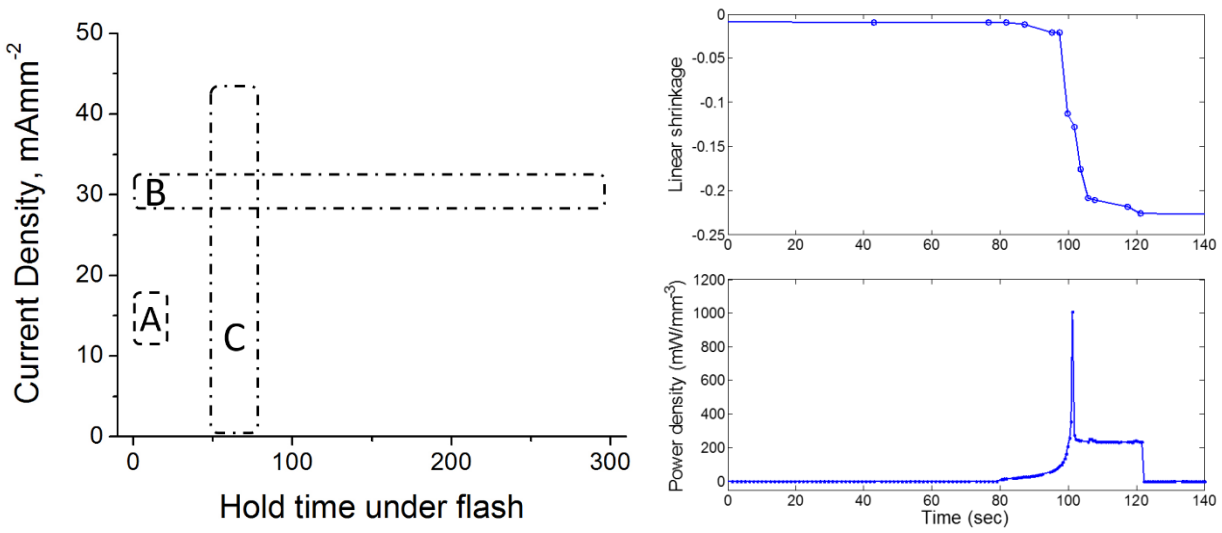

Figure 8.1 (a) Schematic representation of the area of investigation of the current density v/s hold time plot. (Fig 4.6) (b) Densification curve corresponding to point A, with the current density of 15 $mAmm^{-2}$ for 20 seconds along with power dissipation.

The region 'B' corresponds to a higher current density (30 $mAmm^{-2}$) with varying flash hold-time experiments, ranging from 10 sec to 300 sec. At this current density, while the densification is over within 5 seconds, the chemical reactions starts almost instantaneously and continues to happen at depleting rate with time. Third region is varying current density, region C, for a fixed hold time under flash (60 sec).

8.4.2 Current density

First of all the effect of current density was studied. On the left of Fig. 8.2, XRD pattern for a small window of 2θ (bragg angle) shows that peak corresponding to Aluminum titanate (triangle symbol) grows at the expense of alumina (square symbol). With rising current density, not only the flash effect is enhanced but also the temperature of the specimen because of joule heating. This effect is illustrated in right side of Fig. 8.2 where for a fixed hold time (60 sec) the

gap of chemical reaction between the conventional heating and flash results grows with higher current density (higher temperature).

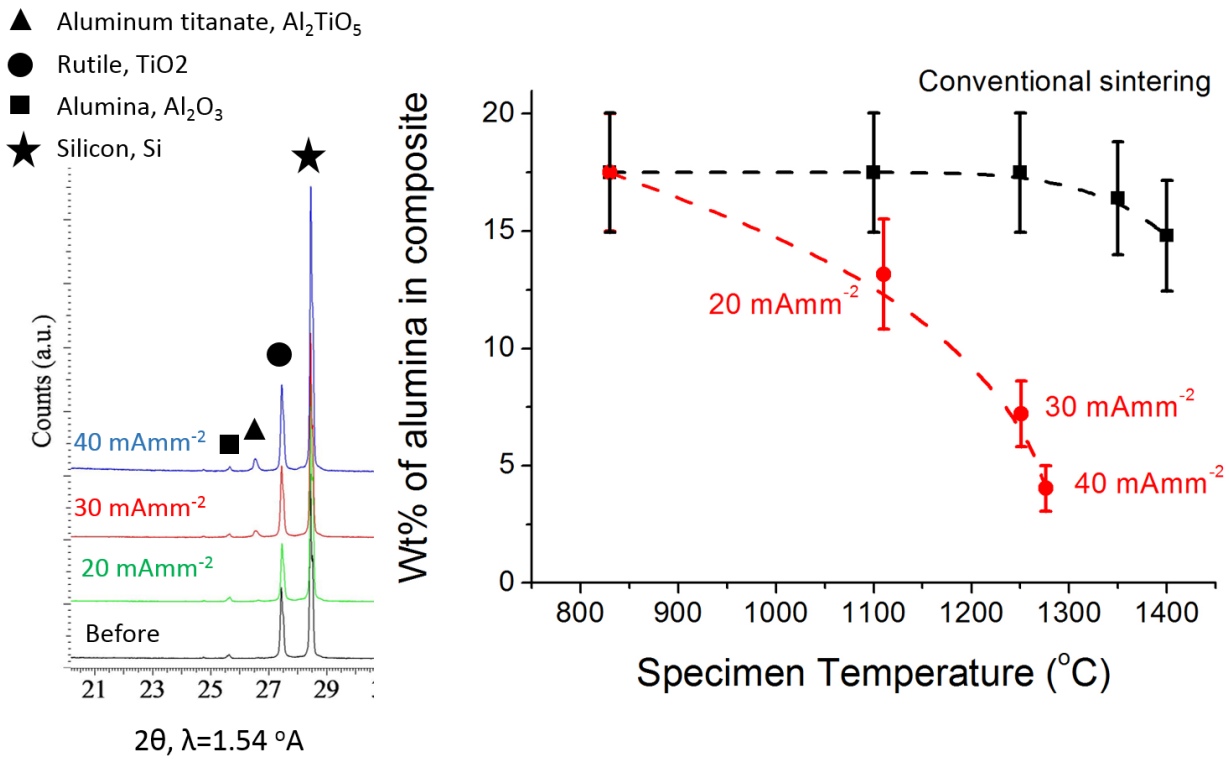

Figure 8.2 Plot of depleting alumina in composite as a function of current density for 60 sec of flash. Current density has been converted into specimen temperature and corresponding conventional sintering results are also included.

8.4.3 Hold time experiments.

Based on Fig. 8.2, 30mAmm^{-2} was chosen for hold time study, since the kinetics of reaction are neither too fast, nor too slow. The hold time under flash was varied from 10 sec to 300 sec. The depleting alumina content and corresponding power dissipation values has been plotted with time in Fig. 8.3. Since power dissipation is directly related to the specimen temperature by black body radiation model with emissivity of 0.9 for oxides [2], the equivalent temperature axis is also

drawn parallel to power density. It is clear from the figure that power increases rapidly from 350 $mWmm^{-3}$ at the initiation of flash and then levels off as the chemical reaction slows down. It is also important to take an account that although temperature of specimen rises during the experiment from ~ 1150°C to 1250°C, the maximum value of temperature (1250°C) has been considered for comparing flash with conventional heating,.

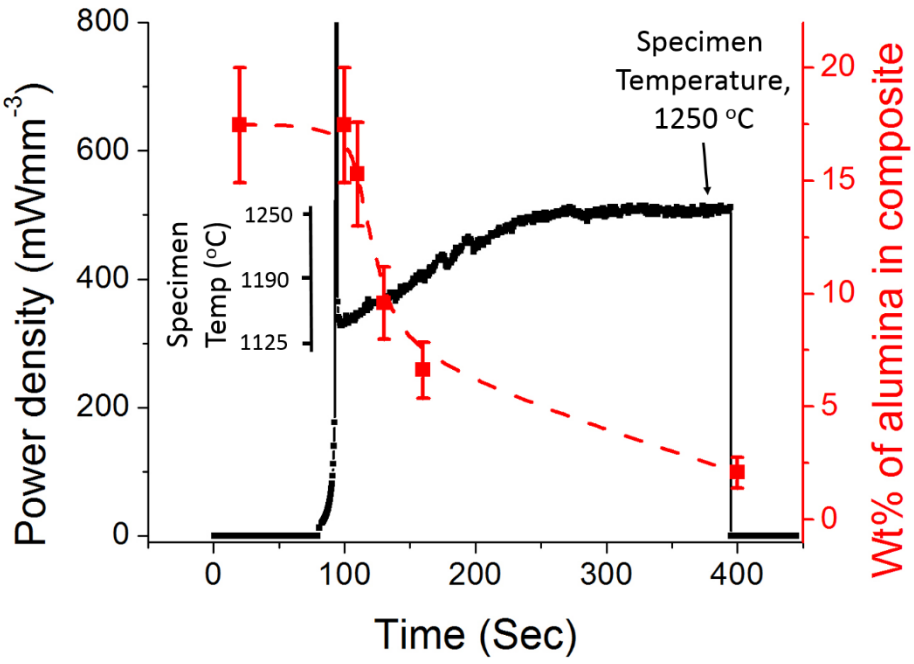

Figure 8.3 Rise in power density during chemical reaction. Temperature was calculated by black body radiation model [2].

As mentioned in experimental section, weight % of alumina remaining in composite has been calculated by the XRD relative intensity ratio (RIR) method [76]. An example of this method has been shown in Fig. 8.4 where intensities of XRD pattern have been plotted against 2θ from 20° to 50°. The intensity of peaks (in a.u.) corresponding to different phases vary with respect to each other in different scans, that are related directly to the amount of the phase in the powder.

Fig. shows that flash experiment with 30 $mAmm^{-2}$ leads to reaction in 60 sec compared to conventional heating at equivalent specimen temperature (1250°C) for 5 hours with no visible peaks of aluminum titanate Al_2TiO_5.

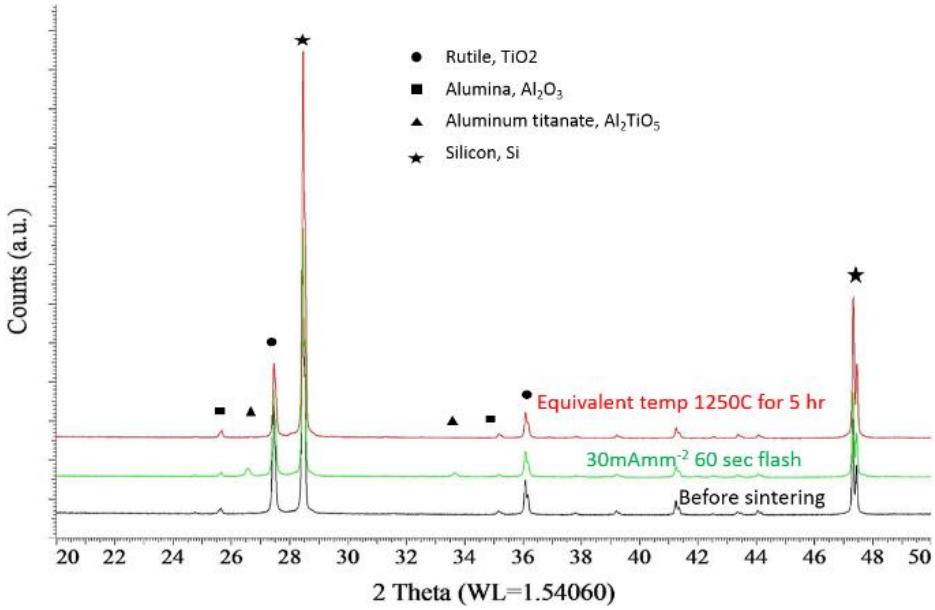

Figure 8.4 Comparison of flash with equivalent temperature calculated by black body radiation, 1250°C for 5 hours.

A similar scan for flash experiments with increasing hold time has been shown on the left of Fig. 8.5. The kinetics of chemical reaction has been analyzed in terms of depleting peak intensity of alumina with respect to that of silicon, using Eq. (4.2). All these results have been consolidated in Fig. 8.5 that shows the amount of alumina diminishing with time under flash compared with conventional heating at temperature 1250°C and 1430°C. No apparent peak of aluminum titanate (Al_2TiO_5) was observed for keeping specimen at 1250°C even for 5 hours as is evident from Fig. 8.4, so a much higher temperature (1430 ^oC) of furnace was used for comparison of kinetics of this transformation. For the flash experiments, the time axis begins when the temperature of the furnace reaches 830°C but electric field is switched 'ON' only after the dwelling time of 100 seconds. The

power supply switches into current modes in the lapse of few seconds because the electric field applied was high (500 V/cm). The chemical reaction is found to be very fast in the beginning but slows down as the alumina content in composite depletes. On comparison with conventional heating, flash was still found to be much faster than 1430°C.

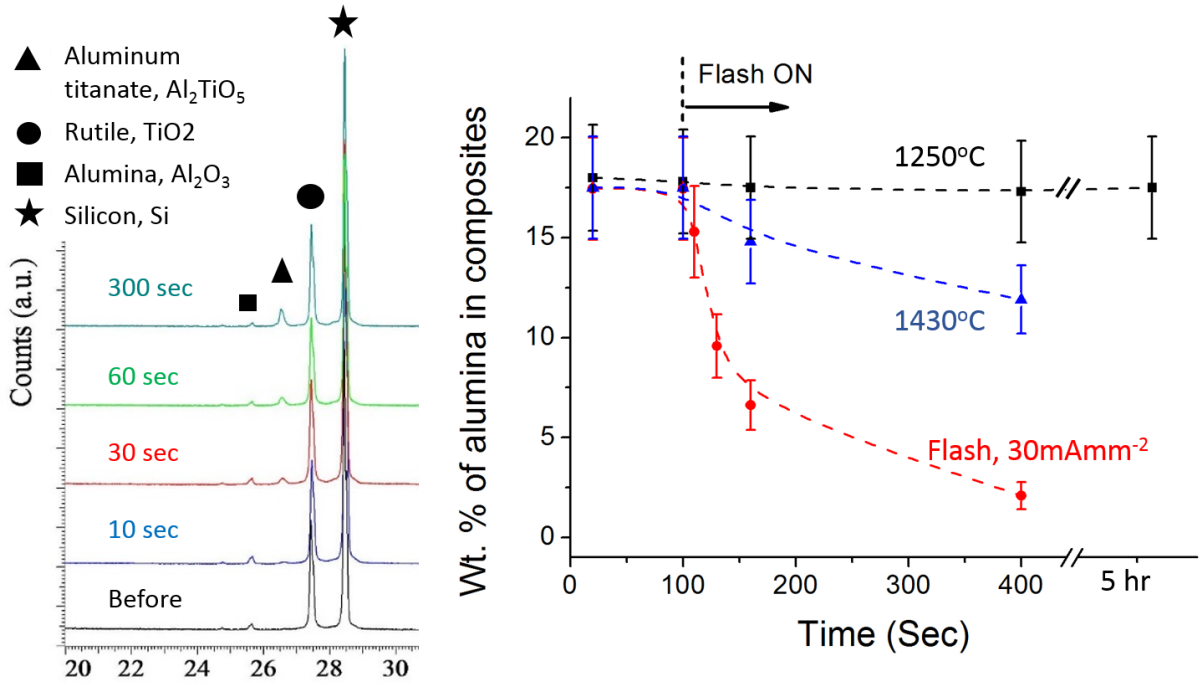

Figure 8.5. XRD pattern for flash hold experiment and kinetics of chemical reaction with flash, compared with conventional sintering at equivalent temperature. Flash starts after 100 seconds of dwelling at 830 °C.

8.4.4 In-situ experiment

Based on the results of hold time experiments, in-situ chemical analysis under electric field at elevated temperature was performed at Synchrotron. The sample was flashed at 900°C

with the help of 500V/cm and the power supply instantly switches to current control mode with the current limit set at 20mAmm^{-2}. The flash is kept 'ON' for another 250 sec before the current limit is pushed up to 25 mAmm^{-2} and held for 400 sec till the reaction gets completed. The XRD spectrum of specimen are measured every second, each one of which contains peaks of alumina, titania, titanium aluminate and platinum. Examples of these spectrum are shown in Fig 8.6 for time 250 sec and 600 sec. Intensity of a peak indicates the quantity of that particular phase while shift of peak in 2θ is a function of lattice expansion because of temperature [36] [63]. Although the depletion of alumina peak is apparent with 20 mAmm^{-2}, formation of $TiAl_2O_5$ becomes evident only when the current density is changed to 25mAmm^{-2}. It is important to note that even with current density as small as 20mAmm^{-2} a small peak corresponding to $TiAl_2O_5$ appears in spectrum 1 within 250 seconds of flash.

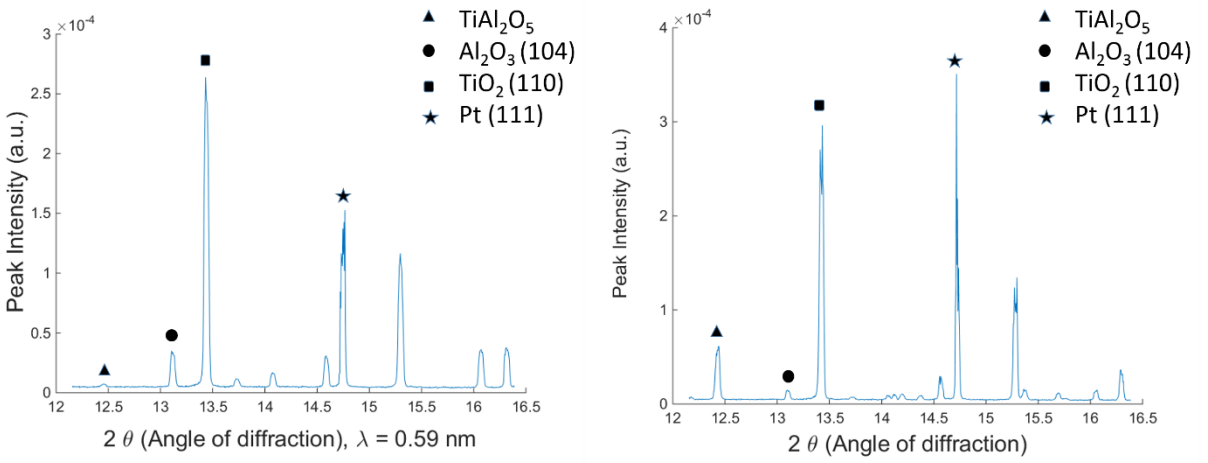

Figure 8.6 The local scan spectra for λ=0.59 nm (a) at 250 sec and (b) 600 sec of the flash experiment shown in Fig. 8.7.

The electrical parameters, peak intensities of different phases and specimen temperature obtained from in-situ experiments were synchronized with time and presented in Fig. 8.7. A jump

in current density to 25 mAmm^{-2} happens at time = 275 sec and resultant change in chemical reaction kinetics can be seen in subplot (b) of the same figure.

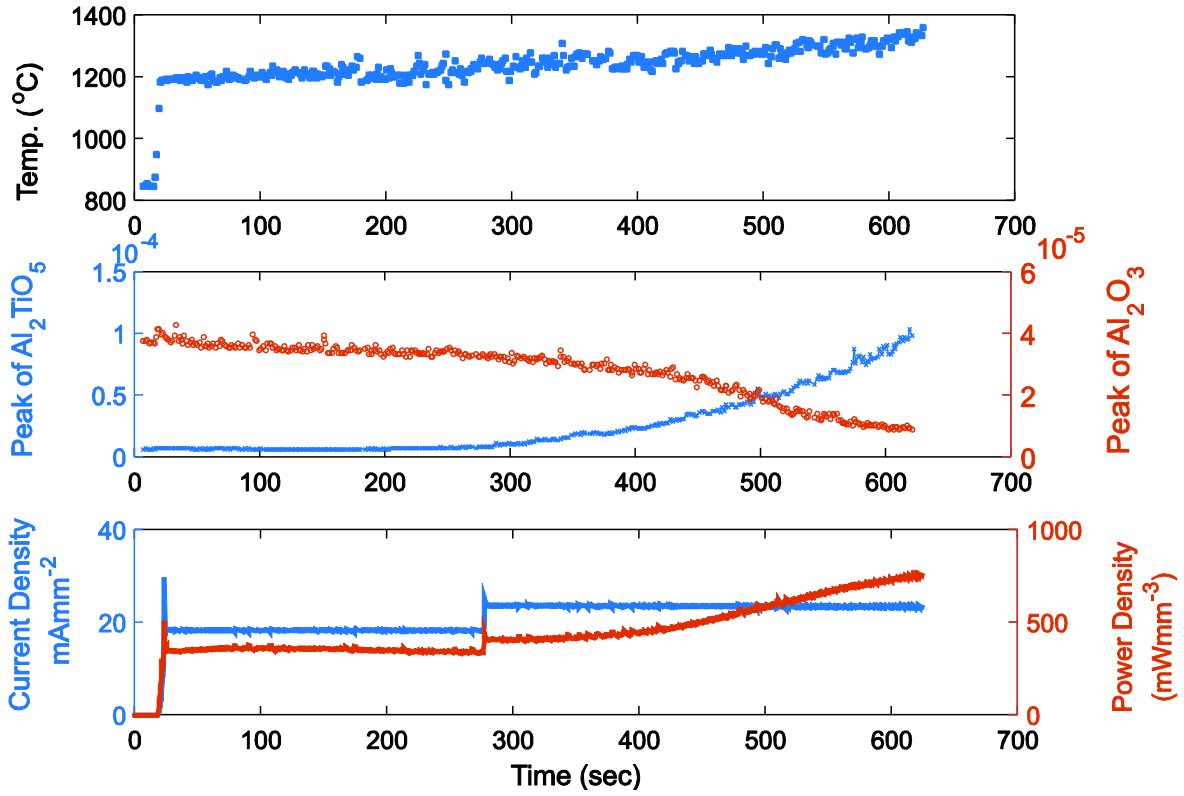

Figure 8.7 Relation of (a) power density and current density, (b) reaction kinetics of alumina and aluminum titanate and (c) specimen temperature of the in-situ experiment have been plotted with respect to time.

The temperature of specimen during the flash experiment, based on the calibration curve for platinum in Fig. 4.9, is shown in subplot (c) of Fig. 8.7. The temperature remains in the range of 1200°C to 1250 °C for current density of 20 mAmm^{-2} and then rises slowly to 1350°C. The black body radiation model gives range of 1150°C to 1300°C for the same experiment, which is in close proximity with synchrotron results. The little lag in black body radiation calculation can

be because of the change in the dimensions of bar during sintering at the earliest stage of flash, which has not been considered in this work. The comparison of black body radiation with synchrotron measurements have already been listed in table 4.5.

8.4.5 Stage II verses stage III

To understand whether the chemical reaction is a stage II (where most of the sintering happens) or stage III (where chemical happens) phenomena, cyclic flash experiments were performed. An example of it is shown in Fig 8.8 (a) with two sets of experiments: cyclic flash with 3 flashes each of 10 sec compared with one continuous flash of 30 sec.

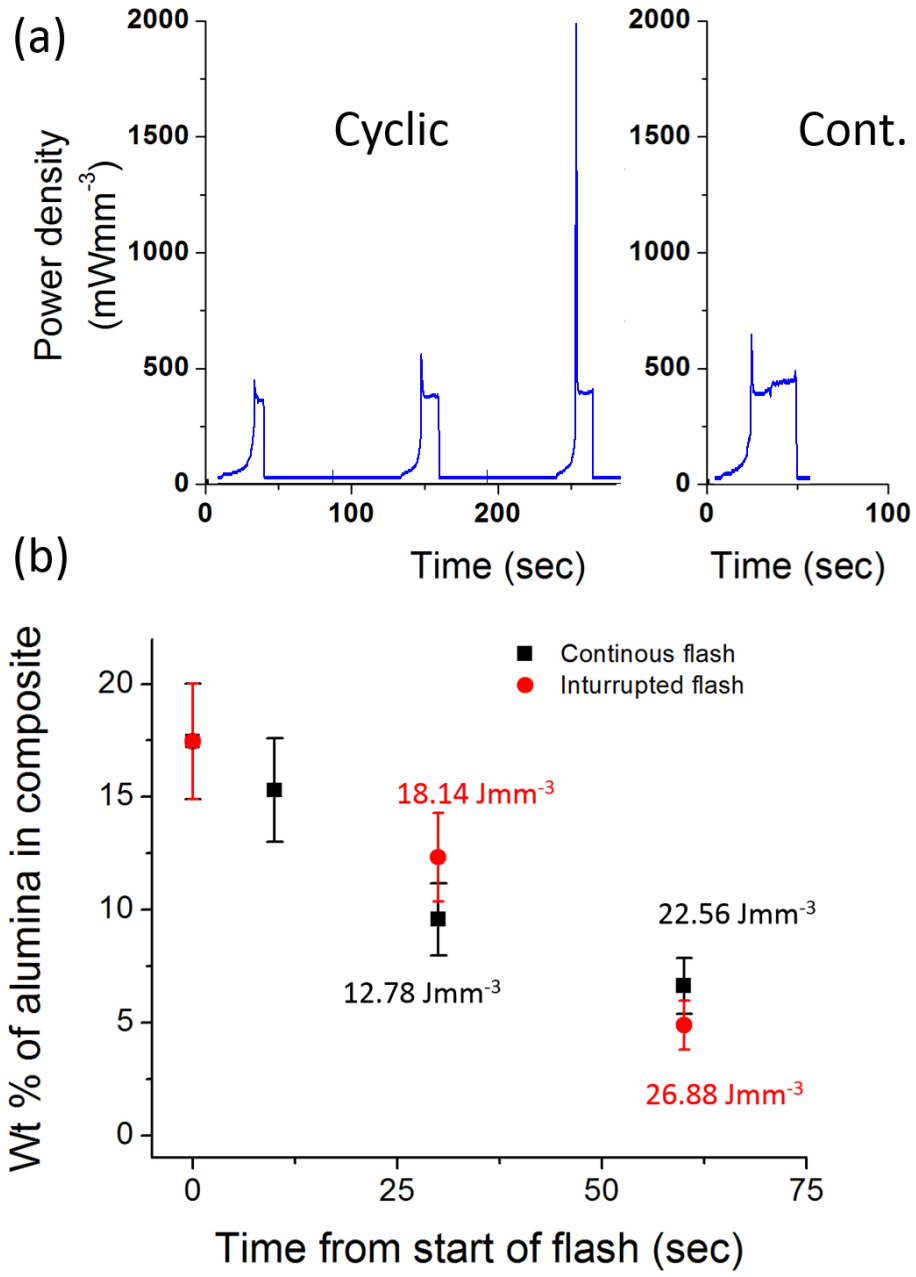

Figure 8.8. (a) An example of cyclic and continuous flash for total of 30 sec (b) Comparison of stage II or stage III in terms of alumina remained after flash.

Two data point have been compared, for 30 sec and 60 sec. If these experiments were to be done for less than 30 sec, flash width of each cycle needed to be smaller than 10 sec and for higher than 60 sec, contribution of power spikes (in terms of total electrical energy/volume) would

significantly higher compared to stage III. So only 30 sec and 60 sec cyclic experiments are considered here. Although the total energy dispensed was higher for cyclic flash experiments (because of power spikes), the extent of chemical reaction were found to be in the error range of each other. The electrical energy expended during the flash experiment, which is the integration of power density curve with time, have also been shown.

8.5 Discussion

A lot of stress has been given in the earlier papers on the contribution of stage II on densification and claimed the extraordinary rise in temperature being the cause of quick densification. Since this transition is too fast to be measured even at synchrotron, no clear consensus has been reached about the possible mechanism behind flash sintering. While Chen *et al* [40] and Steil [62] claimed it to be joule heating alone, Narayan [60] suggested melting at grain boundary (by grain boundary heating) that assists sintering. Raj and coworkers [2], [9] have proposed the theory of Frankel pair defect generation under the effect of electric field as the possible mechanism that can explain rise in sintering rate by three orders of magnitude, optical luminescence [63], and concomitant rise in conductivity [65], [98] with controlled grain growth. Estimate of specimen temperature by Raj [2] on the theory of black body radiation was found to be a few hundred °C below conventional sintering temperature, which were supported by *in-situ* XRD measurement at synchrotron [63].

The electric field has shown chemical reaction to occur at a temperature as low as 1110 °C, well below thermodynamic limit for the phase transformation (1280 °C) [117], [112]. The specimen temperature was thoroughly examined by tracing the shift in (111) peak of Platinum and was found to be in good agreement with estimate from black body radiation model. Expected

temperature gradient from surface to the middle of the specimen thickness has also been examined, by Lebrun and Raj [unpublished data]. As higher temperature cause the peak to move to left (lower bragg angle), temperature gradient would cause the diffraction at varying angles and widen the peak. No such broadening was observed in the stage III, which suggest the temperature of specimen during flash remains same through the thickness.

Earlier study by Mocellin [107] on single crystals of titania and sapphire has establish that reaction is controlled by diffusion of Al_2O_3 specie through Al_2TiO_5 at 1500 °C. We find that flash enhances the kinetics of chemical reaction dramatically when compared to conventional heating. On plotting the reaction kinetics under flash with respect to time on a log-log plot, as shown in Fig. 8.9, we find that slopes of the two experiments were ~ 0.5 which corresponds to diffusion controlled parabolic behavior.

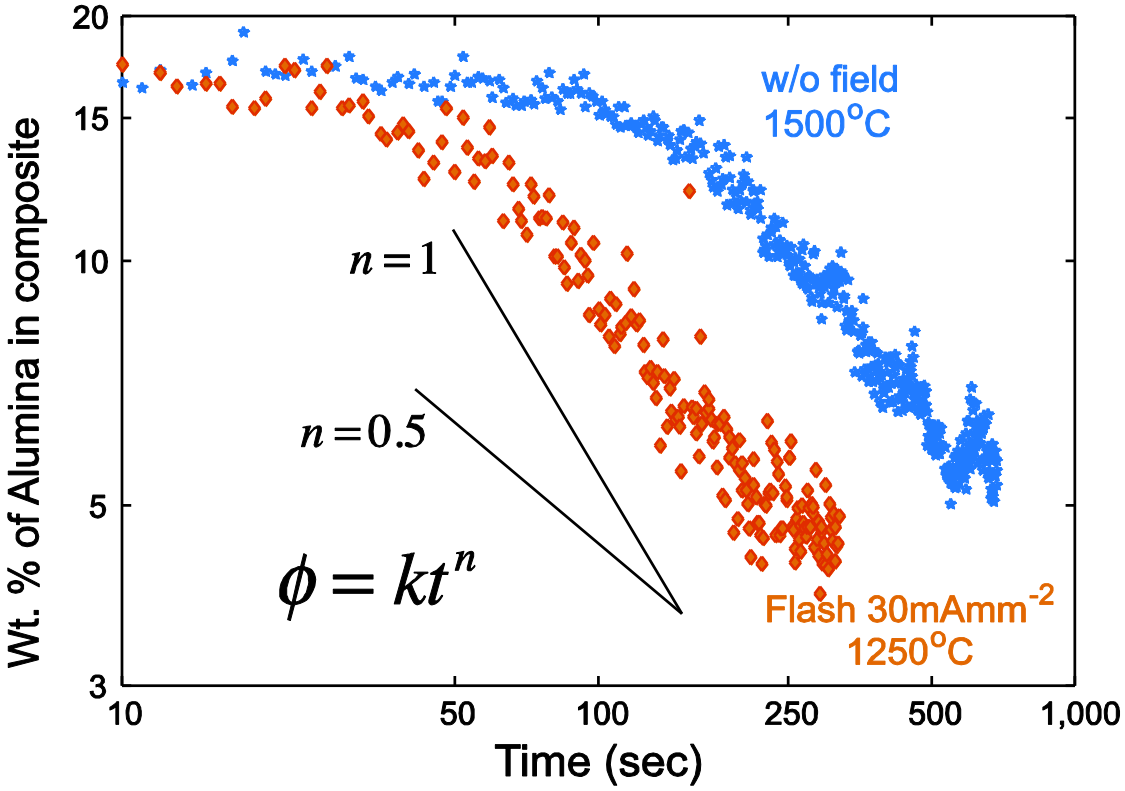

Figure 8.9: Log-log plot of alumina with hold time from live experiments at APS.

It is important to understand that a major difference between sintering and chemical reaction is that while sintering and densification is mostly driven by grain boundary diffusion, the reaction happens when the matter diffuse through the layer of new phase to react on the other side, that is volume diffusion. In the work of Jha *et al* [55] too, it was proposed that defects (vacancy and interstitials) generate within the grains migrate to grain boundaries and pore to produce both volumetric and shear strain at equal rate which is necessary to overcome constrained sintering. If flash were only grain boundary effect [60] then the rate of chemical reaction could not have been enhanced to the extent we see here, as it would be diffusion limited thought the aluminum titanate, Al_2TiO_5, phase. At the same time, assumed local temperature rise during power spike [62] cannot account for this result either since reaction occurs in stage III which have been systematically

studied under synchrotron in earlier studies [63], [70] and the temperature was found to be well below than what would be needed to accomplish the results. This work, in return, also suggest that the power spike in stage II is not very different from stage III of steady-state flash based on the similar extent of chemical reactions for the two scenario, which has earlier been tried to explain quick densification on the basis of partial melting at grain boundaries [60]. In the end, we conclude that generation of defects under flash, which is a volumetric phenomenon, can explain the accelerated reaction rate of TiO_2-Al_2O_3.

9. Conclusion

9.1 Summary

Any mechanism which can be proposed to elucidate the phenomena of flash sintering must at the same time explain all the other behaviors associated with flash, such as, (i) three orders of higher sintering rate, compared with conventional sintering (ii) abrupt, simultaneous non-linear rise in conductivity (iii) optical-luminescence which is different from that of black body radiation [63] (iv) near universality of application across all varieties of ceramics (v) obviating constrained sintering (vi) new phase formation and development of texture in grain orientation (vii) meta-stable phase formation and (viii) improved kinetics of chemical reactions. An important point to note in flash sintering is that while sintering requires charge neutral transport making it limited by slowest diffusion species, ionic conductivity in ceramics is controlled by fastest moving ion.

Joule heating has been proposed by many authors to explain this behavior, but it still falls short of the required number (in terms of temperature) to explain such a high rate of sintering. Black body radiation model and pyrometric measurements [2] estimated the specimen temperature to be a few hundred °C below the typical conventional sintering temperature, which was, later on, also validated by synchrotron experiments [63]. Narayan [60] suggested localized heating at grain boundary which was invalidated by Holland [61] by explaining that such a temperature gradient

is impossible across the grains of 100 nm. It is clear from the above reasoning that temperature rise during flash because of Joule heating cannot explain sintering behavior.

A mechanism was proposed by Raj and coworkers [1], [2], [9] suggested that electric field at elevated temperature induces Frenkel defect pairs (a vacancy and an interstial) in the lattice. These defects then loses their charge (giving out electron and hole pairs) and become charge neutral. These charge neutral vacancies and interstitials are free to move under the bias of the sintering pressure to grain-boundaries and pores respectively, which in effect is same as movement of matter from grain boundary to pores. This charge independence explains the absence of any directionality that can be influenced in the DC electric field. At the same time, the generated electron-hole pairs explain the electronic nature of conduction and the peak in the optical emission spectrum because of occasional recombination of these pairs. There are two important things to notice while comparing conventional densification with densification under flash sintering: (i) there is avalanche of defect generation and (ii) the species of the ceramic are able to move independently of each other. These two factors enhance the sintering behavior by orders of magnitude.

Now, we come back to the results of this thesis:

- ***Flash sintering of titania*:** The two regimes: enhanced densification under electric field (Type A) and flash sintering (type B) are established. Sudden rise in conductivity and concurrent densification suggest a fundamentally different diffusion mechanism under flash. Mode of conduction was found to be electronic, in Type B, compared to mixed (ionic and electronic) conduction, at low field, as determined from Arrhenius relation of

conductivity with temperature. Effect of flash on grain growth is analyzed where a minima was found at the transition point of Type A to Type B (150 V/cm).

- **Texture evolution**: Titanium dioxide (TiO_2) is found to change structure under the electric field. The field induces texture that appears and vanishes immediately when the applied field is turned on and off. The results differ from 3YSZ [70] where a new phase develops under flash and the process is diffusion controlled. The diffraction peaks fluctuate sporadically suggesting a stochastic phenomenon and martensite like transformation in case of TiO_2. A coupling between the phonons and structural changes induced by electric field are proposed.

- **Constrained sintering**: Constrained sintering arises because of the difference in densification rates of two phases that leads to generation of shear stresses that must be relieved for densification to proceed [71]. The longer diffusion distance for shear deformation in comparison to densification, means that densification rate becomes controlled by shear deformation which is considerably slower. We show that constrained sintering induced by the incorporation of large alumina inclusions in titania can be abated in flash sintering, regardless of the volume fraction of alumina. This result is explained by the generation of vacancy-interstitial pairs within the grain matrix of titania that migrate to the grain boundaries and the pores in a similar way to produce both shear and densification strain. Thus, shear deformation occurs at the same rate as densification, and the influence of constrained sintering is largely eliminated.

- **Chemical reaction**: Effect of flash on phase transformation has been studied in stage III. We find that beyond a certain current density ($15mAmm^{-2}$ for titania-alumina composite),

flash effect leads to chemical reaction forming a meta-stable phase and with faster kinetics than conventional heating at higher temperature. The mechanism of reaction in under flash was found to be interface dependent compared to diffusion dependent for conventional heating. Synchrotron source was used to establish the temperature of specimen which agreed with the estimate given by black body radiation model within acceptable range. Defect generation in bulk, rather than a grain boundary effect, under electric field could lead to formation of charge neutral independent species which can explain this enhanced diffusion of species through the volume and explain the high rate of reaction.

The results mentioned in this thesis have been explained on the basis of the proposed mechanism. While the first two works suggest the defect generation that affects the conductivity mechanism and evolution in texture of grain orientation under electric field, the last two works can be explained only by the volumetric defect generation.

9.2 Future work

A number of future experiments have been identified during the period of this research. A few of them are enumerated below:

Grain growth in titania: To further investigate the diffusion mechanism under flash, a grain growth study in titania can be useful, while densification is too rapid in stage II for close observation, grain growth in stage III can be reasonably easily to monitor. Samples can be quenched at regular interval and observed under microscope to quantify the grain size. A determination of the diffusion mechanism can be made based on grain growth rates and their variation with temperature and current density.

Doping with flash sintering: Certain super-saturated solutions of ceramics phases could potentially have significantly improved properties as sensors and the like. Such super saturated solutions are not thermodynamically stable under normal conditions. Flash sintering has been shown to stabilize meta-stable phases at temperatures lower than as suggested by the phase diagrams. Therefore an investigation can be undertaken to explore this possibility.

Metal ceramic composites (Cermets): Cermets can combine desirable properties of toughness of metals and hardness of ceramics. However they sinter at different temperatures and if done in open atmosphere metal would oxidize before ceramics grains could sinter together. With the use of flash, these temperatures are be brought close together. It has also observed that under flash the wetting behavior of metal with ceramic can be improved and nano-penetration of phases has been observed. Further work is warranted to understand this wetting behavior.

EXAF study under flash: Defect generation mechanism within a grain can be investigated by determining the coordination number of a given specie in the lattice. An EXAF (Edge X-ray Absorption Fine Structure) study can be used to determine this. An in-situ isothermal EXAF study with and without flash could be utilized for this purpose.

Superplastic deformation: Ceramics can be deformed into complicated shape using superplastic deformation. Flash sintering can be investigated as a mechanism to reduce the temperature required for the superplastic deformation since it has been shown to enhance the volumetric diffusion in bulk material.

10. Appendix

10.1 Appendix A – On the controversy of joule heating

The extensive review of this manuscript reveals a deep controversy about the mechanism of flash sintering. A highly non-linear rise in conductivity is a signature of this event, which leads us to the rather simplified perception that the sample is suffering a very high level of Joule heating, enough to account for sintering in mere seconds. Indeed that was our impression as well in the first paper published in November 2010 [1]. There are at least a few points that can be made on this issue.

It is becoming increasingly clear to us electric fields *and* currents can influence defect generation and transport in more than one way. What may apply at very high current densities may not be true at low currents. Claims are made in the literature, for example in [40], the samples show melting behavior; however, in this paper there is no information about the current densities used in the experiment: certainly if the current is allowed to rise in an uncontrolled way then I^2R heating will eventually lead to melting. Care is needed when comparing results from different experiments. Just as deformation mechanism maps caution us to recognize that the material response depends on temperature and stress, so does the electrical response of a material depend

upon the field, the current and the temperature. It is critical to state exactly the current density, the field and the temperature when describing the material response. Extrapolations from one mechanism-regime into a different regime can lead to incorrect conclusions [60].

Two papers have discussed the influence of electric field and current on the temperature of the specimen. They are Baraki et al [36] and Raj [2]. Please note that the Raj paper builds on the Baraki et al. paper. When reading these papers please recognize that there are the two regimes of power dissipation. The experiments begin by applying a constant voltage to the specimen, which at a threshold value of the temperature produces a highly non-linear increase in the conductivity (for reasons that we do not understand). In this regime, Regime A, the power dissipation is given by V^2/R; as the resistance falls the power dissipation rises. When the current reaches a preset limit the power supply switches to current control, which happens in 20 ms according to specifications. This is the second regime, Regime B, where the power dissipation is now given by I^2R; the power dissipation now declines since the resistance continues to fall, and quickly reaches a steady state (for reasons that we do not yet understand).

Baraki et al.[36] give the relationship between the specimen temperature and power dissipation in Regime B. These measurements are in good agreement with predictions from a black body radiation model described in Raj [2]. These measurements and comparison with the model have been confirmed many times in different experiments in our laboratory. Typically they produce an increase in specimen temperature in the range 100^oC-400^oC over the furnace temperature for a power dissipation of about 100-400 $mWmm^{-3}$.

Baraki et al. also show the presence of a sharp peak in power dissipation (Regime A) which precedes the steady state (Regime B). However, their measurement of the specimen temperature

does not show a corresponding spike in specimen temperature. This issue is carefully and quantitatively analyzed by Raj in terms of the heat content required to raise the specimen temperature to the steady state levels, as required by the specific heat of the material. It is concluded that in Regime A the spike in power dissipation is damped by the specific heat of the specimen. Measurements of the specimen temperature with a pyrometer in our laboratory are consistent with this expectation: they do not show a spike in the specimen temperature corresponding to the spike in the power dissipation.

Suggestions have been made that the specimen interior can heat to very high levels while the surface remains at a lower temperature. Again, this would depend on the mechanism by which the specimen responds to the applied field and current. In the work reported from our laboratory we have limited our experiments to situations where there is no localization of current in the specimen. The design of the specimens, the dog-bone shape, assures a uniform flow of current through the gage section. Thus the heat dissipation from electric power is uniform as well. Microstructural analyses do not exhibit a gradient from the surface towards the interior. If the power dissipation in the specimen is uniform there is no convincing reason (from the point of view of heat transfer) to expect a large temperature gradient within the specimen since most of the heat loss is from black body radiation (in the temperature regime of interest to us).

However, as stated above, there are different regimes of behavior depending on the field and the current. We have evidence that at very high current settings at the power supply, the current through the specimen can localize causing “tunneling” to some degree. But these current levels spell a different regime of behavior, and we shall be reporting on this in the near future.

Bibliography

[1] M. Cologna, B. Rashkova, and R. Raj, "Flash Sintering of Nanograin Zirconia in <5 s at 850°C," *J. Am. Ceram. Soc.*, vol. 93, no. 11, pp. 3556–3559, 2010.

[2] R. Raj, "Joule heating during flash-sintering," *J. Eur. Ceram. Soc.*, vol. 32, no. 10, pp. 2293–2301, 2012.

[3] W. D. Callister and D. G. Rethwisch, *Material Science and Engineering: An Introduction*, 8th ed. John Wiley & Sons, Inc., 2010.

[4] W. D. Kingery, H. K. Bowen, and D. R. Uhlmann, *Introduction to Ceramics*, 2nd ed. John Wiley & Sons, Inc., 1976.

[5] M. A. Meyers and K. K. Chawla, *Mechanical Behavior of Materials*, 2nd ed. cambridge University Press, 2008.

[6] M. N. Rahaman, *Sintering of Ceramics*, 1st ed. CRC Press, 2007.

[7] S.-J. L. Kang, *Sintering: Densification, Grain Growth and Microstructure*, 1st ed. Elsevier, 2004.

[8] I. Chen and X. Wang, "Sintering dense nanocrystalline ceramics without final-stage grain growth," *Nature*, vol. 404, pp. 168–71, 2000.

[9] R. Raj, M. Cologna, and J. S. C. Francis, "Influence of Externally Imposed and Internally Generated Electrical Fields on Grain Growth, Diffusional Creep, Sintering and Related Phenomena in Ceramics," *J. Am. Ceram. Soc.*, vol. 94, no. 7, pp. 1941–1965, 2011.

[10] M. Cologna, J. S. C. Francis, and R. Raj, “Field assisted and flash sintering of alumina and its relationship to conductivity and MgO-doping,” *J. Eur. Ceram. Soc.*, vol. 31, no. 15, pp. 2827–2837, 2011.

[11] S. K. Jha and R. Raj, “The Effect of Electric Field on Sintering and Electrical Conductivity of Titania,” *J . Am. Ceram. Soc.*, vol. 97, no. 2, pp. 527–534, 2014.

[12] “Wikipedia,” 2015. [Online]. Available: http://en.wikipedia.org/wiki/Pottery.

[13] G. L. E. Roy, J. D. Embury, G. Edwards, and M. F. Ashby, “A Model of Ductile fracture based on the nucleation and growth vbased on voids,” *Acta. Metallurgica.* Vol. 29, pp. 1509-1522, 1981.

[14] T. Cheng and R. Raj, “Measurement of the Sintering Pressure in Ceramic,” *J. Am. Ceram. Soc.*, vol. 71, no. 4, pp. 276–280, 1986.

[15] R. R. Venkatachari K. R., “Shear Deformation and Densification of Powder Compacts,” *J. Am. Ceram. Soc.*, vol. 69, no. 6, pp. 499–506, 1986.

[16] R. Raj, “Analysis of the Sintering Pressure,” *J. Am, Ceram. Soc.*, vol. 70, no. 9, pp. 210–211, 1987.

[17] R. L. Coble, “Sintering Crystalline Solids. I. Intermediate and Final State Diffusion Models,” *J. Appl. Phys.*, vol. 32, no. 5, p. 787, 1961.

[18] J. Stanley C. Francis, “A study on the phenomena of flash-sintering with tetragonal zirconia,” Thesis, University of Colorao, Boulder, 2013.

[19] C. P. Cameron and R. Raj, “Grain-Growth Transition During Sintering of Colloidally Prepared Alumina Powder Compacts,” *J. Am. Ceram. Soc.*, vol. 71, no. 12, pp. 1031–1035, 1988.

[20] J. S. C. Francis, “FAST Ceramics,” 2012. [Online]. Available: http://www.fastceramics.com/innovative-research.html.

[21] K. R. Venkatachari and R. Raj, “Enhancement of Strength through Sinter Forging,” *J. Am. Ceram. Soc.*, vol. 70, no. 7, pp. 514–520, 1987.

[22] M. Oghbaei and O. Mirzaee, “Microwave verses conventional sintering: A review of funcdamentals, advantages and applications,” *J. Alloys Compd.*, vol. 494, no. 1–2, pp. 175–189, 2010.

[23] K. S. Naik, “Sintering of Ceramic Materials Under Electric Field,” Thesis, University of Trento, Italy, 2014.

[24] Z. a. Munir, D. V. Quach, and M. Ohyanagi, “Electric Current Activation of Sintering: A Review of the Pulsed Electric Current Sintering Process,” *J. Am. Ceram. Soc.*, vol. 94, no. 1, pp. 1–19, Jan. 2011.

[25] Z. A. Munir, U. Anselmi-Tamburini, and M. Ohyanagi, “The effect of electric field and pressure on the synthesis and cosolidation of materials : A review of the spark plasma sintering method,” *J. Mater. Sci.*, vol. 41, pp. 763–777, 2006.

[26] H. Conrad and D. Yang, “Influence of an applied dc electric field on the plastic deformation kinetics of oxide ceramics,” *Philos. Mag.*, vol. 90, no. 9, pp. 1141–1157, Mar. 2010.

[27] D. Yang and H. Conrad, “Influence of an electric field on the superplastic deformation of 3Y-TZP,” *Scr. Mater.*, vol. 36, no. 12, pp. 1431–1435, Jun. 1997.

[28] D. Yang, R. Raj, and H. Conrad, “Enhanced Sintering Rate of Zirconia (3Y-TZP) Through the Effect of a Weak dc Electric Field on Grain Growth,” *J. Am. Ceram. Soc.*, vol. 93, no. 10, pp. 2935–2937, 2010.

[29] S. Ghosh, A. H. Chokshi, P. Lee, and R. Raj, “A Huge Effect of Weak dc Electrical Fields on Grain Growth in Zirconia,” *J. Am. Ceram. Soc.*, vol. 92, no. 8, pp. 1856–1859, 2009.

[30] J. S. C. Francis and R. Raj, “Influence of the Field and the Current Limit on Flash Sintering at Isothermal Furnace Temperatures,” *J. Am. Ceram. Soc.*, vol. 96, no. 9, pp. 2754–2758, 2013.

[31] J. S. C. Francis and R. Raj, “Flash-Sinterforging of Nanograin Zirconia: Field Assisted Sintering and Superplasticity,” *J. Am. Ceram. Soc.*, vol. 95, no. 1, pp. 138–146, 2012.

[32] D. Yang and H. Conrad, “Enhanced sintering rate and finer grain size in yttria-stablized zirconia (3Y-TZP) with combined DC electric field and increased heating rate,” *Mater. Sci. Eng. A*, vol. 528, no. 3, pp. 1221–1225, 2011.

[33] H. Conrad and D. Yang, “Dependence of the sintering rate and related grain size of yttria-stabilized polycrystalline zirconia (3Y-TZP) on the strength of an applied DC electric field,” *Mater. Sci. Eng. A*, vol. 528, no. 29–30, pp. 8523–8529, 2011.

[34] H. Conrad, “Space Charge and Grain Boundary Energy in Zirconia (3Y-TZP),” *J. Am. Ceram. Soc.*, vol. 94, no. 11, pp. 3641–3642, 2011.

[35] D. Yang and H. Conrad, “Enhanced sintering rate of zirconia (3Y-TZP) by application of a small AC electric field,” *Scr. Mater.*, vol. 63, no. 3, pp. 328–331, 2010.

[36] R. Baraki, S. Schwarz, and O. Guillon, “Effect of Electrical Field/Current on Sintering of Fully Stabilized Zirconia,” *J. Am. Ceram. Soc.*, vol. 95, no. 1, pp. 75–78, 2012.

[37] C. Schmerbauch, J. Gonzalez-Julian, R. Röder, C. Ronning, and O. Guillon, “Flash Sintering of Nanocrystalline Zinc Oxide and its Influence on Microstructure and Defect Formation,” *J. Am. Ceram. Soc.*, vol. 97, no. 6, pp. 1728–1735, 2014.

[38] Y. Zhang, J.-I. Jung, and J. Luo, “Thermal runaway, flash sintering and asymmetrical microstructural development of ZnO and ZnO–Bi2O3 under direct currents,” *Acta Mater.*, vol. 94, pp. 87–100, 2015.

[39] J. A. Downs and V. M. Sglavo, “Electric Field Assisted Sintering of Cubic Zirconia at 390°C,” *J. Am. Ceram. Soc.*, vol. 96, no. 5, pp. 1342-1344, 2013.

[40] J. Park and I.-W. Chen, “In Situ Thermometry Measuring Temperature Flashes Exceeding 1,700°C in 8 mol% Y 2 O 3 -Stablized Zirconia Under Constant-Voltage Heating,” *J. Am. Ceram. Soc.*, vol. 96, pp. 697-700, 2013.

[41] M. Cologna, A. L. G. Prette, and R. Raj, “Flash-Sintering of Cubic Yttria-Stabilized Zirconia at 750°C for Possible Use in SOFC Manufacturing,” *J. Am. Ceram. Soc.*, vol. 94, no. 2, pp. 316–319, 2011.

[42] A. Gaur and V. M. Sglavo, “Densification of La0.6Sr0.4Co0.2Fe0.8O3 ceramic by flash sintering at temperature less than 100 °C,” *J. Mater. Sci.*, vol. 49, no. 18, pp. 6321–6332, Jun. 2014.

[43] A. Gaur and V. M. Sglavo, “Flash Sintering of (La, Sr)(Co, Fe)O3 - Gd-Doped CeO2 Composite,” *J. Am. Ceram. Soc.*, no. online, pp. 1–6, 2015.

[44] N. Shomrat, S. Baltianski, C. a. Randall, and Y. Tsur, “Flash sintering of potassium-niobate,” *J. Eur. Ceram. Soc.*, vol. 35, no. 7, pp. 2209–2213, 2015.

[45] R. Muccillo, E. N. S. Muccillo, and M. Kleitz, “Densification and enhancement of the grain boundary conductivity of gadolinium-doped barium cerate by ultra fast flash grain welding,” *J. Eur. Ceram. Soc.*, vol. 32, no. 10, pp. 2311–2316, 2012.

[46] R. Muccillo and E. N. S. Muccillo, “Electric field-assisted flash sintering of tin dioxide,” *J. Eur. Ceram. Soc.*, vol. 34, no. 4, pp. 915–923, 2014.

[47] E. N. S. Muccillo and R. Muccillo, “Electric field-assisted sintering of tin dioxide with manganese dioxide addition,” *J. Eur. Ceram. Soc.*, vol. 34, no. 15, pp. 3699–3706, 2014.

[48] J.-C. M’Peko, J. S. C. Francis, and R. Raj, “Field-assisted sintering of undoped BaTiO3: Microstructure evolution and dielectric permittivity,” *J. Eur. Ceram. Soc.*, vol. 34, no. 15, pp. 3655–3660, 2014.

[49] A. Gaur and V. M. Sglavo, “Flash-sintering of MnCo2O4 and its relation to phase stability,” *J. Eur. Ceram. Soc.*, vol. 34, pp. 2391-2400, 2014.

[50] H. Yoshida, Y. Sakka, T. Yamamoto, J.-M. Lebrun, and R. Raj, “Densification behaviour and microstructural development in undoped yttria prepared by flash-sintering,” *J. Eur. Ceram. Soc.*, vol. 34, no. 4, pp. 991–1000, 2014.

[51] J. S. C. Francis, M. Cologna, D. Montinaro, and R. Raj, “Flash Sintering of Anode-Electrolyte Multilayers for SOFC Applications,” *J. Am. Ceram. Soc.*, vol. 96, no. 5, pp. 1352–1354, May 2013.

[52] A. Karakuscu, M. Cologna, D. Yarotski, J. Won, J. S. C. Francis, R. Raj, and B. P. Uberuaga, “Defect Structure of Flash-Sintered Strontium Titanate,” *J. Am. Ceram. Soc.*, vol. 95, no. 8, pp. 2531–2536, 2012.

[53] A. L. G. Prette, M. Cologna, V. Sglavo, and R. Raj, “Flash-sintering of Co2MnO4 spinel for solid oxide fuel cell applications,” *J. Power Sources*, vol. 196, no. 4, pp. 2061–2065, 2011.

[54] K. S. Naik, V. M. Sglavo, and R. Raj, “Field assisted sintering of ceramic constituted by alumina and yttria stabilized zirconia,” *J. Eur. Ceram. Soc.*, vol. 34, no. 10, pp. 2435–2442, 2014.

[55] S. K. Jha and R. Raj, “Electric Fields Obviate Constrained Sintering,” *J. Am. Ceram. Soc.*, vol. 97, no. 10, pp. 3103–3109, 2014.

[56] S. Grasso, T. Saunders, H. Porwal, O. Cedillos-Barraza, D. D. Jayaseelan, W. E. Lee, and M. J. Reece, “Flash Spark Plasma Sintering (FSPS) of Pure ZrB2,” *J. Am. Ceram. Soc.*, vol. 97, no. 8, pp. 2405–2408, 2014.

[57] S. Bonilla, P. R. Wilshaw, and R. I. Todd, “Preliminary investigation of flash sintering of SiC,” *J. Eur. Ceram. Soc.*, vol. 33, pp. 2811–2816, 2013.

[58] J. A. Downs, “Mechanism of flash sintering in cubic zirconia,” Thesis, University of Trento, Italy, 2013.

[59] J. S. C. Francis, M. Cologna, and R. Raj, “Particle size effects in flash sintering,” *J. Eur. Ceram. Soc.*, vol. 32, pp. 3129–3136, 2012.

[60] J. Narayan, “A new mechanism for field-assisted processing and flash sintering of materials,” *Scr. Mater.*, vol. 69, no. 2, pp. 107–111, 2013.

[61] T. B. Holland, U. Anselmi-Tamburini, D. V. Quach, T. B. Tran, and A. K. Mukherjee, “Effects of local Joule heating during the field assisted sintering of ionic ceramics,” *J. Eur. Ceram. Soc.*, vol. 32, no. 14, pp. 3667–3674, 2012.

[62] M. C. Steil, D. Marinha, Y. Aman, J. R. C. Gomes, and M. Kleitz, “From conventional ac flash-sintering of YSZ to hyper-flash and double flash,” *J. Eur. Ceram. Soc.*, vol. 33, no. 11, pp. 2093–2101, 2013.

[63] K. Terauds, J.-M. Lebrun, H.-H. Lee, T.-Y. Jeon, S.-H. Lee, J. H. Je, and R. Raj, “Electroluminescence and the measurement of temperature during Stage III of flash sintering experiments,” *J. Eur. Ceram. Soc.*, vol. 35, no. 11, pp. 3195–3199, 2015.

[64] F. Wakai, Sakaguchi S, and Matsuno Y., “Superplasticity of yttria-stabilized tetrag- onal ZrO2 polycrystals.,” *Adv Ceram Mater*, vol. 1, no. 3, pp. 259–263, 1986.

[65] J.-M. Lebrun and R. Raj, “A first report of Photoemission in Experiments related to Flash Sintering,” *J. Am. Ceram. Soc.*, vol. 97, no. 8, pp. 2427–2430, 2014.

[66] S.-W. Kim, S.-J. L. Kang, and I.-W. Chen, “Electro-Sintering of Yttria-Stabilized Cubic Zirconia,” *J. Am. Ceram. Soc.*, vol. 96, no. 5, pp. 1398–1406, 2013.

[67] J. Narayan, “Grain growth model for electric field-assisted processing and flash sintering of materials,” *Scr. Mater.*, vol. 68, no. 10, pp. 785–788, 2013.

[68] K. S. Naik, V. M. Sglavo, and R. Raj, “Flash sintering as a nucleation phenomenon and a model thereof,” *J. Eur. Ceram. Soc.*, vol. 34, no. 15, pp. 4063–4067, 2014.

[69] R. I. Todd, E. Zapata-Solvas, R. S. Bonilla, T. Sneddon, and P. R. Wilshaw, “Electrical characteristics of flash sintering: thermal runaway of Joule heating,” *J. Eur. Ceram. Soc.*, vol. 33, pp. 2811–2816, 2013.

[70] J.-M. Lebrun, T. G. Morrissey, J. S. C. Francis, K. C. Seymour, W. M. Kriven, and R. Raj, “Emergence and Extinction of a New Phase During On-Off Experiments Related to Flash Sintering of 3YSZ,” *J. Am. Ceram. Soc.*, pp. 1–5, 2015.

[71] R. K. Bordia and R. Raj, “Sintering of TiO2-Al2O3 composites: A model Experimental Investigation,” *J. Am.*, vol. 71, no. 4, pp. 302–310, 1988.

[72] “SOLIDWORKS Student Edition Software.” 2014.

[73] E. A. Barringer, “The synthesis, interfacial electrochemistry ordering and sintering of monodispersed TiO2 powders,” *Ceramic porocessing research laboratory, Rept. no. 28, Volume 1 and 2, Massachusettes Institute of technology*,. 1986.

[74] J. S. C. Francis and J.-M. Lebrun, “Matlab.” 2014.

[75] P. Sarin, W. Yoon, K. Jurkschat, P. Zschack, and W. M. Kriven, “Quadruple Lamp Furncae for High Temperature (up to 2050 K) Synchrotron Powder X-ray Diffraction studies in Air in Reflection Geometry,” *Rev. Sci. Instrum.*, vol. 77, no. 9, 2006.

[76] K. Teradus, “Processing , Structure and High Temperature Oxidation Properties of Polymer-Derived and Hafnium Oxide Based Ceramic Systems,” Thesis, University of Colorado, Boulder, 2014.

[77] ASTM B962-15, “Standard Test Methods for Density of Compacted or Sintered Powder Metallurgy (PM) Products Using Archimedes’ Principle,” *ASTM Int. West Conshohocken, PA*, 2015.

[78] C. Barret and T. B. Massalki, *Structure of Metals*. Pergamon Oxford, 1980.

[79] J.-C. M'Peko, J. S. C. Francis, and R. Raj, "Impedance spectroscopy and dielectric properties of flash versus conventionally sintered yittria doped zirconia electroceramics viewed at the microstructural level," *J. Am. Ceram. Soc.*, vol. 96, no. 12, pp. 3760-3767, 2013.

[80] T. A. Hahn, R. K. Kirby, H. C. Wolfe, M. G. Graham, and H. E. Hagy, "Thermal Expansion of Platinum from 293 to 1900 K," vol. 87, no. 1972, pp. 87–95, 1972.

[81] M. Mendelson, "Average grain size in Polycrystalline Ceramics," *J . Am. Ceram. Soc.*, vol. 52, pp. 443–446, 1969.

[82] H. C. Weerasinghe, P. M. Sirimanne, G. V. Franks, G. P. Simon, and Y. B. Cheng, "Low temperature chemically sintered nano-crystalline TiO2 electrodes for flexible dye-sensitized solar cells," *J. Photochem. Photobiol. A Chem.*, vol. 213, no. 1, pp. 30–36, 2010.

[83] N.-G. Park, K. M. Kim, M. G. Kang, K. S. Ryu, S. H. Chang, and Y.-J. Shin, "Chemical Sintering of Nanoparticles: A Methodology for Low-Temperature Fabrication of Dye-Sensitized TiO2 Films," *Adv. Mater.*, vol. 17, no. 19, pp. 2349–2353, 2005.

[84] T. Bak, J. Nowotny, M. K. Nowotny, and L. R. Sheppard, "Defect Engineering of Titanium Dioxide," *J. Aust. Ceram. Soc.*, vol. 44, no. 2, pp. 63–67, 2008.

[85] S. Chao, V. Petrovsky, and F. Dogan, "Effects of sintering temperature on the microstructure and dielectric properties of titanium dioxide ceramics," *J. Mater. Sci.*, vol. 45, no. 24, pp. 6685–6693, 2010.

[86] M. Radecka, "Effect of High-Temperature Treatment on n – p Transition in Titania," *J. Am. Ceram. Soc.*, vol. 85, no. 2, pp. 346–354, 2002.

[87] Y. Liu and A. R. West, "Semiconductor-Insulator Transition in Undoped Rutile, TiO2 , Ceramics," *J. Am. Ceram. Soc.*, vol. 96, no. 1, pp. 218–222, 2013.

[88] et. al. Ming Zou, Yuan Wang, “Influence of Donar additives and properties of TiO2-Based Varistor,” *Adv. Mater. Res.*, vol. 105, pp. 320–323, 2010.

[89] H. Hahn, J. Logas, and R. S. Averback, “Sintering characteristics of nanocrystalline TiO2,” *J. Mater. Res.*, vol. 5, no. 3, pp. 609–614, 1990.

[90] M. Mazaheri, a. M. Zahedi, M. Haghighatzadeh, and S. K. Sadrnezhaad, “Sintering of titania nanoceramic: Densification and grain growth,” *Ceram. Int.*, vol. 35, no. 2, pp. 685–691, 2009.

[91] Y. Liu, X. Hao, Z. Wang, J. Wang, J. Qiao, Y. Yan, and K. Sun, “A newly-developed effective direct current assisted sintering technique for electrolyte film densification of anode-supported solid oxide fuel cells,” *J. Power Sources*, vol. 215, pp. 296–300, 2012.

[92] M. Cologna, V. M. Sglavo, and M. Bertoldi, “Sintering and Deformation of Solid Oxide Fuel Cells Produced by Sequential Tape Casting,” *Int. J. Appl. Ceram. Technol.*, vol. 7, no. 6, pp. 803–813, 2010.

[93] R. Muccillo, M. Kleitz, and E. N. S. Muccillo, “Flash grain welding in yttria stabilized zirconia,” *J. Eur. Ceram. Soc.*, vol. 31, no. 8, pp. 1517–1521, 2011.

[94] R. Muccillo and E. N. S. Muccillo, “An experimental setup for shrinkage evaluation during electric field-assisted flash sintering: Application to yttria-stabilized zirconia,” *J. Eur. Ceram. Soc.*, vol. 33, no. 3, pp. 515–520, 2013.

[95] D. Yang, R. Raj, and H. Conrad, “Enhanced Sintering Rate of Zirconia (3Y-TZP) Through the Effect of a Weak dc Electric Field on Grain Growth,” *J. Am. Ceram. Soc.*, vol. 93, no. 10, pp. 2935–2937, 2010.

[96] A. L. Linsebigler, G. Lu, and J. T. Yates, “Photocatalysis on TiO2 Surfaces: Principles, Mechanisms, and Selected Results,” *Chem. Rev.*, vol. 95, no. 3, pp. 735–758, 1995.

[97] S. K. Jha, J. M. Lebrun, K. C. Seymour, W. M. Kriven, and R. Raj, “Electric Field Induced Texture in Titania during Experiments Related to Flash Sintering,” *J . Am. Ceram. Soc.*, in preperation, 2015.

[98] R. Muccillo and E. N. S. Muccillo, “Light emission during electric field-assisted sintering of electroceramics,” *J. Eur. Ceram. Soc.*, vol. 35, no. 5, pp. 1653–1656, May 2015.

[99] P. D. Clapp, “A localized soft mode theory for martensitic transformation,” *Phys. Status Solidi*, vol. 57, no. 2, pp. 561–569, 1973.

[100] R. K. Bordia and R. Raj, “Sintering Behavior of Ceramic Films Constrained by a Rigid Substrate,” *J . Am. Ceram. Soc.*, vol. 68, no. 6, pp. 287–292, 1985.

[101] R. Raj and R. K. Bordia, “Sintering behavior of bi-modal powder compacts,” *Acta Met.*, vol. 32, no. 7, pp. 1003–1019, 1984.

[102] R. K. Bordia and R. Raj, “Role of shear in the sintering of composites,” *pp 27-39 in Tailoring multitude Compos. Ceram. Ed. by R.E. Tressler, G.L. Messin. C.G. Pantano R.E. Newnham , Plenum, New York*, 1986.

[103] A. M. Segadges, “Combustion Synthesis of Aluminium Titanate,” *J. Eur. Ceram. Soc.*, vol. 18, pp. 771–781, 1998.

[104] I. Stamenkovic, “Aluminium Titanate-Titania Ceramics Synthesized by Sintering and Hot Presstng,” *Ceram. Int.*, vol. 15, pp. 155–160, 1989.

[105] S. K. Jha, J. M. Lebrun, and R. Raj, “Asynchronicity of the electric current-induced sintering and phase transformation in the alumina titania system,” *J. Am, Ceram. Soc.*, p. in preparation, 2015.

[106] B. Freudenberg and A. Mocellin, “Aluminum Titanate Formation by Solid-state Reaction of Fine A1203 and Ti02 Powders,” *J. Am. Ceram. Soc.*, vol. 70, no. 1, pp. 33–38, 1987.

[107] B. Freudenberg and A. Mocellin, “Aluminium titanate formation by solid state reaction of AI203 and TiO2 single crystals,” *J. Mater. Sci.*, vol. 25, pp. 3701–3708, 1990.

[108] R. Uribe, C. Baudin, L. Mazerolles, and D. Michel, “Sub-micron sized Al 2 TiO 5 powders prepared by high-energy ball milling,” *J. Mater. Sci.*, vol. 36, pp. 5105–5113, 2001.

[109] V. Buscaglia, P. Nanni, G. Battilana, G. Aliprandi, and C. Carry, “Reaction sintering of aluminium titanate: II—Effect of different alumina powders,” *J. Eur. Ceram. Soc.*, vol. 13, no. 5, pp. 419–426, 1994.

[110] H. Okamura, E. A. Barringer, and H. K. Bowen, “Preparation and Sintering of Monosized A1203-Ti02 Composite Powder,” *J. Am, Ceram. Soc.*, vol. 69, no. 2, pp. 22–24, 1986.

[111] V. Buscaglia, G. Battilana, M. Leoni, and P. Nanni, “Decomposition of Al2TiO5-MgTi2O5 solid solutions: a thermodynamic approach,” *J. Mater. Sci.*, vol. 31, no. 19, pp. 5009–5016, 1996.

[112] V. Buscaglia, M. Alvazzi Delfrate, M. Leoni, C. Bottino, and P. Nanni, “The effect of MgAl2O4 on the formation kinetics of Al2TiO5 from Al2O3 and TiO2 fine powders,” *J. Mater. Sci.*, vol. 31, no. 7, pp. 1715–1724, 1996.

[113] T. Korim, “Effect of Mg2+-and Fe3+-ions on formation mechanism of aluminium titanate,” *Ceram. Int.*, vol. 35, no. 4, pp. 1671–1675, 2009.

[114] M. Ishitsuka, T. Sato, T. Endo, and M. Shimada, “Synthesis and Thermal Stability of Aluminum Titanate Solid Solutions,” *J. Am. Chem. Soc.*, vol. 70, no. 2, pp. 69–71, 1987.

[115] X. Hao, Y. Liu, Z. Wang, J. Qiao, and K. Sun, “A novel sintering method to obtain fully dense gadolinia doped ceria by applying a direct current,” *J. Power Sources*, vol. 210, pp. 86–91, 2012.

[116] A. Gaur and V. M. Sglavo, “Flash-sintering of MnCo2O4 and its relation to phase stability,” *J. Eur. Ceram. Soc.*, vol. 34, pp. 2391–2400, 2014.

[117] E. Kato, K. Daimon, and J. Takahashi, “Decomposition temperature of beta Al2TiO5,” *J . Am. Ceram. Soc.*, no. June, pp. 355–356, 1980.